# Nucleon and pion distribution functions in the valence region

Roy J. Holt*

*Physics Division, Argonne National Laboratory, Argonne, Illinois 60439, USA*

Craig D. Roberts†

*Physics Division, Argonne National Laboratory, Argonne, Illinois 60439, USA and Department of Physics, Peking University, Beijing 100871, China*

(Published 28 October 2010)

An experimental and theoretical perspective is provided on the behavior of unpolarized distribution functions for the nucleon and pion on the valence-quark domain, namely, Bjorken $x \gtrsim 0.4$. This domain is a key to much of hadron physics; e.g., a hadron is defined by its flavor content and that is a valence-quark property. Furthermore, its accurate parametrization is crucial to the provision of reliable input for large collider experiments. The focus is on experimental extractions of distribution functions via electron and muon inelastic scattering, and from Drell-Yan interactions; and on theoretical treatments that emphasize an explanation of the distribution functions, providing an overview of major contemporary approaches and issues. Valence-quark physics is a compelling subject, which probes at the heart of our understanding of the standard model. There are numerous outstanding and unresolved challenges, which experiment and theory must confront. In connection with experiment, an explanation that an upgraded Jefferson Laboratory facility is well suited to provide new data on the nucleon is provided, while a future electron-ion collider could provide essential new data for the mesons. There is also great potential in using Drell-Yan interactions, at FNAL, CERN, J-PARC, and GSI, to push into the large-$x$ domain for both mesons and nucleons. Furthermore, it is argued that explanation, in contrast to modeling and parametrization, requires a widespread acceptance of the need to adapt theory: to the lessons learnt already from the methods of nonperturbative quantum-field theory and a fuller exploitation of those methods.

DOI: 10.1103/RevModPhys.82.2991 PACS number(s): 12.38.Qk, 12.38.Bx, 12.38.Lg, 13.60.Hb

## CONTENTS



*holt@anl.gov
†cdroberts@anl.gov

 

## I. INTRODUCTION

From the first deep inelastic-scattering experiments (Bloom *et al.*, 1969; Breidenbach *et al.*, 1969) and the advent of the parton model (Bjorken, 1967; Bjorken and Paschos, 1969; Feynman, 1969), there has been a tremendous effort to deduce the parton distribution functions of the most stable hadrons—the proton, neutron, and pion. The long sustained and thriving interest in these structure functions is motivated by the necessity to understand hadron structure at a truly fundamental level. While it is anticipated that quantum chromodynamics (QCD) will provide the explanation of hadron structure, a quantitative description of hadrons within QCD is not yet at hand. An explanation and prediction of the behavior of parton distribution functions in the valence-quark region,[1] viz., Bjorken $x \gtrsim 0.4$, poses an important challenge for QCD and related models of hadron structure. This is the domain on which the transition takes place from deep inelastic scattering, with incoherent elastic scattering from numerous loosely correlated small-$x$ partons, to scattering from dressed quarks that become increasingly well correlated as $x \to 1$. We focus our attention herein on the behavior of unpolarized structure functions on the valence-quark domain.

The parton distributions are also essential to an understanding of QCD's role in nuclear structure. It has been known (Aubert *et al.*, 1983) for more than two decades that the parton distribution functions in a nucleus cannot simply be obtained by adding together the distributions within the constituent nucleons. This mismatch is the so-called European Muon Collaboration (EMC) effect, and although concerted efforts have led to the identification of some of the ingredients necessary to an explanation, we still lack a completely satisfactory understanding of the nuclear dependence of parton distribution functions. This hampers us enormously. For example, an accounting for the EMC effect in light nuclei is key to extracting the neutron structure function. That is a necessary precursor to a veracious determination of the differences between the parton distribution functions of the light quarks.

An accurate determination of the pointwise behavior of distribution functions in the valence region is also important to very high-energy physics. Particle discovery experiments and standard model tests with colliders are only possible if the QCD background is completely understood. QCD evolution, apparent in the so-called scaling violations by parton distribution functions, entails that with increasing center-of-mass energy $\sqrt{s}$ the support at large $x$ in the distributions evolves to small $x$ and thereby contributes materially to the collider background.

Deep inelastic scattering (DIS) of electrons from protons and bound neutrons at the Stanford Linear Accelerator Center (SLAC) led to the discovery of quarks. These experiments observed more electrons scattering with high energy at large angles than could be explained if protons and neutrons were uniform spheres of matter.[2] In the approximately 40 intervening years, electron DIS has played a central role in measuring structure functions, and SLAC has been especially effective in mapping the proton's structure functions in the valence-quark region.

More recently, muon scattering experiments—performed by the EMC, the New Muon Collaboration (NMC), and the Bologna-CERN-Dubna-Munich-Saclay Collaboration (BCDMS)—have contributed to our store of information. There have also been a substantial number of neutrino scattering experiments. However, they have generally used nuclear targets rather than pure hydrogen targets. Drell-Yan experiments have been effective at measuring the antiquark distributions in the proton and nuclei. Putting all this together, it can be said that as a consequence the proton structure function is extremely well known, at least for $x \lesssim 0.7$.

Herein we discuss the status of charged-lepton and Drell-Yan experiments, as well as prospects for new experiments at, e.g., the Thomas Jefferson National Accelerator Facility (JLab) and FermiLab (FNAL). On the other hand, although a number of experiments at the Conseil Européen pour la Recherche Nucléaire (CERN) and Deutsches Elektronen-Synchrotron have also provided measurements of the proton structure function, many of these efforts focused on the low-$x$ behavior and hence they will not be discussed.

An experimental determination of the neutron structure function at high Bjorken $x$ has proved especially troublesome, the main reason being that most of our information about the neutron structure function is obtained from DIS experiments on a deuteron target, for which the nature of the EMC effect is simply unknown. Consequently, inference of the neutron structure function from proton and deuteron measurements is model dependent. We treat this topic in some depth and, in addition, canvass prospects for the future.

On the theoretical side the challenge is first to parametrize and ultimately to calculate the parton distribution functions. We write *ultimately* because the distribution functions are essentially nonperturbative and therefore cannot be calculated in perturbation theory. Thus, in the absence of a truly accurate, quantitative, and predictive nonperturbative tool, the QCD calculation of parton distribution functions remains an alluring but distant

[1] As will become clear, for a given hadron in its infinite-momentum frame, a parton's Bjorken-$x$ value specifies the fraction of the hadron's momentum carried by this parton. There is no unambiguous beginning to the valence-quark domain. We choose $x \gtrsim 0.4$ because thereafter the gluon distribution can be said to be much smaller than the valence $u$-quark distribution in the proton.

[2] In both method and results this series of experiments, conducted from 1966 to 1978 and for which Taylor, Kendall, and Friedman were awarded the 1990 Nobel Prize in Physics, was kindred to that which led Rutherford to discovery of the nucleus in 1911.

prospect. Herein we provide both an historical perspective on past attempts at a theoretical interpretation and an overview of recent progress toward this goal. Notably, today, there are no computations of the pointwise behavior of the nucleon's valence-quark distribution function that agree with the predictions of the QCD parton model.

There has, on the other hand, been much success to date with parametrization. A number of independent groups have analyzed and performed a global fit to the vast body of extant DIS and Drell-Yan nucleon structure-function data. In this approach the physical processes are factorized into the product of short- and long-distance contributions. The so-called short-distance parts are calculable in perturbation theory, whereas the long-distance parts are determined by the parton distribution functions. In this way, via the operator product expansion in QCD, scattering processes involving hadrons are connected to subprocesses involving partons. The utility of this approach is grounded on the fact that as long as factorization is valid, the parton distribution functions are universal; namely, all hadron-level interactions for which factorization applies are described by the same small body of parton distribution functions. This being true, the nonperturbative problem is reduced to that described above: instead of calculating all cross sections from scratch, one has *merely* to calculate the distribution functions. Herein we introduce the modern parametrizations.

At its simplest, the nucleon is a three-body problem. As ostensibly a two-body problem, it would appear theoretically simpler to calculate properties of the pion and hence the parton distributions therein. However, the pion is, in fact, both a bound state and the Goldstone mode associated with dynamical chiral-symmetry breaking (DCSB) in QCD. This amplifies the importance of understanding its properties. However, it also significantly complicates the calculation of the pion's distribution functions and places additional constraints on any framework applied to the task: the pion simply cannot veraciously be described as a constituent quark-antiquark pair. Instead, key features of nonperturbative quantum-field theory must be brought to bear.

Although it is not presently possible to perform deep inelastic scattering on a free pion, the pion structure function has been measured in pionic Drell-Yan experiments at CERN and FNAL. Owing to predictions from the QCD parton model, the form of the pion's valence-quark distribution function provides a stringent test of our understanding of both QCD and QCD-based approaches to hadron structure. The FNAL Drell-Yan experiment (Conway *et al.*, 1989) measured the pion structure function up to high Bjorken $x$, where the QCD predictions were expected to be realized. However, they were not manifest, so that a puzzling discrepancy remains at this time. The status of structure-function measurements of the pion as well as prospects for future experiments at JLab and a possible future electron-ion collider (EIC) will be presented, as will a full description of the theoretical perspective.

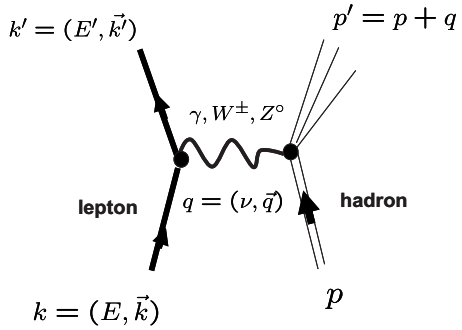


FIG. 1. Feynman diagram representing deep inelastic lepton scattering from a hadron.

The purpose of this article is not to present a comprehensive review of all the issues involved in extracting structure functions from high-energy data, as in Sterman (1995), nor an exhaustive digest of theoretical developments in the field. Rather the focus will be on structure functions in the valence region, which have chiefly been extracted from electron and muon inelastic scattering, as well as from Drell-Yan interactions. Moreover, we focus on the theoretical treatments that emphasize an explanation of these structure functions and summarize the major contemporary approaches and issues. To end this Introduction, a brief remark on notation: unless denoted otherwise, when addressing a distribution function, it will be that associated with the proton, e.g., $u_v(x)$ will mean the proton's valence $u$-quark distribution.

## II. NUCLEON STRUCTURE FUNCTIONS FROM ELECTRON AND MUON SCATTERING

### A. Kinematics

The Feynman diagram for lepton inelastic scattering from a hadron is given in Fig. 1. Practically, the leptons in a laboratory scattering process can be electrons, muons, or neutrinos, as shown in the figure, and the current can be a photon, a charged weak current $W^{\pm}$, or a neutral weak current $Z^0$ of four-momentum transfer $q$. The incident lepton has incoming and outgoing four-momenta of $k$ and $k'$, respectively, so that the momentum and energy transfers are given by

$$q = k - k', \tag{2.1}$$

$$\nu = E - E', \tag{2.2}$$

where the incident momentum and mass of the hadron are given by $p$ and $M$, while the outgoing debris after the inelastic event has a momentum $p'$.

The invariants in the scattering process are the following: the square of the four-momentum transfer; the square of the invariant mass; $p \cdot q$, which is related to the energy transfer in the target rest frame; and the square of the total energy in the center-of-mass frame. The square of the four-momentum transfer depends on the energy of the beam and scattered lepton as well as the lepton scattering angle: neglecting the lepton's mass,

$$Q^2 := -q^2 = 4EE' \sin^2\frac{\theta}{2}. \tag{2.3}$$

The square of the invariant mass $W$ is given by

$$W^2 = (p+q)^2 = M^2 - Q^2 + 2p\cdot q = M^2 + \frac{1-x}{x}Q^2, \tag{2.4}$$

where $M$ is the mass of the hadron and

$$x = Q^2/2p\cdot q \tag{2.5}$$

is the Bjorken variable. The square of the total energy in the center of mass is given by the Mandelstam variable $s$,

$$s = (k+p)^2. \tag{2.6}$$

A final useful invariant is

$$y = p\cdot q/p\cdot k, \tag{2.7}$$

which, in the target rest frame, is a measure of the fractional energy loss by the incident lepton.

The Bjorken limit is theoretically defined as

$$Q^2 \to \infty, \quad 2p\cdot q \to \infty, \quad x = \text{fixed}. \tag{2.8}$$

In this limit, $x$ can be shown to equal the fraction of the hadron's momentum carried by the struck quark. Empirically, in order to avoid complications associated with the production of hadron resonances, the Bjorken scaling regime is explored via

$$W \to \infty, \quad Q^2 \to \infty, \quad x = \frac{Q^2}{Q^2 + W^2 - M^2} = \text{fixed}. \tag{2.9}$$

In principle, the deep inelastic approximation is only good when

$$\nu^2/Q^2 = Q^2/4M^2x^2 \gg 1. \tag{2.10}$$

However, it is empirically well established that scaling in DIS sets in at tractable values of $W$ and $Q^2$. As a practical matter, evaluations of data typically impose the requirement that $Q^2 \geqslant 4$ GeV$^2$ and $W \geqslant 3.5$ GeV. As discussed and explored, e.g., by Malace *et al.* (2009) and Accardi *et al.* (2010), data at high Bjorken $x$ but not meeting these kinematic requirements would be subject to large target-mass corrections, which are kinematic and owe to binding of partons in the hadron. Before discussing these topics in more detail, the cross section for inelastic electron scattering will be presented.

### B. The cross section for charged-lepton scattering

The cross section for inelastic charged-lepton scattering from a hadron via a one-photon exchange process, as shown in Fig. 1, is well known and given by

$$\frac{d\sigma}{d\Omega dE'}(E,E',\theta) = \left(\frac{\alpha_e^2}{Q^4}\right)\left(\frac{E'}{E}\right)L^e_{\mu\nu}W^{\mu\nu}, \tag{2.11}$$

where $L^e_{\mu\nu}$ is the leptonic tensor and $W^{\mu\nu}$ is the hadronic tensor. The leptonic tensor has the following straightforward dependence on the kinematic variables:

$$L_e^{\mu\nu} = 2\{k^\mu k'^\nu + k^\nu k'^\mu + g^{\mu\nu}[m^2 - (k\cdot k')]\}, \tag{2.12}$$

where $m$ is the lepton's mass. Conserving current and parity, the hadronic tensor for a spin-$\frac{1}{2}$ charged particle depends on two structure functions $W_1(\nu,Q^2)$ and $W_2(\nu,Q^2)$, viz.,

$$W_{\mu\nu} = W_1\left(-g_{\mu\nu} + \frac{q_\mu q_\nu}{q^2}\right) + \frac{W_2}{M^2}\left(p_\mu - \frac{p\cdot q}{q^2}q_\mu\right)\left(p_\nu - \frac{p\cdot q}{q^2}q_\nu\right). \tag{2.13}$$

Contracting the leptonic tensor with the hadronic tensor yields the well-known cross section of the form

$$\frac{d\sigma}{d\Omega dE'}(E,E',\theta) = 4\frac{\alpha_e^2 E'^2}{Q^4}\left[W_2(\nu,Q^2)\cos^2\frac{\theta}{2} + 2W_1(\nu,Q^2)\sin^2\frac{\theta}{2}\right]. \tag{2.14}$$

The quantities $W_1$ and $W_2$ in Eq. (2.14) are often written in terms of dimensionless structure functions $F_1$ and $F_2$ for the nucleon

$$MW_1(\nu,Q^2) = F_1(x,Q^2), \tag{2.15}$$

$$\nu W_2(\nu,Q^2) = F_2(x,Q^2). \tag{2.16}$$

In turn, these structure functions are frequently written in terms of the transverse ($F_T$) and longitudinal ($F_L$) structure functions, which correspond to absorption of transverse and longitudinal virtual photons, respectively,

$$F_T(x,Q^2) = 2xF_1(x,Q^2), \tag{2.17}$$

$$F_L(x,Q^2) = F_2(x,Q^2) - 2xF_1(x,Q^2). \tag{2.18}$$

They can, in principle, be measured separately by performing a longitudinal/transverse ($L/T$) separation, as will be discussed in Sec. II.H. The most intuitive physical picture of the interaction in the deep inelastic-scattering regime is provided by the parton model.

### C. The parton model

It was discovered at SLAC in the late 1960s that the structure functions appeared to scale; i.e., their evolution with $x$ is nearly independent of $Q^2$ over a very large kinematic range. These important points are well documented not only in the original papers (Bjorken, 1967; Bjorken and Paschos, 1969; Bloom *et al.*, 1969; Breidenbach *et al.*, 1969; Feynman, 1969) but also in the Nobel lectures summarized by Friedman (1991), Kendall (1991), and Taylor (1991) and here will only be reviewed briefly.

The observed scaling feature means that the cross section is not separately a function of the two kinematic variables, energy transfer $\nu$ and $Q^2$. Instead, the behavior of the cross section can be expressed in a dependence on only one scaling variable, namely, Bjorken $x$. Indeed, in the Bjorken limit [Eq. (2.9)], the proton struc-

ture functions $W_1$ and $W_2$ assume a form consistent with elastic scattering from a point fermion, viz.,

$$2MW_1(\nu,Q^2) \to 2F_1(x) \sim \frac{Q^2}{2M\nu x^2}\delta\left(1-\frac{Q^2}{2M\nu x}\right), \tag{2.19}$$

$$\nu W_2(\nu,Q^2) \to F_2(x) \sim \delta\left(1-\frac{Q^2}{2M\nu x}\right), \tag{2.20}$$

where $x$ is given by Eq. (2.5). This near dependence on only a single dimensionless variable is referred to as Bjorken scaling. Assuming this to be the case, then the expression for the cross section [Eq. (2.11)] becomes

$$\frac{d\sigma}{d\Omega dE'}(E,E',\theta) = 4\frac{\alpha_e^2 E'^2}{Q^4}\left[\frac{F_2(x)}{\nu}\cos^2\frac{\theta}{2} + \frac{2F_1(x)}{M}\sin^2\frac{\theta}{2}\right]. \tag{2.21}$$

Capitalizing on these results and assumptions, further analysis leads to (Callan *et al.*, 1969)

$$F_2(x) = 2xF_1(x). \tag{2.22}$$

This Callan-Gross relation is observed to be approximately valid, a feature that is often cited as evidence that the pointlike constituents of the proton, i.e., the quarks, are spin-$\frac{1}{2}$ degrees of freedom.

An intuitive understanding of the observed scaling behavior is provided by the quark-parton model (QPM) or QCD parton model. In this model the electron collides with a collection of partons within the hadron. Owing to Lorentz contraction of the hadron at extremely high momentum, these partons are practically frozen in time during the extremely brief collision process. Moreover, the probability of finding two partons near enough to interact with each other drops as $1/Q^2$. Thus, initial- and final-state interactions are suppressed in the DIS regime. Within this model, the photon interacts incoherently with individual partons and the cross section depends in a simple way on the probability of finding a quark of flavor $i$ with fraction $x$ of the proton's momentum. These properties are realized in the following simple expression for the electromagnetic structure function:

$$F_2(x) = 2xF_1(x) = \sum_i e_i^2 x[q_i(x)+\bar{q}_i(x)], \tag{2.23}$$

where $e_i$ are the charges of the individual quarks and $q_i(x)$ are the probability densities for finding quark $i$ with fraction $x$ of the hadron's momentum. Assuming that only the relatively light quarks $(u,d,s,c)$ and their respective antiquarks contribute to the proton structure function, then the proton structure function can be written as

$$\frac{1}{x}F_2^p(x) = \frac{4}{9}[u(x)+\bar{u}(x)+c(x)+\bar{c}(x)] + \frac{1}{9}[d(x)+\bar{d}(x)+s(x)+\bar{s}(x)]. \tag{2.24}$$

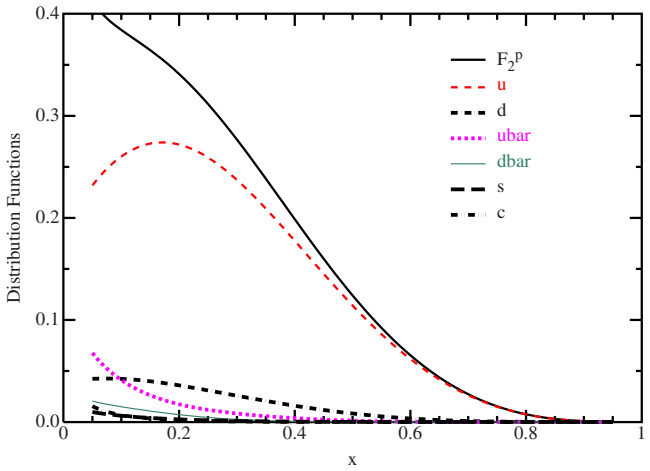


FIG. 2. (Color online) Quark flavor dependence of the proton structure function according to the CTEQ6L (leading-order) evaluation at a scale $Q^2=10$ GeV$^2$ (Stump *et al.*, 2003; Martin *et al.*, 2004). We plot the quantities $e_i^2 x q_i(x)$ in order to emphasize the contribution to the structure function from the various quark flavors.

In Fig. 2 we show the contributions of these quark flavors to the structure function in the valence region. The CTEQ6L leading-order (LO) evaluation (Stump *et al.*, 2003; Martin *et al.*, 2004), a modern global evaluation of existing data, was used for illustration. The distribution of up- and down-quark flavors is fixed primarily by electron and muon scattering from the proton and neutron, while the distribution of the $u$ and $d$ quark sea is largely determined by Drell-Yan processes. The strange and charm quark sea is determined by neutrino interactions. The $u$-quark distribution is the dominant contribution to the proton structure function, while the $d$ and anti-$u$ quarks are significant. The charm and strange quark distributions are small and are not easily distinguishable in the figure. We note that semi-inclusive electron scattering from the proton and deuteron is emerging as an important tool for determining the strange quark distribution, thereby providing an important complement to the method of neutrino scattering from complex nuclei as a probe of nonvalence proton structure functions. Of course, the $u$- and $d$-quark distributions in the valence region are particularly important for testing descriptions of nucleon structure, and it is therefore vital to obtain accurate and precise data and a reliable flavor separation in this region.

A primary goal of modern theory is the computation of valence-quark distribution functions using QCD-motivated or QCD-based models and nonperturbative methods in QCD. Naturally, valence quarks have no strict empirical meaning because experiment cannot readily distinguish a valence from a sea quark. However, valence-quark distributions for the $u$ and $d$ quarks in the nucleon can be defined as the following flavor-nonsinglet combinations:

$$u_v(x) := u(x) - \bar{u}(x), \tag{2.25}$$

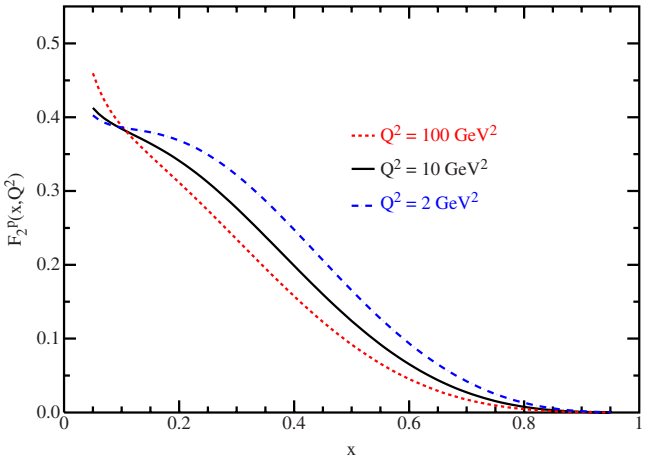


FIG. 3. (Color online) Structure function of the proton at three values of $Q^2$, computed from the CTEQ6L leading-order evaluation.

$$d_v(x) := d(x) - \bar{d}(x). \tag{2.26}$$

Conservation of charge leads to important normalization conditions,

$$\int_0^1 dx u_v(x) = 2, \quad \int_0^1 dx d_v(x) = 1. \tag{2.27}$$

Naturally,

$$\int_0^1 dx s_v(x) = 0, \tag{2.28}$$

with the same result for all heavier quarks. However, it does not follow that $s_v(x)$ must be identically zero.

Consistent with nomenclature, the combinations in Eqs. (2.25) and (2.26) have nonzero values of various flavor quantum numbers, such as isospin and baryon number. Singlet distributions also play a role and are constituted from a sum of quark distribution functions: $\Sigma(x)=\Sigma_i[q_i(x)+\bar{q}_i(x)]$. Under QCD evolution, discussed below, singlet distributions mix among themselves and with the gluon distribution, but the nonsinglet distributions do not.

### D. QCD and scaling violations

The proton structure function in the valence region is shown in Fig. 3 as a function of Bjorken $x$ and for three values of $Q^2$ for the CTEQ6L LO evaluation. Although the $Q^2$ range illustrated is relatively large, from 2 to 100 GeV$^2$, the structure function does not exhibit a strong dependence on $Q^2$. This result validates the parton model as an approximation to a QCD description of the structure function. Of course, the structure functions have a dependence on $Q^2$, indicating the necessity of QCD rather than a parton model to describe the data. This relatively small $Q^2$ dependence is known as a scaling violation.

The validity of the QPM led to the idea of factorization in deep inelastic scattering. In factorization, the cross section is separated into two distinct contributions: a short-distance part, described by perturbative QCD (pQCD), and a long-distance part. The $Q^2$-dependence driving scaling violation originates in the pQCD part and owes to the same phenomena that generate running of the strong-coupling constant $\alpha_s$ and hence asymptotic freedom. This factorization for the moments of the structure functions can be shown rigorously using the operator product expansion and the renormalization-group equations. Alternatively, a distribution function where the moments can be written as products can be expressed in terms of a convolution of two distributions. Naturally, the long-distance part is only calculable using nonperturbative methods and presents a challenge for modern hadron theory.

At small distances or, equivalently, large momentum transfers in QCD, the effective coupling constant becomes small. This feature is known as asymptotic freedom (Gross and Wilczek, 1974; Politzer, 1974). In terms of the renormalization scale $\Lambda_{\rm QCD}$, the strong-coupling constant has the perturbative form,

$$\frac{\alpha_s(t)}{4\pi} = \frac{1}{\beta_0 t} - \frac{\beta_1 \ln(t)}{\beta_0^3 t^2} + \mathcal{O}\left(\frac{1}{t^3}\right), \tag{2.29}$$

where $t=\ln(Q^2/\Lambda_{\rm QCD}^2)$, $\beta_0=11-2n_f/3$, $\beta_1=102-38n_f/3$, and $n_f$ is the number of quark flavors involved in the process. From Eq. (2.29) it is apparent that $\alpha_s\to 0$ as $Q^2\to\infty$, so that a parton-model limit is contained within QCD; e.g., as will become clear below, Eq. (2.23) is obtained from Eq. (2.37) in this limit.

Plainly, the definition of short- and long-distance phenomena is ambiguous, and associated with a separation of the cross section into these two contributions is a factorization scale, namely, a mass scale chosen by the practitioner as the boundary between hard and soft. If that scale is large enough, then the hard part of the scattering cross section can be calculated in pQCD. This, however, introduces another scale, associated with renormalization. For convenience and economy, the factorization and renormalization scales are usually chosen to be the same. It follows, in addition, that factorization is scheme dependent because the choice of renormalization scheme implicitly specifies a division of the finite pieces of the cross section into those that are retained in the hard contribution and those understood to be contained in the soft piece. The part identified as owing to long-distance effects is basically the parton density distribution function.

In fitting data to construct PDFs, it is usual to use the $\overline{\rm MS}$ (modified minimal subtraction) renormalization scheme whereas, with regard to factorization, there are two commonly used schemes. The DIS scheme (Altarelli *et al.*, 1978) was designed to ensure there are no higher-order corrections to the expression for the $F_2$ structure function in terms of the quark PDFs; i.e., all finite contributions are absorbed into the PDF. On the other hand, in the more widely used $\overline{\rm MS}$ scheme (Bardeen *et al.*, 1978), in addition to the divergent piece, only the usual $(\ln 4\pi-\gamma_E)$ combination is absorbed into $q(x)$ and

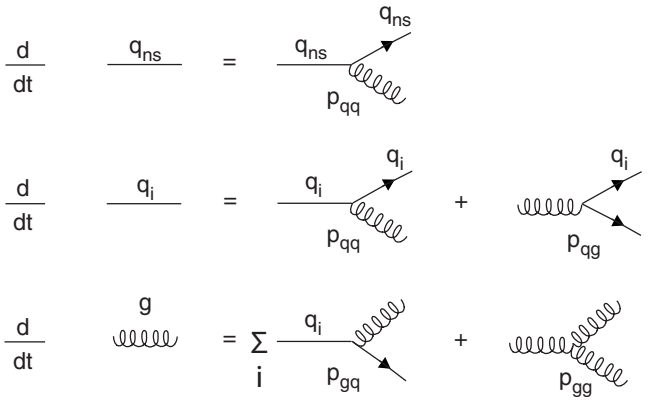


FIG. 4. Graphical representation of the leading-order DGLAP equations.

hence the expression for $F_2$ exhibits explicit $O(\alpha_s)$ corrections [see Sterman *et al.* (1995) for more on these points].

The CTEQ6L (leading-order) structure functions shown in Fig. 3 were evaluated using the $\overline{\text{MS}}$ scheme. At leading order there is no difference between factorization schemes. As we will subsequently see (Fig. 4), radiated gluons give rise to the scaling violation or $Q^2$ dependence of the structure functions. They, and the quark distribution functions defined therefrom, then depend on both $x$ and $Q^2$. The $Q^2$ dependence is now routinely described within the framework of next-to-leading-order (NLO) QCD evolution.

An important and extremely useful feature of factorization is that a measurement of a structure function at relatively low $Q^2$ permits the calculation, through the use of pQCD, of the structure function at high $Q^2$. In leading order, a set of integrodifferential equations, now known as the Dokshitzer-Gribov-Lipatov-Altarelli-Parisi (DGLAP) evolution equations (Gribov and Lipatov, 1972; Lipatov, 1975; Altarelli and Parisi, 1977; Dokshitzer, 1977), is used for this purpose. Intuitively, one may think that as $Q^2$ increases, a parton can sometimes be resolved into two partons; e.g., a quark can split into a quark and a gluon or a gluon into two gluons—see Fig. 4 for a graphical representation of the leading-order DGLAP equations. The two resolved partons then share in the fraction of the nucleon momentum carried by the initial unresolved parton at lower $Q^2$. The parton distribution thus becomes a function of $Q^2$. Such evolution of the parton distribution function (PDF) can be seen in Fig. 3. At the highest values of $Q^2$ the structure function is shifted toward lower values of $x$. This work has been generalized to other reaction processes (Furmanski and Petronzio, 1982).

We note that, in principle, the domain of "relatively-low $Q^2$" means, nevertheless, $Q^2 \gg \Lambda^2_{\rm QCD}$. Notwithstanding this, in some empirical determinations of PDFs through data fitting (see Sec. V.C) and in the application of models to their calculation (see Sec. VI), evolution is sometimes applied from low $Q^2 \sim 4\Lambda^2_{\rm QCD}$. In such cases an interpretation of the low-$Q^2$ distribution as a parton-model density is questionable owing to the probable importance of nonperturbative corrections. However, contributions from such corrections are suppressed by DGLAP evolution to larger $Q^2$ and hence one anticipates that in these applications there is always a $Q^2$ whereafter the desired interpretation becomes valid.

As stated above, the evolution equations enable the accurate calculation of the PDFs at a general $Q^2$, provided they are known at another scale $Q_0^2$ so long as pQCD is a valid tool at both scales. At next-to-leading order the QCD evolution equations have the form (Herrod and Wada, 1980)

$$dq_{NS\pm}(x,Q^2)/dt = P_{NS\pm} \otimes q_{NS\pm}(x',Q^2), \tag{2.30}$$

where the convolution is defined as

$$C \otimes f := \int_x^1 \frac{dy}{y} C(y) f\left(\frac{x}{y}\right) \tag{2.31}$$

and

$$\frac{d}{dt}\begin{pmatrix}\Sigma(x,Q^2)\\ g(x,Q^2)\end{pmatrix} = P \otimes \begin{pmatrix}\Sigma(x',Q^2)\\ g(x',Q^2)\end{pmatrix}. \tag{2.32}$$

In these formulas, $q_{NS-}=u-\bar{u}$, $d-\bar{d}$ and $q_{NS+}=(u+\bar{u})-(d+\bar{d})$ or $(u+\bar{u})+(d+\bar{d})-2(s+\bar{s})$ are the nonsinglet PDFs, while $\Sigma=\Sigma_i(q_i+\bar{q}_i)$ is the singlet combination. The splitting functions are given by

$$P_{NS\pm} = \frac{\alpha_s}{2\pi} P^0_{qq}(x) + \left(\frac{\alpha_s}{2\pi}\right)^2 P^1_{NS\pm}(x), \tag{2.33}$$

$$P = \frac{\alpha_s}{2\pi} P^0(x) + \left(\frac{\alpha_s}{2\pi}\right)^2 P^1(x), \tag{2.34}$$

where

$$P^j = \begin{pmatrix} P^j_{qq} & 2n_f P^j_{qg} \\ P^j_{gq} & P^j_{gg}\end{pmatrix}. \tag{2.35}$$

The leading-order DGLAP equations are obtained simply by eliminating the $\alpha_s^2$ terms in the equations above.

It will be apparent from Eqs. (2.30) and (2.31) that $x=1$ is a fixed point, namely, that the $x=1$ value of each distribution function is invariant under evolution—it is the same at every value of the resolving scale $Q^2$. This is because the right-hand side of each evolution equation vanishes at $x=1$. Naturally, when Bjorken $x$ is unity, then $q^2+2p\cdot q=0$ and hence one is strictly dealing with the situation in which the invariant mass of the hadronic final state is precisely that of the target: $W=M$ in Fig. 1, viz., elastic scattering. The structure functions inferred experimentally in the neighborhood of $x=1$ are therefore determined by the target's elastic form factors, which all vanish in the limit $Q^2\to\infty$. This fact *per se* is not interesting. However, the rate at which distribution functions vanish with $x$ is important because it can lead to nonzero renormalization-scale-invariant distribution-function ratios at $x=1$. For example, the value of $\lim_{x\to 1} d_v(x)/u_v(x)$ in the nucleon is an unambiguous scale-invariant feature of QCD and hence a discrimina-

tor between models. [For an illustration of this point, see also Fig. 42, which shows $u_v^K(x)/u_v^\pi(x)$.] This is an important consequence, and one much discussed and explored in experiment and theory (see Secs. II.G and VI).

We reiterate, however, that the neighborhood of $x=1$ poses difficulties for experiment and for theory too, owing, e.g., to the importance on this domain of target-mass corrections and higher-twist contributions (explained below). While the equivalence between $x=1$ and elastic scattering cannot be avoided, one might choose to approach the limit obliquely. For example, noting from Eq. (2.9) that

$$1-x=1-\frac{Q^2}{Q^2+W^2-M^2}\overset{Q^2\gg W^2-M^2}{\approx}\frac{(W-M)(W+M)}{Q^2}, \tag{2.36}$$

one would ideally choose a path such that both $Q^2$ and $W-M$ are simultaneously kept as large as kinematically possible. This is experimentally very difficult, as discussed in connection with Fig. 7. Future experimental possibilities are outlined in Sec. IV.

A great triumph of QCD is the good agreement between the evolved structure function for the proton and experiment over many orders of magnitude in $Q^2$. Of course, the structure function should be calculated at the same order as the PDFs. The equation for the structure function at NLO in the DIS scheme is given by

$$F_2(x,Q^2)=x\sum_i e_i^2\Bigg\{q_i(x,Q^2)+\bar{q}_i(x,Q^2)+\frac{\alpha_s(Q^2)}{2\pi}\{C_i\otimes[q_i(x,Q^2)+\bar{q}_i(x,Q^2)]+2C_g\otimes g(x,Q^2)\}\Bigg\}, \tag{2.37}$$

where $g(x,Q^2)$ is the gluon distribution and the Wilson coefficients $\{C_{i,g}\}$ are given by Furmanski and Petronzio (1982) and Glück *et al.* (1995).

During the past several years rather complete NNLO fits (Martin *et al.*, 2007) in the $\overline{\text{MS}}$ scheme have been performed for the data. These fits have made use of next-to-next-to-leading-order (NNLO) splitting functions (Moch *et al.*, 2004; Vogt *et al.*, 2004). The LO, NLO, and NNLO $u$-quark distribution functions are plotted at a scale of $Q^2=10$ GeV$^2$ in Fig. 5 for comparison. Naturally, the structure functions themselves are measured quantities and do not depend on the order of the fit. In the valence region, the largest difference occurs between LO and NLO as expected. There is some evidence (Yang and Bodek, 2000) from early NNLO analyses that evolution at NNLO largely offsets the effect of high twist in an NLO analysis on the large-$x$ domain. However, a more recent analysis (Blumlein *et al.*, 2007) performed up to next-to-next-to-next-to-leading order (N3LO) contradicts this finding.

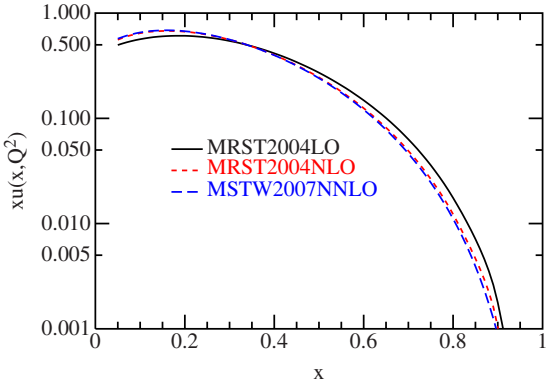


FIG. 5. (Color online) Comparison of the proton's $u(x)$ distributions in LO, NLO, and NNLO at $Q^2=10$ GeV$^2$.

### E. High twist effects and target-mass corrections

As we have seen, the interactions between partons at short distances that give rise to scaling violations are reasonably well described in a pQCD approach through the $Q^2$-evolution equations. Probes of a hadron at intermediate values of $Q^2$ might expose correlations among the partons. Thus far, we have only considered the case in DIS where structure functions are governed by incoherent scattering from the partons. As we move to lower $Q^2$ where nucleon resonances could dominate or to very high $x$ where the elastic-scattering limit and complete coherence dominate, then correlations between the partons must be taken into account. Ultimately a theoretical treatment of these correlations demands an understanding of the way that quarks and gluons bind to form hadrons. Although perturbative QCD cannot explain binding effects, it does permit one to construct a model of power corrections to the perturbative result. It was found (Ellis *et al.*, 1982, 1983) that the first power correction $1/Q^2$ to the structure function is governed by the intrinsic transverse components of the parton momentum.

The operator product expansion is normally used to order contributions to a DIS structure function according to their twist $\tau$ which is defined as the difference between the naive mass dimension of an operator and its "spin." Here spin means the number of vector indices contracted with the configuration-space four-vector $z$. For example, Sterman (1995) considered the expansion of a dimension six$=2d_J$ current-current correlator, typical of DIS,

$$J^\alpha(z)J_\alpha(0)\sim\sum_{\tau=2}^{\infty}\sum_{n=0}^{\infty}C_{\tau,n}(z^2,\mu^2)z^{\nu_1}\cdots z^{\nu_n}\times O^\tau_{\nu_1\cdots\nu_n}\quad(z=0,\mu^2), \tag{2.38}$$

where $\mu$ is the factorization scale. One is interested in the $z^2\sim 0$ behavior of the coefficient function $C_{\tau,n}(z^2,\mu^2)=(z^2)^{-d_C/2}\hat{C}(z^2\mu^2)$ because the more highly singular is this function on the light cone, the more important is the associated operator at large $Q^2$. Now, sup-

pose the operator $O^{\tau}_{\nu_1\cdots\nu_n}(\mu^2)$ has dimension $d_{O_n}$, then, in order to balance dimensions on both sides of Eq. (2.38), one must have $d_C=2d_J-(d_{O_n}-n)$ since each factor of $z$ on the right-hand side contributes mass dimension negative-one. Plainly, the largest value of $d_C$ is obtained with the smallest value of twist $\tau=d_{O_n}-n$, and the associated operators are those which dominate the large-$Q^2$ behavior of the correlator. As Eq. (2.38) indicates, numerous operators with different dimensions have the same twist and all such operators are associated with the same degree of light-cone singularity.

As evident in the example above, the leading-twist contributions in DIS are twist 2. In unpolarized DIS, the higher-twist components, i.e., twist=4,6,…, are suppressed by $1/Q^2,1/Q^4,\ldots$, respectively. Thus, in general, a structure function should be expressed in the form (Alekhin *et al.*, 2004)

$$F_2(x,Q^2) = F_2^{LT}(x,Q^2) + H_2(x,Q^2)/Q^2 + \mathcal{O}(1/Q^4), \tag{2.39}$$

where $F_2^{LT}$ refers to the leading-twist part. As a practical matter, the magnitudes of higher-twist terms are generally unknown and the estimates are therefore somewhat controversial. Before one can claim discovery of higher-twist components, it is essential that these be distinguished from target-mass corrections and $Q^2$-evolution effects.

Several analyses have shown that higher-twist coefficients can become quite large at high $x$ and relatively low $Q^2$. An analysis (Virchaux and Milsztajn, 1992) of BCDMS and SLAC data indicated that the twist-4 coefficient is sizable for the proton and deuteron. Here, however, the inclusion of target-mass corrections reduced the magnitude of the twist-4 coefficient. This finding was supported in an analysis that included NNLO (Yang and Bodek, 2000). It was found that the NNLO contribution can partially compensate for a large higher-twist effect. More recently, an analysis (Blumlein *et al.*, 2007) of world data indicated that the twist-4 coefficient is sizable for NLO, NNLO, and N3LO for the proton and deuteron. While increasing the order of the QCD analysis of the data reduces the twist-4 coefficient, the coefficient is significant at high $x$. This is shown in Fig. 6, which plots an empirically determined correction defined via

$$F_2(x,Q^2) = O_{TMC}[F_2^{\text{twist-2}}(x,Q^2)][1 + C_{HT}(x,Q^2)/Q^2], \tag{2.40}$$

where $O_{TMC}$ describes inclusion of target-mass corrections of the twist-2 contributions to the structure function. At present, there exists no statistically significant determination of the magnitude of the twist-6 coefficient.

In connection with the size of higher-twist contributions, it is relevant to consider their impact on Bloom-Gilman duality (Bloom and Gilman, 1971). This is an expectation that the nucleon structure function, when measured in the region dominated by low-lying nucleon resonances, should follow a global scaling curve that is

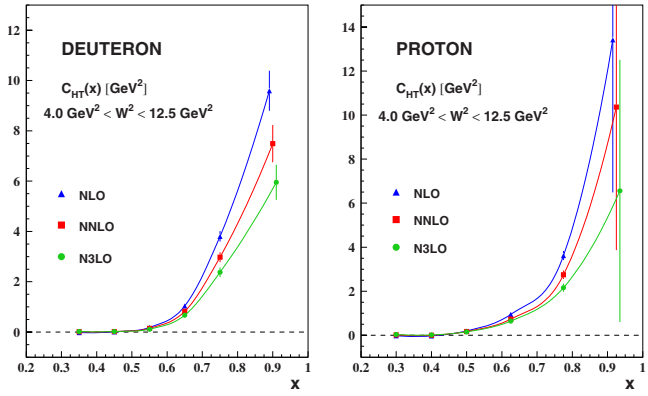


FIG. 6. (Color online) Empirical nonsinglet higher-twist coefficient, denoted $C_{HT}$, as a function of Bjorken $x$, for the proton (left panel) and deuteron (right panel), as obtained when the twist-2 contributions are treated at NLO, NNLO, and N3LO. Adapted from Blumlein *et al.*, 2007.

determined by high-energy data. It is important to note that although the standard application of DGLAP evolution to deep inelastic structure functions can appear to be inconsistent with Bloom-Gilman duality at fixed $W$, this apparent conflict is resolved if one takes into account the fact that the struck quark is far-off shell in the $x\to 1$ domain (Lepage and Brodsky, 1980; Brodsky, 2005).

Underlying Bloom-Gilman duality is the assumption of quark-hadron duality, namely, a belief that one obtains equivalent descriptions of physical phenomena irrespective of whether one uses partonic or hadronic degrees of freedom (Shifman, 2000; Melnitchouk *et al.*, 2005). While this assumption is probably correct in principle, in comparisons between computations that use finite-order truncations, it can and is violated in practice. The presence of large higher-twist contributions can therefore entail an apparently strong violation of Bloom-Gilman duality.

Experiments, particularly at the highest values of $x$, might not be performed at sufficiently large momentum transfer to avoid high-twist effects and target-mass corrections. A pQCD treatment is truly valid only in the limit that the mass of the hadron is negligible in comparison with the dominant scale $Q^2$. The target-mass corrections are kinematic and owe to binding of partons in the hadron. Nachtmann (1973) first pointed out that at finite $Q^2$ and nonvanishing target mass, the scaling variable should be the fraction $\xi$ of the nucleon's light-front momentum carried by the parton, viz.,

$$\xi(x,Q^2) = 2x/(1+\kappa), \quad \kappa = \sqrt{1+4x^2M^2/Q^2}. \tag{2.41}$$

Naturally, this Nachtmann variable reduces to Bjorken $x$ for $M^2/Q^2\to 0$.

It was subsequently shown (Georgi and Politzer, 1976) that at leading order, if the quantity $x^2M^2/Q^2$ is reasonably small, then it is straightforward to apply corrections for finite mass to the structure function. If the leading-twist structure function is denoted by $F_i^{LT}$ and the target-mass corrected structure function by $F_i^{TM}$, then one has

$$F_1^{TM}(x,Q^2) = \frac{x}{2\kappa}F_1^{LT}(\xi) + \frac{M^2x^2}{Q^2\kappa^2}\int_\xi^1 dx' F_1^{LT}(x') + 2\frac{M^4x^3}{Q^4\kappa^3}\int_{x'}^1 dx'' F_1^{LT}(x''), \quad (2.42)$$

$$F_2^{TM}(x,Q^2) = \frac{x^2}{\kappa^3}F_2^{LT}(\xi) + 6\frac{M^2x^3}{Q^2\kappa^4}\int_\xi^1 dx' F_2^{LT}(x') + 12\frac{M^4x^4}{Q^4\kappa^5}\int_{x'}^1 dx'' F_2^{LT}(x''). \quad (2.43)$$

A concern with the Nachtmann or the Georgi-Politzer approach is the so-called "threshold problem." This problem results from the fact that the maximum kinematic value of $\xi$ is less than unity, which means that the corrected leading-twist structure function does not vanish at $x=1$.

Target-mass corrections have been extended to NLO QCD (DeRújula *et al.*, 1977) and generalized to include charge and neutral weak current deep inelastic scattering (Kretzer and Reno, 2004). De Rújula *et al.* argued that the threshold problem could be solved by considering higher-twist effects.

A recent interesting approach (Steffens and Melnitchouk, 2006) to the threshold problem followed the original Georgi-Politzer approach but with one critical difference. Namely, the upper limit of the integrals in Eq. (2.42) becomes the upper limits of $x'$ and $x''$ that are permitted by kinematics at $x=1$ rather than merely unity. In terms of existing data, this solution does not result in a large effect for $Q^2>2$ GeV$^2$ but can have a significant effect below 1 GeV$^2$ where the underlying assumption of factorization becomes questionable anyway.

In addition to target-mass corrections, there are also effects from nonzero current-quark mass (Barbieri *et al.*, 1976). Such corrections will not be discussed herein because of our focus on high $x$, where heavy quarks have little effect in nucleons and Goldstone bosons. These effects, in addition to those arising from target-mass corrections, are discussed in a recent review (Schienbein *et al.*, 2008). Furthermore, recent work (Accardi and Qiu, 2008) has pointed out that changing the upper limit of the integrals in the Georgi-Politzer equations leads to an abrupt cutoff at $x=1$ and proposed a "quark jet" mechanism to give a more reasonable approach to the very large $x$ behavior.

### F. The proton structure function

Measurements of structure functions at very high values of $x$ are extremely challenging. The main problems can be seen from Fig. 7. Here $Q^2$ is plotted from Eq. (2.4) as a function of $x$. Typical evaluations of the parton distribution functions require that $W\geqslant 3.5$ GeV. Clearly, the $Q^2$ necessary to meet this demand is extremely high and impractical, at present, for $x\geqslant 0.7$.

The first DIS measurements, performed at SLAC, were limited to a beam energy of 24.5 GeV. Although this beam energy limit is a serious problem for very high $x$ measurements, the SLAC experiments had good control of systematic errors. Relatively high luminosities were possible, the incident electron energy was very well known, and the spectrometer properties were relatively well understood. A consistent reanalysis of all the early SLAC experiments was performed by Whitlow *et al.* (1992), and the result is shown in Fig. 8.

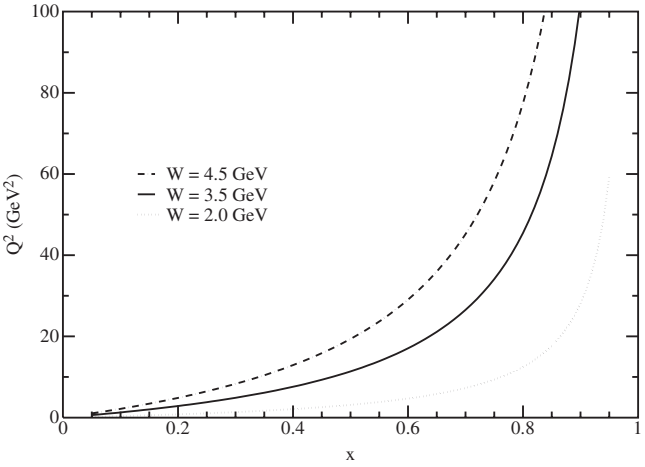


FIG. 7. $Q^2$ vs $x$ for three values of $W$. Measurements at very high $x$ demand very high $Q^2$ to remain in the DIS region.

After the importance of the early SLAC experiments was realized, the quest for additional data, particularly at high $Q^2$, led to muon scattering experiments at CERN and FNAL. At CERN a series of experiments was performed at muon energies between 90 and 280 GeV by the NMC Collaboration (Amaudruz *et al.*, 1992), between 120 and 280 GeV by the BCDMS Collaboration (Benvenuti *et al.*, 1990b), and at 280 GeV by the EMC

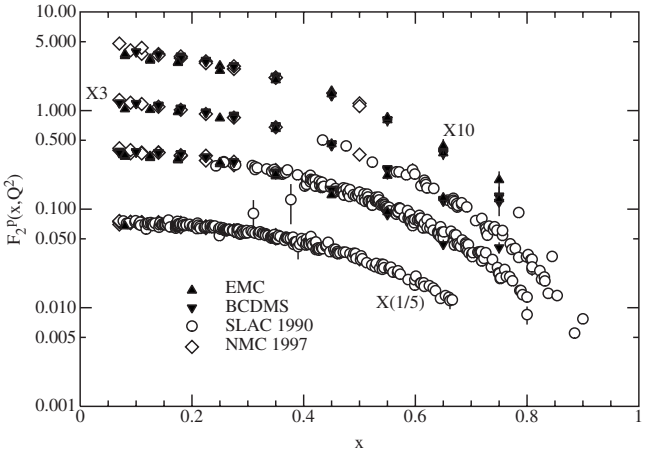


FIG. 8. Proton structure function vs Bjorken $x$ with $W\geqslant 2.0$ GeV. For ease of representation: the upper bands of data were multiplied by a factor of 10 and correspond to the domain $25\leqslant Q^2\leqslant 40$ GeV$^2$; the next bands are scaled by a factor of 3 and cover the domain $15\leqslant Q^2\leqslant 25$ GeV$^2$; the third-lowest bands are unscaled and cover $7\leqslant Q^2\leqslant 15$ GeV$^2$; and the lowest bands are scaled by a factor of 1/5 and cover $2\leqslant Q^2\leqslant 7$ GeV$^2$.

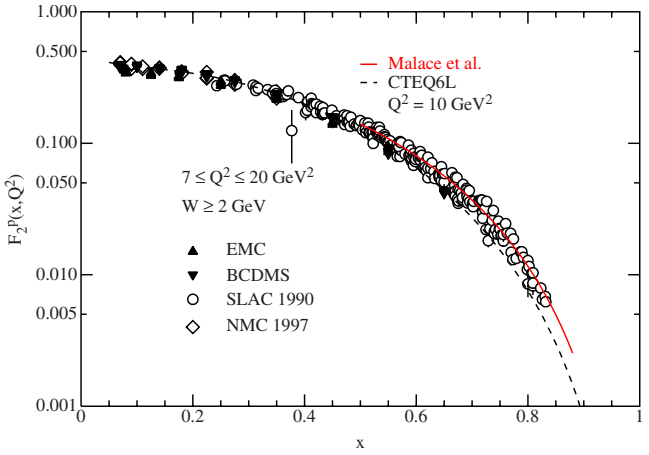


FIG. 9. (Color online) The proton structure functions vs Bjorken $x$ with $W \geqslant 2$ GeV. The dashed black curve represents the CTEQ6L evaluation with $Q^2=10$ GeV$^2$, while the solid curve indicates the result obtained when target-mass corrections are incorporated. From Malace *et al.*, 2009.

collaboration (Aubert *et al.*, 1987). In this case, the combination of very high beam energies and relatively low luminosities makes it difficult to obtain structure-function data at very high $x$. The practical limit is about $x=0.75$ as shown in Fig. 8. The FNAL E665 experiment provides data at even lower $x$ than the CERN experiments since the beam energy was 470 GeV.

Data for various $Q^2$ ranges from the BCDMS (Benvenuti *et al.*, 1990b), EMC (Aubert *et al.*, 1983, 1987), NMC (Amaudruz *et al.*, 1992; Arneodo *et al.*, 1997a), and SLAC (Whitlow *et al.*, 1990) experiments are plotted in Fig. 8. The effect of the kinematic constraints on the reach in $x$ is evident throughout the relatively wide range of values for $Q^2$. The SLAC data persist out to the highest values of $x$ but only for relatively low values of $W$.

If the condition on $W$ is relaxed to $W \geqslant 2$ GeV, then data from SLAC exist up to $x=0.85$ as shown in Fig. 9. Clearly, the CTEQ6L evaluation at the highest values of $x$ deviates from the data. However, if target-mass corrections are taken into account, as shown by the dashed curve in the figure, then good agreement is restored. This illustrates that target-mass corrections are indispensable in order to fully understand and extract parton distributions at very high $x$.

### G. The neutron structure function

Interest in the neutron structure function at very high $x$ has burgeoned during the past decade. The neutron structure function or at least the ratio of the neutron structure function to that of the proton is believed to be one of the best methods to determine the $d(x)/u(x)$ ratio. A knowledge of this ratio in the valence region would provide an important constraint on models for the nucleon (Brodsky *et al.*, 1995; Isgur, 1999). For example, if one were to assume that a simple SU(6) flavor symmetric model for the nucleon is valid, then the $d/u$ ratio would just be $1/2$ for the valence-quark distributions. In this model, the nucleon and $\Delta$ would be degenerate, so this is clearly not a correct description of the nucleon. Other interesting limits occur, for example, where the $d$ quark in the proton is "sequestered" in a pointlike scalar diquark. In this model, $d/u|_{x\to 1}=0$ and $F_2^n/F_2^p|_{x\to 1}=1/4$. Furthermore, in a world where pQCD could be applied naively and scattering at large $x$ involves only quarks with the same helicity as the target hadron, then $d/u|_{x\to 1}=1/5$ and $F_2^n/F_2^p|_{x\to 1}=3/7=0.43$. (An extensive discussion of these issues is provided in Sec. VI, where it is argued, e.g., that $F_2^n/F_2^p|_{x\to 1}=0.36$ and only with reliable data at $x\geqslant 0.8$ will one be empirically able to determine the $x\to 1$ behavior.)

The parton model is a good starting point for introducing the neutron structure function. Under the assumption of isospin symmetry and recalling Eqs. (2.27), the neutron structure function is simply obtained from Eq. (2.24) by the operation $u\leftrightarrow d$, viz.,

$$\frac{1}{x}F_2^n(x)=\frac{4}{9}[d(x)+\bar{d}(x)+c(x)+\bar{c}(x)] + \frac{1}{9}[u(x)+\bar{u}(x)+s(x)+\bar{s}(x)]. \tag{2.44}$$

Neglecting the $c$ quarks, the expression for the neutron-to-proton structure-function ratio is

$$\frac{F_2^n(x)}{F_2^p(x)}=\frac{u(x)+\bar{u}(x)+4[d(x)+\bar{d}(x)]+s(x)+\bar{s}(x)}{4[u(x)+\bar{u}(x)]+d(x)+\bar{d}(x)+s(x)+\bar{s}(x)}. \tag{2.45}$$

From this equation it is readily apparent that the ratios are $1/4$ when $u$ quarks dominate and 4 when $d$ quarks dominate, and, if the sea dominates, the ratio approaches unity. Within the parton model, Eq. (2.45) leads to the Nachtmann limit (Nachtmann, 1972),

$$\tfrac{1}{4}\leqslant F_2^n(x)/F_2^p(x)\leqslant 4. \tag{2.46}$$

As interest has grown, a number of new methods for measuring the $F_2^n/F_2^p$ ratio have been proposed. One approach (Fenker *et al.*, 2003) is to tag very low-momentum protons emerging from the deuteron when deep inelastic scattering from the neutron is performed. This technique minimizes off-shell effects since at very low momentum the neutron is practically a spectator in the deuteron. Another method (Afnan *et al.*, 2000, 2003; Bissey *et al.*, 2001; Petratos *et al.*, 2006) is to perform deep inelastic scattering from $^3$He and $^3$H at very high $x$. In forming the ratio of the scattering rates from these two nuclei, the nuclear effects cancel to a high degree in extracting the $F_2^n/F_2^p$ ratio.

Two proposed methods avoid nuclear effects altogether. Both a ratio of charge-current neutrino to antineutrino scattering from the proton and parity-violating deep inelastic electron scattering at high $x$ from the proton are sensitive to the $d/u$ ratio. Nevertheless, both of these methods are fraught with technical difficulties, particularly at high $x$.

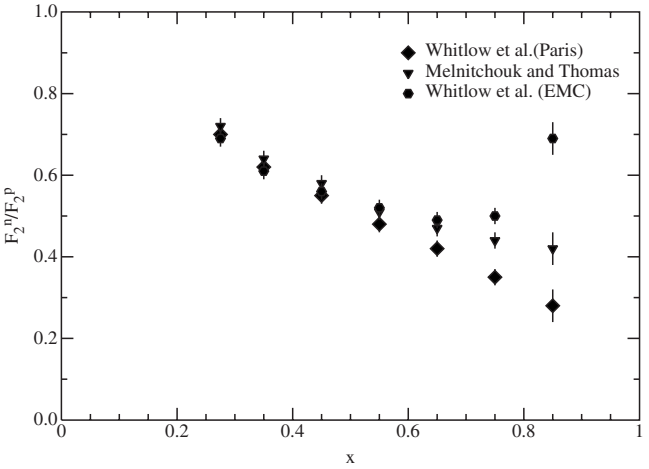


FIG. 10. The ratio of the neutron-to-proton structure functions as a function of $x$. The results of three extraction methods are shown.

The primary problem with measuring the neutron structure function is that there exists no practical free neutron target. Typically, a deuteron target is employed in experiments. The neutron structure function is then extracted from a measurement of the proton and deuteron structure functions by employing a model for the deuteron wave function. As an example, we consider the covariant approach of Thomas and Melnitchouk (1998). In this case, the proton and neutron structure functions are convoluted with a nucleon density function in the deuteron. The neutron is also off shell, so that a model for the off-shell behavior is necessary. The expression for the deuteron structure function is then given by

$$F_2^D(x) = \frac{1}{2}\sum_N \int_x^{M_D/M} dy' \rho_{N/D}(y') F_2^N\left(\frac{x}{y'}, Q^2\right) + \delta^{\rm off} F_2^D, \tag{2.47}$$

where $\rho_{N/D}(y')$ is the probability of finding a nucleon of momentum $y'$ in the deuteron and $\delta^{\rm off}F_2^D$ is the off-shell correction. The extraction process is iterative. First the off-shell effect is subtracted from the measured deuteron structure function. Then the proton structure function, convoluted as indicated by the first term in Eq. (2.47), is subtracted from the remainder, leaving the convoluted neutron structure function. This remaining piece is then deconvoluted to give the neutron structure function. The last three steps are then repeated until convergence is achieved.

The results (Thomas and Melnitchouk, 1998) of this procedure for the ratio of the neutron-to-proton structure functions are shown in Fig. 10. In this work a covariant deuteron wave function and a consistent off-shell correction were used (Melnitchouk *et al.*, 1994). Another application (Burov *et al.*, 2004) of the covariant approach indicates that data for the deuteron structure function at very high $x$ are essential for constraining the high $x$ neutron structure function. Although the convolution approach has been used by many as a step toward explaining the EMC effect, the convolution method has no firm theoretical basis.

Two other extractions, also shown in Fig. 10, yield different results at high $x$. The extraction, labeled "Whitlow *et al.* (Paris)" (Whitlow *et al.*, 1992), made use of light-front kinematics with the null vector along the incident-beam direction and an early deuteron wave function. The extraction, labeled "Whitlow *et al.* (EMC)" (Whitlow *et al.*, 1992), made a density-dependent extrapolation of the EMC effect in heavy nuclei to that in the deuteron. There is significant controversy (Yang and Bodek, 1999, 2000; Melnitchouk *et al.*, 2000) surrounding the density-dependent extrapolation method.

A recent approach (Arrington *et al.*, 2009) made use of the light front, with null-plane dynamics and modern deuteron wave functions. This framework, which can be applied even when the constraints of DIS kinematics are not met, greatly simplifies the convolution equation in terms of the nucleon structure functions. The analysis established that it is important to account properly for the $Q^2$ dependence of the data and incorrect to use a simple convolution formula to analyze data if those data do not satisfy the DIS kinematic constraints. When the CD-Bonn potential is used to determine the deuteron wave function, the method of Arrington *et al.* (2009) produces a ratio similar to that labeled Whitlow *et al.* (Paris) in Fig. 10, which was obtained using a light-front approach with the null vector aligned along the direction of the incident electron beam (Frankfurt and Strikman, 1981). While this particular choice of null-vector orientation is consistent with DIS kinematics, the very high $x$ SLAC data, included in the analysis, are not. They are usually excluded when fitting PDFs.

### H. The longitudinal structure function

Before the $F_2$ structure function can be extracted from data, one must either know or measure the $R$ structure function. By combining Eqs. (2.14)–(2.16), the expression for the cross section in terms of $F_1(x,Q^2)$ and $F_2(x,Q^2)$ is given by

$$\frac{d\sigma}{d\Omega dE'}(E,E',\theta) = 4\frac{\alpha_e^2 E'^2}{Q^4}\left[\frac{F_2(x,Q^2)}{\nu}\cos^2\frac{\theta}{2} + \frac{2F_1(x,Q^2)}{M}\sin^2\frac{\theta}{2}\right]. \tag{2.48}$$

This cross section is often expressed in terms of the $F_2$ and $R$ structure functions in the following way:

$$\frac{d\sigma}{d\Omega dE'}(E,E',\theta) = 4\frac{\alpha_e^2 E'^2}{Q^4}\frac{F_2(x,Q^2)}{\nu}\cos^2\frac{\theta}{2} \times\left[1+\frac{1-\epsilon}{\epsilon}\frac{1}{1+R(x,Q^2)}\right], \tag{2.49}$$

where

$$\epsilon = \left[1 + 2(1+\nu^2/Q^2)\tan^2\frac{\theta}{2}\right]^{-1} \quad (2.50)$$

and

$$R(x,Q^2) \equiv \frac{\sigma_L}{\sigma_T} = \frac{F_2(x,Q^2)}{2xF_1(x,Q^2)}\left(1+\frac{2Mx}{\nu}\right) - 1. \quad (2.51)$$

Here $\sigma_L$ and $\sigma_T$ refer to the longitudinal and transverse cross sections, respectively. Since the quarks are point-like spin-$\frac{1}{2}$ objects, the cross section for absorption of a longitudinal photon is small in comparison with that for a transverse photon. Furthermore, a vector-vector interaction preserves chirality, so the longitudinal cross section will depend on violations of this chirality. Violations of order $m_q^2/Q^2$ would be expected, where $m_q$ is the struck quark's current mass. Intrinsic transverse quark momentum $k_T$ as well as higher orders in $\alpha_s$ from the gluon distribution can give rise to an increase in the longitudinal cross section. For example, the Bjorken-Feynman model gives the result (Feynman, 1972) that

$$R = 4(m_q^2 + \langle k_T^2\rangle)/Q^2. \quad (2.52)$$

The QCD contribution to $F_L$ and, consequently, to $R$ of order $\alpha_s$ is given by (Reya, 1981; Altarelli, 1982)

$$F_L(x,Q^2) = \frac{\alpha_s}{2\pi}x^2\int_x^1 \frac{dy}{y^3}\left[\frac{8}{3}F_2(y,Q^2) + \frac{40}{9}\left(1-\frac{x}{y}\right)yG(y,Q^2)\right] + \mathcal{O}(\alpha_s^2), \quad (2.53)$$

where $G$ is the gluon distribution function, and only four flavors of quarks are considered in the second term. An excellent extraction (Whitlow *et al.*, 1990) of $F_2$ and $R$ was performed from a global analysis of the SLAC data.

It has long been believed that a tight constraint on the gluon structure function can be built from good measurements of $F_L$. The best extractions for $R$ in the valence region are from the lower energy SLAC and JLab data (Whitlow *et al.*, 1990; Yang and Bodek, 2000; Tvaskis *et al.*, 2007). The best extractions of $F_L$ are from HERA-DESY (Hadron Electron Ring Accelerator, Deutsches Elektronen-Synchrotron) data but at lower $x$ than the subject of this review. Nevertheless, the deduced gluon distribution is very sensitive to the order of $\alpha_s$ used in the analysis (Martin *et al.*, 2006).

### I. The gluon structure function

Interest in the gluon structure function has grown markedly during the past decade. Part of the interest resides in the fact that gluons comprise more than 98% of the rest mass of the nucleon as well as more than half of its light-front momentum. This interesting aspect of the role of glue in the nucleon can be seen from Fig. 11. Here the mass of a light quark is plotted as a function of the quark's momentum. The "data" in the plot are results from lattice simulations, while the curves are from Dyson Schwinger equation (DSE) calculations. The curve labeled "chiral limit" is the DSE result obtained with the current-quark mass set to zero. Clearly, even if the current-quark mass vanishes, the quark mass rises rapidly to near 0.3 GeV at low quark momentum. This is DCSB and a clear demonstration in QCD of the effect on the quark mass produced by the presence of gluons with strong self-interactions.

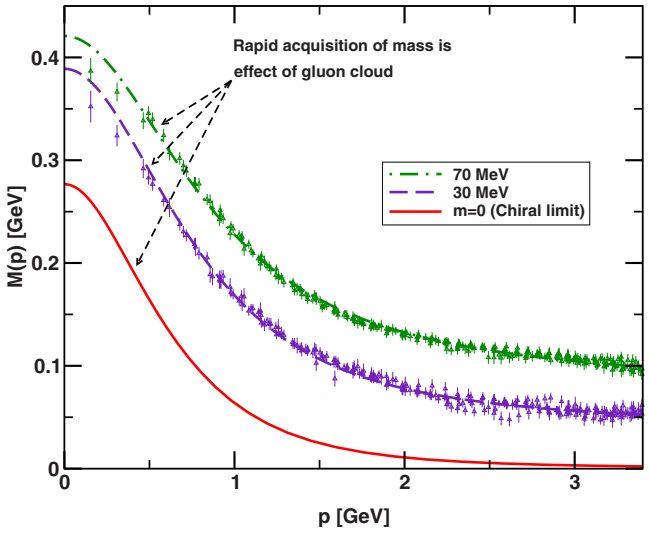


FIG. 11. (Color online) Dressed-quark mass function $M(p)$: curves—Dyson-Schwinger equation (DSE) results, obtained as explained by Bhagwat *et al.* (2003) and Bhagwat and Tandy (2006); data—numerical simulations of unquenched lattice-QCD (Bowman *et al.*, 2005). In the momentum dependence of $M(p)$, one observes the current quark of perturbative QCD evolving into a constituent quark as its momentum becomes smaller. The constituent-quark mass arises from a cloud of low-momentum gluons attaching themselves to the current quark. This is dynamical chiral-symmetry breaking (DCSB): an essentially nonperturbative effect that generates a quark mass from nothing, namely, it occurs even in the chiral limit. Adapted from Bhagwat *et al.*, 2007.

Sensitivity to the gluon structure function via lepton beams can be produced by a careful measurement of scaling violations, i.e., measurements of the longitudinal structure function or the partial derivative of $F_2(x,Q^2)$ with respect to $\ln Q^2$. This is particularly effective at low values of $x$ where this derivative is directly proportional to the gluon distribution function at first order.

## III. DISTRIBUTION FUNCTIONS FROM DRELL-YAN INTERACTIONS

Informative reviews on the Drell-Yan process exist (Kenyon, 1982; Reimer, 2007). In this section we emphasize that the Drell-Yan interaction provides (i) the cleanest access to the antiquark distributions in the valence region in hadrons, (ii) a means to determine the quark distributions in the proton at very high $x$, and (iii) the most information on the parton distributions in mesons. Naturally, in order to isolate the valence-quark distributions in the proton, it is imperative to measure the antiquark distributions.

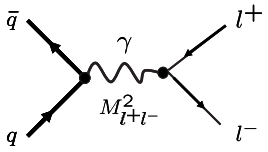


FIG. 12. Feynman diagram representing the Drell-Yan interaction.

### A. The Drell-Yan interaction

The Drell-Yan process was devised (Drell and Yan, 1970a, 1971) to explain hadron-hadron collisions where an antilepton-lepton pair is produced. For example, two hadrons $A$ and $B$ collide and produce the lepton pair $l^+l^-$,

$$A + B \to l^+ + l^- + X. \tag{3.1}$$

At relatively large values of momentum transfer, say greater than a few GeV$^2$, the underlying process is believed to be dominated by antiquark-quark annihilation,

$$\bar{q} + q \to l^+ + l^-. \tag{3.2}$$

The Feynman diagram for this underlying Drell-Yan interaction is given in Fig. 12. Here two hadrons collide and a timelike photon of mass $M_{l^+l^-}$ is formed from the annihilation of a quark in one of the hadrons with an antiquark in the other. The photon then decays by emitting an antilepton-lepton pair. In a typical experiment, the lepton pair is often an antimuon-muon pair as a matter of technical convenience.

In this process the square of the four-momentum transfer is given by the square of the dilepton mass, $M^2_{l^+l^-}$. At leading order, the Drell-Yan cross section can be determined in a straightforward manner to yield

$$\frac{d\sigma}{dx_b dx_t} = \frac{4\pi\alpha_e^2}{9M^2_{l^+l^-}} \sum_i e_i^2 [q_{bi}(x_b, Q^2)\bar{q}_{ti}(x_t, Q^2) + \bar{q}_{bi}(x_b, Q^2) q_{ti}(x_t, Q^2)], \tag{3.3}$$

where $q_{b(t)i}(x_{b(t)i})$ refers to the distribution function of the quark of flavor $i$ in the beam ($b$) or target ($t$) hadron, respectively. It has been shown (Altarelli *et al.*, 1979) that if the distribution functions have the same definition as those in deep inelastic scattering, namely, that if one employs the DIS factorization scheme, then the NLO part is calculable and becomes a multiplicative factor to the expression above, as discussed in Sec. III.B.

### B. QCD and higher-order corrections

The NLO QCD processes that contribute to Drell-Yan scattering are shown in Fig. 13. These processes lead to a modification of the Drell-Yan cross section by introducing the so-called $K$ factor,

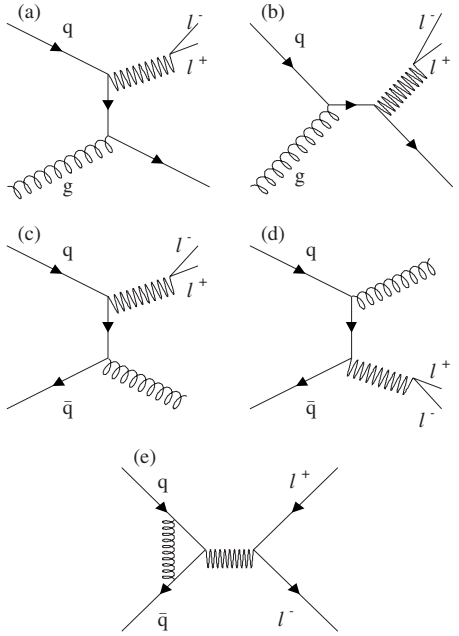


FIG. 13. Feynman graphs of NLO corrections to the Drell-Yan process. Top row, Compton-like scattering in QCD, viz., $gq \to \gamma^*$ (and also $g\bar{q} \to \gamma^*$, not shown explicitly). Middle row, QCD radiative correction, viz., $q\bar{q} \to \gamma^*$. Bottom diagram, QCD vertex correction. Adapted from Reimer, 2007.

$$\frac{d\sigma}{dx_b dx_t}(\mathrm{NLO}) = K_{\mathrm{NLO}} \frac{d\sigma}{dx_b dx_t}(\mathrm{LO}). \tag{3.4}$$

With PDFs defined in the DIS factorization scheme, the $K_{\mathrm{NLO}}$ factor is given by (Altarelli *et al.*, 1979)

$$K_{\mathrm{NLO}} \approx 1 + \frac{\alpha_s}{2\pi}\left(1 + \frac{4}{3}\pi^2\right) \tag{3.5}$$

and assumes a value between 1.5 and 2. Consideration of NNLO as well as NLO diagrams leads to a simple factorization of the cross section and an approximate factor of 2 for $K$. The factorization scheme dependence of the $K$ factor is described by van Neerven and Zijlstra (1992). We note in addition that the $K$ factor depends on kinematics, a fact shown by Wijesooriya *et al.* (2005) to be important at very high $x$ for pionic Drell-Yan studies.

### C. High-$x$ quark distribution functions

The Drell-Yan process presents a valuable method for measuring parton distribution functions in hadrons at very high $x$. For example, it can be used to probe the quark distribution in the beam proton. To see how, consider that if $s$ and $c$ quarks are neglected and the beam-target kinematics are chosen such that $x_F := x_b - x_t$ is large, then for proton+proton collisions Eq. (3.3) can be rewritten (Webb, 2003) as

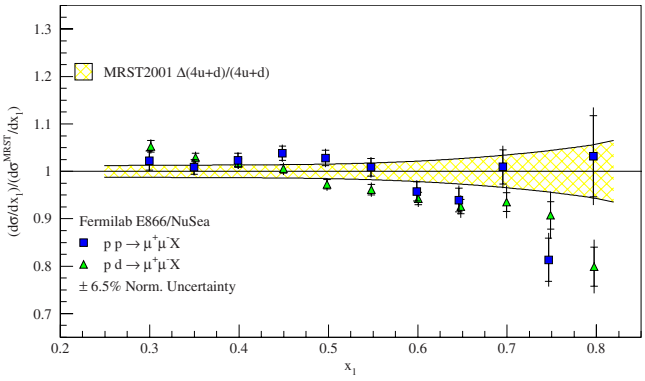


FIG. 14. (Color online) Ratios of the measured Drell-Yan $pp$ (squares) and $pd$ (triangles) cross sections to NLO calculations based on the MRST 2001 PDF fit (Martin *et al.*, 2002a), plotted as a function of beam momentum fraction, here labeled $x_1$, with averaging over the target momentum fraction. The shaded area between the solid lines represents the experimental uncertainty ranges (Martin *et al.*, 2003) on $4u(x)+d(x)$ in the MRST 2001 PDF fit. The data are from the FNAL E866 experiment. Adapted from Webb, 2003 and Webb *et al.*, 2003.

$$\frac{d\sigma}{dx_b dx_t} \approx \frac{4\pi\alpha_e^2 K}{81s}[4u_b(x_b,Q^2)\bar{u}_t(x_t,Q^2) + d_b(x_b,Q^2)\bar{d}_t(x_t,Q^2)] \tag{3.6}$$

because $\bar{q}_b(x_b) \ll q_b(x_b)$ and $q_t(x_t) \ll \bar{q}_t(x_t)$ for large $x_F$. Now suppose that the target is a deuteron with a similar kinematic setup, then Eq. (3.4) can be written (Webb, 2003) as

$$\frac{d\sigma}{dx_b dx_t} \approx \frac{4\pi\alpha_e^2 K}{81s}[4u_b(x_b,Q^2) + d_b(x_b,Q^2)] \times[\bar{u}_t(x_t,Q^2) + \bar{d}_t(x_t,Q^2)], \tag{3.7}$$

where, as usual herein, $q(x)$ means the distribution of flavor-$q$ quarks in the proton, and one has assumed isospin symmetry and neglected nuclear binding effects in the weakly bound deuteron. It is thus apparent that this kinematic setup produces Drell-Yan cross sections that are primarily sensitive to the valence distributions in the proton beam and the antiquark distributions at small $x_t$ in the proton and deuteron targets.

Some results from analysis of the FNAL E866 Drell-Yan data are reproduced in Fig. 14. In this figure the E866 results for $pp$ and $pd$ collisions are divided by the appropriate differential cross section computed using the Martin-Roberts-Stirling-Thorne (MRST) 2001 PDFs (Martin *et al.*, 2002a). Analogous ratios plotted as a function of $x_t$ (Webb *et al.*, 2003) indicate that the MRST 2001 PDFs provide a good description of the $pp$ cross section's $x_t$ dependence on the complete $x_t$ domain and a good description of the $pd$ cross section for $x_t < 0.15$. In this light, consider first the $pp$ data, which hint that the plotted ratio is smaller than one at $x_b \gtrsim 0.6$. Given that the $u$ quark is responsible for roughly 80% of the cross section, this observation can be interpreted as an indication that the MRST 2001 PDFs overestimate the proton's valence $u$-quark distribution. There is a strong signal from the $pd$ cross section that the plotted ratio is less than unity for $x_b \gtrsim 0.5$. Given that this cross section is proportional to $4u(x)+d(x)$ and the greater suppression, one can argue that the PDFs overestimate the proton's valence $d$-quark distribution. A consideration of the impact of this and other recent data on PDF fits is presented by Owens *et al.* (2007).

### D. $\bar{d}/\bar{u}$ ratio and the Gottfried sum rule

One of the most celebrated applications of the Drell-Yan process is the measurement of the flavor dependence of the antiquark sea in the proton. This was first suggested more than 20 years ago (Bickerstaff *et al.*, 1984, 1986; Garvey, 1987; Ellis and Stirling, 1991) at which time it was usually assumed that the light-quark sea was flavor symmetric. Such experiments led subsequently to a demonstration that this is not true; namely, the light-quark sea is flavor asymmetric.

One of the first indications that the light-quark sea might be flavor asymmetric was the observation of the violation of the Gottfried sum rule. The Gottfried sum rule is defined by (Gottfried, 1967)

$$S_G := \int_0^1 \frac{dx}{x}[F_2^p(x) - F_2^n(x)]. \tag{3.8}$$

Using Eqs. (2.25)–(2.27) and assuming isospin invariance, $S_G$ becomes

$$S_G = \frac{1}{3} - \frac{2}{3}\int_0^1 dx[\bar{d}(x) - \bar{u}(x)] =: \frac{1}{3} - \frac{2}{3}\mathcal{I}_{\bar{d}-\bar{u}}. \tag{3.9}$$

If the sea is flavor symmetric, then the Gottfried sum just evaluates to 1/3. Any other value is termed a "violation" of the sum rule.

The earliest hints of a possible violation of the sum rule can be found in data from SLAC (Bodek *et al.*, 1973) and Fermilab (Ito *et al.*, 1981). The NMC experiment at CERN gave the result (Amaudruz *et al.*, 1991; Arneodo *et al.*, 1994, 1997a),

$$S_G = 0.235 \pm 0.026, \tag{3.10}$$

significantly different from 1/3. A more recent reevaluation of the Gottfried sum, using a neural network parametrization of all available data on the nonsinglet structure function $F_2^{NS} = F_2^p - F_2^n$ (Benvenuti *et al.*, 1989, 1990a; Arneodo *et al.*, 1997b), yielded $S_G = 0.244 \pm 0.045 \Rightarrow \mathcal{I}_{\bar{d}-\bar{u}} = 0.134 \mp 0.068$ (Abbate and Forte, 2005), in agreement with the earlier analyses.

It was pointed out long ago that Pauli blocking would give some enhancement of the ratio $\bar{d}/\bar{u}$ (Field and Feynman, 1977). This mechanism might have been sufficient to explain the early SLAC data but Drell-Yan experiments have since given far more information about the magnitude of the effect. Pion cloud models also generate such an effect (Thomas, 1983).

A compilation (Peng, 2003) of values for $\mathcal{I}_{\bar{d}-\bar{u}}$, which characterizes the second term in Eq. (3.9), is given in

TABLE I. Values of $\mathcal{I}_{\bar{d}-\bar{u}}$, which appears in the Gottfried sum rule [Eq. (3.9)], compiled by Peng (2003). The original sources are the following: NMC (DIS) (Amaudruz *et al.*, 1991; Arneodo *et al.*, 1994), HERMES (semi-inclusive DIS) (Ackerstaff *et al.*, 1998), and E866 (Drell-Yan) (Hawker *et al.*, 1998; Peng *et al.*, 1998; Towell *et al.*, 2001). At NNLO, $\mathcal{I}_{\bar{d}-\bar{u}}$ is almost scale independent for $Q^2 \in [1,100]$ GeV$^2$, as shown in Fig. 3 of Abbate and Forte (2005).

| Experiment | $\mathcal{I}_{\bar{d}-\bar{u}} = \int_0^1 dx[\bar{d}(x) - \bar{u}(x)]$ |
|---|---|
| NMC | $0.147 \pm 0.039$ |
| HERMES | $0.16 \pm 0.03$ |
| E866 | $0.118 \pm 0.011$ |

Table I. The relative agreement is reasonable among these determinations. The most accurate result quoted is from the Drell-Yan experiment, FNAL E866, and the comparison is meaningful because $\mathcal{I}_{\bar{d}-\bar{u}}$ is almost scale independent for $Q^2 \in [1,100]$ GeV$^2$.

The power of the Drell-Yan technique can be illustrated by making some simple assumptions. Consider the yield per nucleon from a proton beam incident on a target nucleus of atomic mass $A$, charge $Z$, and neutron number $N$. Assuming that the yield $Y_{pA}$ from the process factorizes into a simple sum of $pp$ and $pn$ interactions, then

$$Y_{pA} \sim (Z\sigma_{pp} + N\sigma_{pn})/A, \tag{3.11}$$

where $\sigma_{pp}$ and $\sigma_{pn}$ are the proton-proton and proton-neutron Drell-Yan cross sections, respectively. If it is further assumed that $pp$ Drell-Yan interactions are dominated by the target proton's $\bar{u}_p$-quark distribution and those for $pn$ are dominated by the neutron's $\bar{u}_n = \bar{d}_p$-quark distribution, then

$$\sigma_{pp}/\sigma_{pn} \approx \bar{u}_p/\bar{d}_p. \tag{3.12}$$

With Eqs. (3.11) and (3.12), it is readily seen that the ratio of yields for proton-nucleus to that of proton-deuteron interactions becomes

$$\frac{Y_{pA}}{Y_{pd}} \approx 1 + \frac{(N-Z)(\bar{u}-\bar{d})}{A(\bar{u}+\bar{d})}, \tag{3.13}$$

where we now return to our convention of omitting the subscript $p$ when distribution functions in the proton are meant. Clearly, if the flavor of the light-quark sea is symmetric; i.e., $\bar{u} = \bar{d}$, then this ratio of yields becomes unity. By considering the ratio of $pp$ to $pd$ Drell-Yan scattering, then the ratio becomes

$$\frac{Y_{pp}}{Y_{pd}} \approx 1 + \frac{\bar{u}-\bar{d}}{\bar{u}+\bar{d}} \tag{3.14}$$

and the ratio $\bar{d}/\bar{u}$ becomes accessible experimentally (Bickerstaff *et al.*, 1984, 1986; Garvey, 1987). Of course, the experiments are analyzed in a more sophisticated manner without these simplifying assumptions.

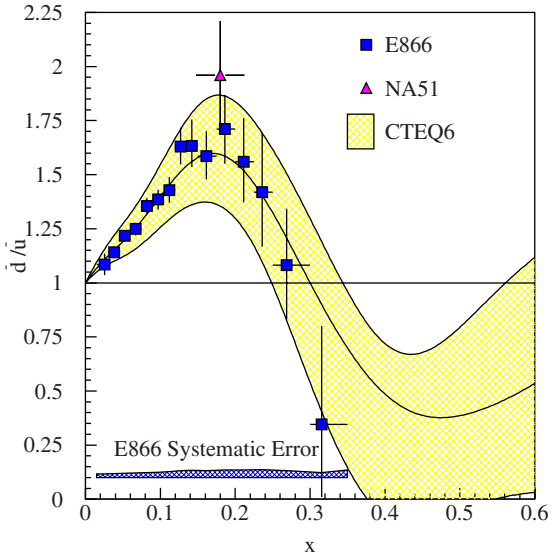


FIG. 15. (Color online) $x$ dependence of $\bar{d}/\bar{u}$. The solid squares represent the measurements from FNAL E866 (Hawker *et al.*, 1998; Towell *et al.*, 2001), while the triangle indicates the CERN NA51 measurement (Baldit *et al.*, 1994). The shaded region indicates the uncertainty from the CTEQ6 evaluation of the world data.

The first Drell-Yan experiment that indicated that the sea is not flavor symmetric was experiment NA51 at CERN (Baldit *et al.*, 1994). This experiment found that $\bar{u}/\bar{d} = 0.51 \pm 0.04 \pm 0.05$ at $x = 0.18$. Experiment E866 made a more comprehensive study by extending the $x$ range of the experiment (Hawker *et al.*, 1998; Towell *et al.*, 2001). These results are shown in Fig. 15.

As argued, e.g., by Steffens and Thomas (1997), Pauli blocking is not sufficient to explain the large effect observed in modern experiments. A number of theoretical explanations have been advanced to explain this effect in the context of models: pion cloud, chiral quark, chiral soliton, and instanton. As real information about this phenomenon is only available for $x \lesssim 0.3$ and our focus is $x \gtrsim 0.4$, we do not discuss it further herein but refer the interested reader to Speth and Thomas (1997), Kumano (1998), and Garvey and Peng (2001), and references therein.

From Eq. (3.13) it should be apparent that the protonic Drell-Yan interaction with nuclei is an especially valuable means to measure antiquark distributions in nuclei. In fact, this method has been used (McGaughey *et al.*, 1992) and proposed (Reimer, 2007) to search for an antiquark or, equivalently, a pion excess in nuclei. It is believed (Friman *et al.*, 1983; Thomas, 1983) that observation of the pion excess in nuclei would provide a stringent confirmation of our understanding of conventional nuclear theory, where the nuclear binding is produced by pion exchange. Thus far, no evidence for a pion or antiquark excess in nuclei has been discovered (McGaughey *et al.*, 1992; Gaskell *et al.*, 2001).

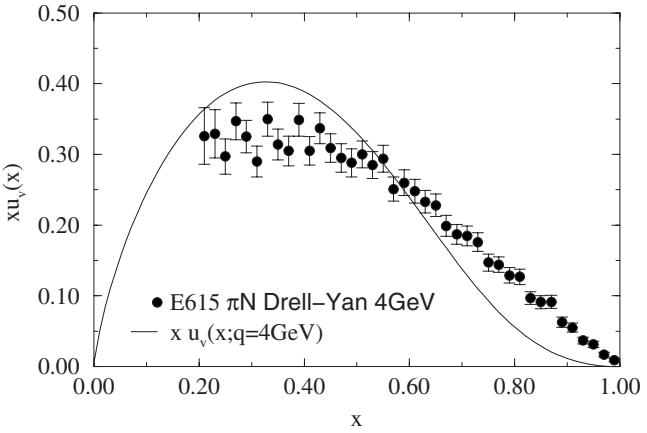


FIG. 16. The $\bar{u}$ quark distribution function in the $\pi^-$. The data are from a LO analysis of the FNAL E615 experiment (Conway *et al.*, 1989). The curve reproduces a Dyson-Schwinger equation calculation (Hecht *et al.*, 2001), described in Sec. VI.B.3, which is consistent with QCD expectations. The discrepancy is disturbing and hitherto unresolved.

### E. The pion structure function

The pion plays a key role in nucleon and nuclear structure. It has been used not only to explain the long-range nucleon-nucleon interaction, forming a basic part of the standard model of nuclear physics (Pieper and Wiringa, 2001; Wiringa, 2006), but also, e.g., to explain the flavor asymmetry observed in the quark sea in the nucleon. However, compared to that of other hadrons, the pion mass is anomalously small. This owes to dynamical chiral-symmetry breaking and any veracious description of the pion must properly account for its dual role as a quark-antiquark bound state and the Nambu-Goldstone boson associated with DCSB (Maris *et al.*, 1998). It is this dichotomy and its consequences that make an experimental and theoretical elucidation of pion properties so essential to understanding the strong interaction.

Experimental knowledge of the parton structure of the pion arises primarily from pionic Drell-Yan scattering from nucleons in heavy nuclei (Badier *et al.*, 1983; Betev *et al.*, 1985; Falciano *et al.*, 1986; Conway, 1987; Guanziroli *et al.*, 1988; Conway *et al.*, 1989; Heinrich *et al.*, 1991). A LO analysis of results from FNAL E615 (Conway *et al.*, 1989) is shown in Fig. 16 but the shape of the empirically extracted pion distribution function at high $x$ is contentious.

Indeed, theoretical descriptions disagree. The QCD parton model (Ezawa, 1974; Farrar and Jackson, 1975), which determines the pion distribution function from the process shown in Fig. 17, indicates that at very high $x$ the distribution should behave as $(1-x)^2$. Perturbative quantum chromodynamics (pQCD) (Brodsky *et al.*, 1995; Ji *et al.*, 2005) and continuum nonperturbative calculations, such as DSE studies (Bloch *et al.*, 1999, 2000; Hecht *et al.*, 1999, 2001; Maris and Roberts, 2003), which express the momentum dependence of the dressed-quark mass function that is evident in Fig. 11, indicate

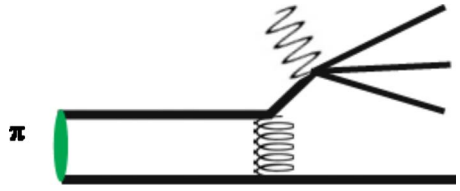


FIG. 17. (Color online) Feynman diagram of the parton picture of DIS on the pion, where one hard gluon exchanges prior to absorption of the highly energetic photon, so that the struck parton carries most of the momentum of the pion. Evaluation of this diagram leads to a $(1-x)^2$ dependence of the pion structure function at very high $x$ (Ezawa, 1974; Farrar and Jackson, 1975).

that the high- $x$ behavior should be $(1-x)^{2+\gamma}$, with an anomalous dimension $\gamma>0$.

In contrast, anti–de Sitter/QCD models using light-front holography (Brodsky and de Teramond, 2008) yield $(1-x)^a$ with $a=0$, as do Nambu–Jona-Lasinio models when a translationally invariant regularization is used (Davidson and Ruiz Arriola, 1995; Bentz *et al.*, 1999; Weigel *et al.*, 1999). On the other hand, the Nambu–Jona-Lasinio (NJL) models yield $a=1$ with a hard cutoff (Shigetani *et al.*, 1993), as do duality arguments (Melnitchouk, 2003). Relativistic constituent-quark models (Frederico and Miller, 1994; Szczepaniak *et al.*, 1994) give $(1-x)^a$ with $0<a<2$ depending on the form of model wave function, and instanton-based models produce $(1-x)^a$ with $1<a<2$ (Dorokhov and Tomio, 2000). A full discussion is presented in Sec. VI and, in particular, in Sec. VI.B.3.

Given the importance of the shape of the pion distribution function at high $x$ as a test of QCD, a NLO analysis of the FNAL E615 data was performed (Wijesooriya *et al.*, 2005). The results of this analysis are compared with those of the original LO analysis in Fig. 18. The solid curve is from the NLO analysis and in comparison with the LO analysis (dashed curve) has some strength shifted from the very high $x$ region to the lower $x$ region, as one should expect from the gluon radiation involved in the NLO processes shown in Fig. 13. Nevertheless, the amount of additional depletion thus uncovered is not yet sufficient to agree with the nonperturbative DSE calculation, given by the black dotted curve in the figure, or the pQCD prediction, which both give a very high-$x$ dependence of the form $(1-x)^{2+\gamma}$, where $\gamma>0$.

This discrepancy remains a crucial mystery for a QCD description of the lightest and subtlest hadron, and a number of explanations have been advanced to explain it. These range from simple experimental resolution-in-$x$ problems (Wijesooriya *et al.*, 2005) to a higher-twist effect that, at fixed $Q^2(1-x)$ with $Q^2\to\infty$, accentuates the structure function associated with longitudinal photon polarization (Berger and Brodsky, 1979) and theoretical factorization issues (Kopeliovich *et al.*, 2005) of Drell-Yan at high $x$. Given this and some questions regarding the Boer-Mulders effect, which are discussed in Sec.

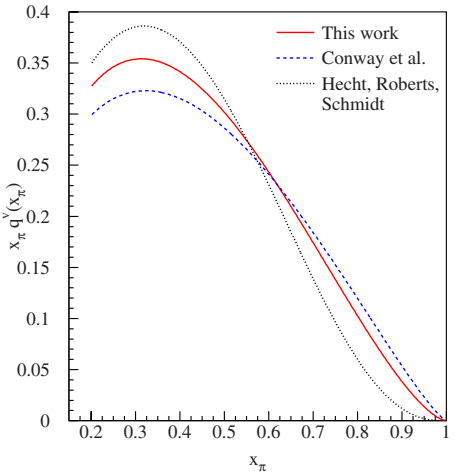


FIG. 18. (Color online) The pion distribution function. Dashed curve, fit from the LO analysis of the FNAL E615 data; solid curve, NLO fit to the E615 data (Wijesooriya *et al.*, 2005); and dotted curve, calculation of the distribution function using a Dyson-Schwinger equation approach (Hecht *et al.*, 2001), which manifestly incorporates the momentum dependence of the dressed-quark mass function that is shown in Fig. 11.

III.F, a new pionic Drell-Yan experiment with better resolution is warranted.

### F. Azimuthal asymmetries

The decay angular distribution of the lepton pair in Drell-Yan interactions provides interesting additional insight into the valence structure of the hadron. In the simplest case, the decay angular distribution for a purely transversely polarized Drell-Yan photon is given by

$$\frac{1}{\sigma}\left(\frac{d\sigma}{d\Omega}\right) = \frac{3}{16\pi}(1+\cos^2\theta), \tag{3.15}$$

where the angles are defined in Fig. 19. For the more general case where the Drell-Yan photon also has a longitudinal component, the decay angular distribution with angles defined in Fig. 19 can be written as (Collins and Soper, 1977)

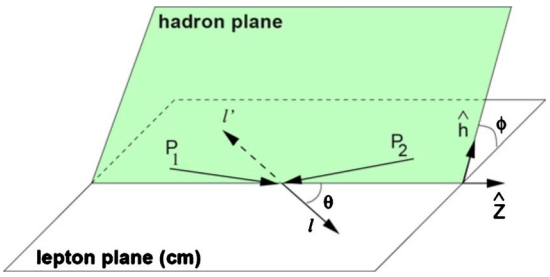


FIG. 19. (Color online) The decay angular distribution of the Drell-Yan process in the Collins-Soper frame.

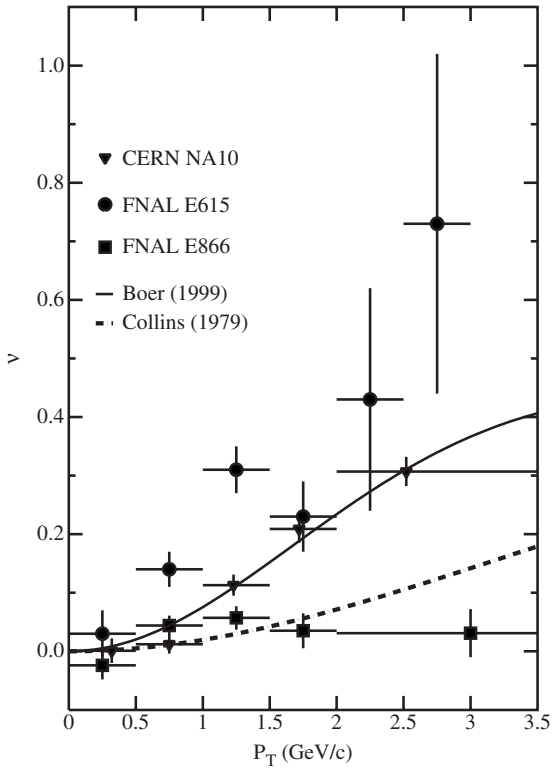


FIG. 20. The $\nu$ or $\cos 2\phi$ component of the Drell-Yan angular distributions obtained with a pion (NA10 and E615) or proton (E866) beam plotted as a function of the transverse momentum of the lepton pair. The dotted curve depicts a pQCD prediction (Collins, 1979) [Eq. (3.17) and associated discussion]. The solid curve, which represents the Boer-Mulders effect (Boer, 1999), was adjusted to describe the NA10 data [Eq. (3.22) and associated discussion].

$$\frac{1}{\sigma}\left(\frac{d\sigma}{d\Omega}\right) = \left[\frac{3}{4\pi}\frac{1}{\lambda+3}\right]\left[1+\lambda\cos^2\theta+\mu\sin 2\theta\cos\phi + \frac{\nu}{2}\sin^2\theta\cos 2\phi\right]. \tag{3.16}$$

This expression is valid in all reference frames. Commonly used reference frames are the $u$ channel, in which the $z$ axis is chosen antiparallel to the target beam direction; Gottfried and Jackson (1964) ($t$ channel)—$z$ axis is chosen parallel to the beam nucleon; and Collins and Soper (1977)—$z$ axis bisects the angle between the $z$ axes in the other two frames. The quantities $\lambda$, $\mu$, and $\nu$ in one frame can readily be related to their forms in another (Conway *et al.*, 1989).

For pionic Drell-Yan interactions, an interesting result is that the parameter $\nu$ in Eq. (3.16) was found (Badier *et al.*, 1983; Betev *et al.*, 1985; Falciano *et al.*, 1986; Conway, 1987; Guanziroli *et al.*, 1988; Conway *et al.*, 1989; Heinrich *et al.*, 1991) to be large and dependent on the transverse momentum of the lepton pair, as shown in Fig. 20.

In the late 1970s, two processes were investigated that could produce an azimuthal asymmetry in Drell-Yan processes. The first was a higher-twist effect (Berger and Brodsky, 1979), while the second was a single gluon ra-

diation process (Collins, 1979). In the former, the high-twist diagrams considered gave rise to a $\cos\phi$ dependence in the Drell-Yan process. This is considered to be important at very high $x$ and relatively low $Q^2$. It is now believed (Boer, 1999) that high-twist effects, such as those explored by Brandenburg *et al.* (1994), cannot simultaneously describe the observed $\mu$ and $\nu$ in the Drell-Yan experiments.

In connection with the latter process, diagrams (c) and (d) in Fig. 13 were considered. The gluon radiation gives rise to the transverse quark momentum. This simple process produces a $\cos 2\phi$ dependence in the angular distribution of the Drell-Yan lepton pair. For example, it was found that (Collins, 1979)

$$\nu = \frac{P_T^2}{Q^2 + \frac{3}{2}P_T^2}, \tag{3.17}$$

where $P_T$ is the total transverse momentum observed in the process. It appears that this simple pQCD process could explain a significant fraction of the large $\nu$ observed in the pionic Drell-Yan experiments, as shown by the dotted curve in Fig. 20.

It is notable that for some time it was believed that if soft gluon resummation is included (Chiappetta and Le Bellac, 1986), then this process predicts very small values of $\nu$ and restores in large part the naive Drell-Yan cross section given by Eq. (3.15). However, it was recently shown (Boer and Vogelsang, 2006) that the gluon resummation in that work was not applied to both the numerator and denominator in the $\cos 2\phi$ component of the cross section. When the gluon resummation is applied correctly, then the effect partially cancels out, leaving the simple pQCD process as dominant. This result is verified by Berger *et al.* (2007). It remains mysterious why the simple pQCD process overestimates $\nu$ for the proton Drell-Yan experiment, shown by the filled squares in Fig. 20.

The mystery increases when the Lam-Tung relation is considered. In the context of the parton model, a relationship exists between two of the decay angular distribution parameters in Eq. (3.16) (Lam and Tung, 1980),

$$1 - \lambda = 2\nu. \tag{3.18}$$

The Lam-Tung relation is a consequence of the spin-$\frac{1}{2}$ nature of quarks. It is an analog of the Callan-Gross relation in DIS [Eq. (2.22)] but is less sensitive to QCD corrections. Nevertheless, a violation of the Lam-Tung relation would suggest a rather significant nonperturbative process. The pionic Drell-Yan data indicate a large violation of the Lam-Tung relation, whereas the proton data do not indicate a violation. A more recent treatment (Berger *et al.*, 2007) demonstrated that a resummed part of the helicity structure functions preserves the Lam-Tung relation as a function of $P_T$ to all orders in $\alpha_s$.

The observed violation of the Lam-Tung relation led to the suggestion of a new nonperturbative process (Brandenburg *et al.*, 1993). Therein, the violation of the Lam-Tung relation was parametrized in terms of $\kappa$

$$1 - \lambda - 2\nu = -4\kappa, \tag{3.19}$$

where an *Ansatz* was proposed for the $P_T$ dependence of $\kappa$. After that work, a new structure function was advocated (Boer and Mulders, 1998), known now as the Boer-Mulders structure function. The quantity $h_1^\perp(x,k_T)$ represents the $T$-odd, chiral-odd structure function that describes quarks with the Bjorken $x$ and intrinsic transverse momentum $k_T$ in one hadron, while $\bar{h}_1^\perp(\bar{x},p_T)$ represents the antiquarks in the second hadron. The $\cos 2\phi$ term arises from a double helicity flip process (Brandenburg *et al.*, 1993) and is generally expressed by the product of two single chiral-odd, time-reveral odd ($T$-odd) helicity flip amplitudes, one for each of the hadrons involved in the process. Then the expression for $\nu$ is proportional to the product of the two $T$-odd structure functions,

$$\nu \propto h_1^\perp(x,k_T) \otimes \bar{h}_1^\perp(\bar{x},p_T) \tag{3.20}$$

[see also Bodwin *et al.* (1989), Boer *et al.* (2003), and Collins and Qiu (2007)]. It is notable that a similar product gives rise to the $\cos 2\phi$ asymmetry in semi-inclusive DIS, where the antiquark distribution is replaced by the Collins fragmentation function. A nonzero Boer-Mulders function would signal a correlation between the transverse spin and the transverse momentum of quarks inside an unpolarized hadron.

We note that in contrast to the parton distribution functions with whose properties we are primarily concerned, the Boer-Mulders and Collins functions are examples of "dynamic" structure functions, which do not have a probabilistic interpretation. As we have indicated here, if nonzero, these functions can lead to a wide range of effects that are not usually apparent in the parton model (Brodsky, 2009).

An *Ansatz* similar to that from Brandenburg *et al.* (1993) was used in later work (Boer, 1999), wherein it was advocated that the parametrization of the Boer-Mulders structure function should assume the same form as that for the Collins fragmentation function (Collins, 1993). This parametrization uses a quark mass scale $M_c$, in a modified fermion propagator,

$$h_1^\perp(x,p_T) = \frac{\alpha_T}{\pi} C_H \frac{M_c M_H}{p_T^2 + M_c^2} \exp(-\alpha_T p_T^2) f(x), \tag{3.21}$$

where $M_H$ is the hadron mass, the parameter $C_H$ is chosen to be unity, $\alpha_T = 1\ \mathrm{GeV}^{-2}$, and $f(x)$ is a parton distribution function. In assuming that the Boer-Mulders structure function and the Collins fragmentation function have exactly the same form, the result for $\nu$ reduces to

$$\nu = 2\kappa = \kappa_1 P_T^2 M_c^2/(P_T^2 + 4M_c^2)^2. \tag{3.22}$$

The solid curve in Fig. 20 results from Eq. (3.22) and gives a reasonable description of the NA10 (pion) data. However, to be consistent with these data, the quark mass-scale parameter must be unnaturally large [~2.3 GeV in Boer (1999)] in comparison with the chiral-symmetry-breaking scale, typically 0.3 GeV, as

evident in Fig. 11. There is no sound basis for this and so, clearly, an improved theoretical description of this structure function is necessary. In order to accept this simple model as the explanation for the large asymmetry in pionic Drell-Yan data, one would also require an understanding of how it may correctly be combined with the apparently large pQCD component identified by Collins (1979).

The Boer-Mulders asymmetry was found (Zhu *et al.*, 2007) to be extremely small in the proton Drell-Yan data of FNAL E866 shown in Fig. 20. This small asymmetry is not understood, but it might be our first indication that the Boer-Mulders structure function is small for sea quarks and the pQCD part is suppressed. The pionic Drell-Yan data involve valence quarks in both the pion and the nucleon target, while these proton Drell-Yan data were taken with kinematics that focused attention mainly on the valence domain in the beam proton and the sea region in the target. An interesting test of this idea would be a Drell-Yan experiment with an antiproton beam and a proton target where the kinematics were chosen such that the annihilating quarks could both be valence quarks. Experiments of this type are planned for the Facility for Antiproton and Ion Research (FAIR) at Darmstadt. New studies of the pionic Drell-Yan data will be initiated in the near future in the Common Muon Proton Apparatus for Structure and Spectroscopy (COMPASS) experiment at CERN.

A new suggestion (Lu *et al.*, 2006, 2007) is to make use of the $\cos 2\phi$ dependence in unpolarized Drell-Yan scattering to measure the flavor dependence of the Boer-Mulders structure function for both quarks and antiquarks. In order to measure the quark (antiquark) distribution, a pion (proton) beam on both hydrogen and deuteron targets is proposed to perform the flavor separation.

The Boer-Mulders asymmetry can also be measured in unpolarized semi-inclusive DIS (SIDIS). The general expression for this cross section (Ahmed and Gehrmann, 1999), written to emphasize the azimuthal dependence, is given by

$$\frac{d\sigma}{dxdQ^2dzdP_T^2d\phi} = \frac{\alpha_e^2\pi}{2Q^6z}(A + B\cos\phi + C\cos 2\phi), \tag{3.23}$$

where $z$ is the fraction of the energy transfer imparted to the produced hadron. In this case, the Boer-Mulders structure function also gives rise to an azimuthal asymmetry $\cos 2\phi$. In fact, the parameter $C$ in Eq. (3.23) has a term that is proportional to the product of the Boer-Mulders structure function and the Collins fragmentation function.

This asymmetry must, however, be disentangled from the Cahn effect (Cahn, 1978, 1989), which also gives rise to $\cos\phi$ and $\cos 2\phi$ dependence. The Cahn effect can arise from the transverse momentum of the quark in a manner similar to that for $R$ given by Eq. (2.52). At relatively large values of $P_T$, say $P_T \geqslant 1$ GeV/$c$, the parameters $B$ and $C$ can also arise from gluon radiation effects (Georgi and Politzer, 1978). The azimuthal asymmetries arising from these effects have been very well established in SIDIS from the CERN EMC experiment (Arneodo *et al.*, 1987), FNAL E665 (Adams *et al.*, 1993), and HERA (Derrick *et al.*, 1996). At Jefferson Laboratory the azimuthal asymmetries were found (Mkrtchyan *et al.*, 2008) to be small and consistent with the Cahn and Boer-Mulders effects at very low values of $P_T$. Future results from HERMES and COMPASS and an upgraded JLab facility (Avakian *et al.*, 2006) will probe a more comprehensive kinematic space, so as to pin down these effects in the valence region and provide new information about the Boer-Mulders asymmetry.

Given the importance of DCSB in QCD, it is also worth mentioning in connection with SIDIS that a leading-twist mechanism within QCD has been identified which can generate a transverse spin asymmetry that directly probes partonic structure associated with chiral-symmetry breaking (Brodsky *et al.*, 2002a). This is the so-called "Sivers asymmetry" (Sivers, 1990, 1991). In hadron-induced hard processes, e.g., Drell-Yan, this asymmetry exists and is reversed in sign and thereby violates naive universality of parton densities (Brodsky *et al.*, 2002b; Collins, 2002). Indeed, in the Drell-Yan process, even when both the beam and target are unpolarized, the annihilating quark and antiquark have a transverse-momentum-dependent transversity. Extensive discussions of distributions associated with quark spin asymmetries are presented by Barone *et al.* (2002) and D'Alesio and Murgia (2008).

We close this section by reiterating that antiproton-proton Drell-Yan interactions, of the type planned for FAIR, are a particularly powerful method for isolating the Boer-Mulders structure function. In this case, the $\cos 2\phi$ term is again given by Eq. (3.20), where now the process involves annihilation of the quarks in the valence region of the proton with the valence antiquarks in the antiproton. Similarly, the Collins fragmentation function can be determined from $e^+e^- \to h\bar{h}$, where $h$ and $\bar{h}$ refer to the outgoing hadron and antihadron. Work (Ogawa *et al.*, 2007) has been performed at Belle in this regard. A recent review (D'Alesio and Murgia, 2008) of azimuthal asymmetries and single spin asymmetries in hard scattering processes covers these topics in more detail.

### G. The kaon distribution functions

The valence structure of the kaon is comprised of a light $u$ or $d$ quark or antiquark and a strange quark or antiquark. If our understanding of meson structure is correct, then the large difference between the current masses of the $s$ quark and the $u$ and $d$ quarks should give rise to some interesting effects in the kaon structure function. For example, owing to its larger mass, the $s$ quark should carry more of the charged kaon's momentum than the $u$ quark. Then the $u_v$ quark distribution in the kaon should be weighted to lower values in $x$ than that in the pion. A Nambu–Jona-Lasinio model calcula-

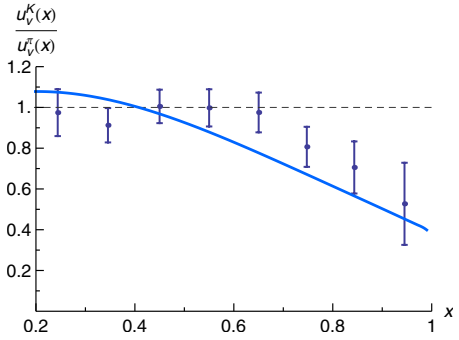


FIG. 21. (Color online) Ratio of kaonic to pionic Drell-Yan cross sections, which is usually interpreted as the ratio of the $\bar{u}$ quark distribution function in the $K^-$ to that in the $\pi^-$. Data from Badier *et al.* (1980), which are obtained from a sample of dimuon events with invariant mass $4.1<M<8.5$ GeV, and solid curve from Shigetani *et al.* (1993), an NJL-model result evolved from $Q_0=0.5$ to 4.5 GeV (see also Fig. 42 and associated discussion).

tion (Shigetani *et al.*, 1993) exhibits this behavior, as shown in Fig. 21. A modern DSE prediction, discussed in Sec. VI.B.3 and shown in Fig. 42, confirms this trend and provides an improved understanding of its origin.

Experimentally, a Drell-Yan measurement (Badier *et al.*, 1980) of the ratio of $K^-$ to $\pi^-$ is consistent with unity over most of the $x$ region, with a suggestion that the ratio is dropping at high $x$. However, the data are not of sufficient quality to test and verify our understanding of pion and kaon structure. To explain, we note that one might claim from the data in Fig. 21 that for $x>0.7$ there is a deviation from $u_v^K(x)=u_v^\pi(x)$ at the $3.8\sigma$ level. However, following Badier *et al.* (1980), which relied on simple models for motivation, we observe that the entire data set is fitted by (see Fig. 42)

$$R_{K^-/\pi^-}(x)=1.1(1-x)^{0.22}, \tag{3.24}$$

with $\chi^2/8=0.45$, and this drops to just $\chi^2/3=0.032$ for data at $x>0.7$. Such values are unreasonably small. Hence, it is essential to make a high accuracy measurement of the structure function of the kaon at $x>0.6$ before the behavior in Fig. 21 can be viewed as anything more than a hint.

## IV. FUTURE EXPERIMENTS AT JLab, EIC, FNAL, CERN, J-PARC, AND FAIR

The 12 GeV upgrade at JLab permits a new opportunity to study structure functions at extremely high $x$. Although the greater energy that will be available at JLab will not be sufficient to avoid target-mass corrections for the nucleon at the higher values of $x$, it does present the prospect of obtaining precise data on the proton and neutron structure functions. It might also represent a new opportunity to study the pion structure function, although assumptions concerning virtual pions would have to be invoked (Wijesooriya *et al.*, 2001). This is because, in determining meson structure functions from

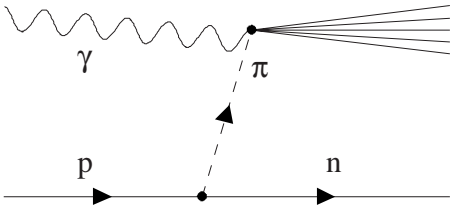


FIG. 22. Feynman diagram for a possible DIS interaction with a virtual pion in the proton.

deep inelastic scattering, it is necessary to consider scattering from virtual mesons, as shown in Fig. 22.

An electron-ion collider (EIC) is aimed at polarization studies of the nucleon structure function at lower values of $x$. Nevertheless, it will permit access to the virtual pion and kaon structure function through measurements of the forward nucleon structure functions (Holt and Reimer, 2001). For example, the scattering process shown in Fig. 22 can be simulated using the RAPGAP Monte Carlo program (Jung, 1995). These processes include DIS from an exchanged pion or pomeron (Holtmann *et al.*, 1996; D'Alesio and Pirner, 2000). A comparison of results from RAPGAP with HERA data shows reasonable agreement for fast outgoing neutrons (Adloff *et al.*, 1999).

The expected accuracy of a possible DIS experiment from a virtual pion was estimated using events in which a "spectator" neutron was identified (Holt and Reimer, 2001). In general, the neutron is scattered less than 50 mrad from the nominal proton beam axis. Events were cut on $Q^2>1$ GeV$^2$. For a 5 GeV electron beam on a 25 GeV proton beam, the expected errors are shown in Fig. 23. A modest luminosity of $10^{32}$ cm$^{-2}$ s$^{-1}$ was assumed for a run lasting $10^6$ s. Such an experiment should be feasible because a similar experiment was conducted at HERA (Chekanov *et al.*, 2007). This experiment gave the interesting result that the shape of the sea distribution for the virtual pion is the same as that for the proton.

The $K^+$ structure function can be measured by considering deep inelastic scattering from the kaon cloud surrounding a proton. The basic Feynman diagram would be the same as in Fig. 22, with the pion replaced by a kaon and the neutron replaced by a $\Lambda$. The probability

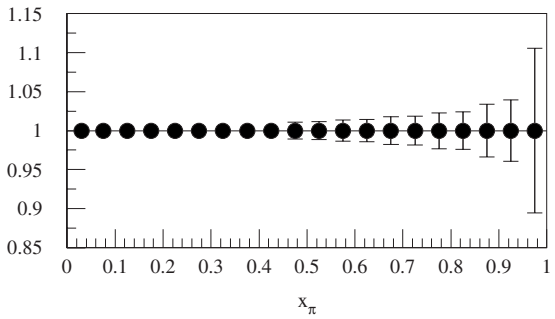


FIG. 23. The expected statistical error for a future experiment to measure the $\pi^+$ structure function at an electron-ion collider. Adapted from Holt and Reimer (2001).

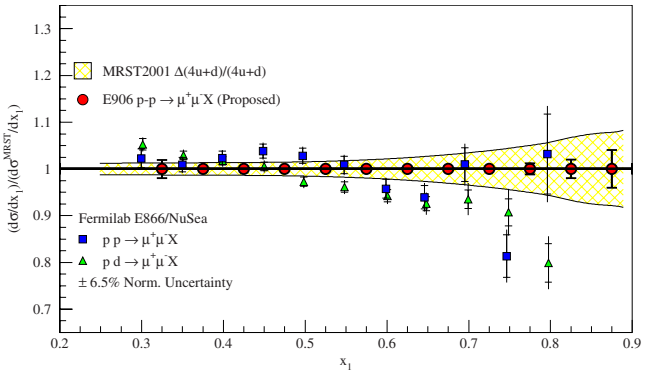


FIG. 24. (Color online) (Color online) The absolute Drell-Yan cross section is proportional to $4u(x)+d(x)$ in the beam proton. The data are from the FNAL E866 experiment. The solid circles are projected data from experiment E906 at FNAL. Adapted from Webb, 2003, Webb *et al.*, 2003, and Reimer *et al.*, 2006.

for scattering from the $K^+$ cloud surrounding the proton should be comparable to that for the $\pi^+$ because the $KN\Lambda$ coupling constant is comparable to that of the $\pi NN$ vertex. In fact, one would only expect about a factor of 2 reduction in the vertex function for the kaon compared to the pion.

The difficulty with this process is in the detection of the $\Lambda$. The $\Lambda$ decays predominantly (64%) to a proton and a $\pi^-$. Thus, a special forward proton spectrometer as well as a forward pion spectrometer would be necessary. This should be feasible since the ZEUS and H1 experiments at HERA have already successfully employed forward proton spectrometers.

It is also likely that an EIC will permit measurements of the $F_2^n/F_2^p$ ratio at extremely high $x$. The technique should be analogous to the method that would be used for the pion and kaon structure function, with a deuteron target beam in this case. The scattered electron would be detected in coincidence with either a forward-going spectator proton or neutron, depending on whether the DIS occurred on a neutron or proton, respectively. In this case, a 5 GeV electron beam on a 25 GeV deuteron beam at a relatively modest luminosity should be sufficient.

Reliable results at extremely high $x$ are also expected from forthcoming Drell-Yan measurements. For example, the solid circles in Fig. 24 indicate the error limits expected for the proposed Drell-Yan experiment at FNAL (E906) (Reimer *et al.*, 2006). The assumptions that went into this simulation were a 120 GeV proton beam from the FNAL main injector and a total integrated luminosity of $5\times10^{33}$ cm$^{-2}$.

Finally, the Japanese Proton Accelerator Research Center (J-PARC) facility, currently under construction at Tokai, Japan, could make polarized Drell-Yan studies possible. Serious consideration is being given to experiments aimed at measuring parton distribution functions in mesons. For example, pionic Drell-Yan experiments are planned for the COMPASS II experiment at CERN. In addition, FAIR, under construction at GSI (Gesellschaft für Schwerionenforschung) in Darmstadt, would make it possible to directly measure the Drell-Yan process from high-$x$ antiquarks in the antiproton annihilating with quarks in the proton.

## V. PRESENT-DAY PARAMETRIZATIONS OF THE PDFs

Excellent reviews of the parametrization of distribution functions exist. In fact, a good starting point for most of the distribution functions can be found at the Durham website.[3] At this website, one can access compilations of data, codes, and grids associated with the following distribution functions: MRST/MSTW—Sec. V.A; CTEQ—Sec. V.B; GRV/GJR—Sec. V.C; and ALEKHIN—Sec. V.D, as well as an online PDF calculator. Here we consider primarily the CTEQ, the MRST, and the GRV parametrizations, emphasizing the differences between them. Another very useful website is that of CTEQ.[4] Here the CTEQ QCD handbook (Sterman *et al.*, 1995) can readily be accessed. The recent status of the MRST/MSTW PDFs can be found in Thorne *et al.* (2009), wherein the MSTW2008 distribution functions (Martin *et al.*, 2009) are recommended.

The primary source of variations between the parametrizations are the different

- Data sets used in the fits.
- Selections of data within the data sets.
- pQCD choices—e.g., evolution order, factorization scheme, renormalization scale, $\alpha_s$.
- Parametric forms for the PDF.
- Theoretical assumptions about the $x\to1$ behavior.

Although there are also distinct treatments of heavy flavors, assumptions of sea flavor asymmetry, and $x\to0$ behavior, these do not have a large impact on the valence region.

Most parametrizations begin with valencelike input, which means that at some infrared scale $Q_0\lesssim1$ GeV all distribution functions are represented as

$$xf(x,Q_0^2)\sim x^{\alpha_f}(1-x)^{\beta_f}, \tag{5.1}$$

where $\alpha_f>0$ and $\beta_f>0$ are fit parameters, so that even those of the sea and glue distributions are nonzero but finite at the infrared boundary. Then, typically, the distribution functions are evolved to higher scales, commensurate with experiment, and the parameters fitted to obtain agreement with data. Some detailed starting distributions for the various parametrizations are given in the identified sections below.

### A. MRST and MSTW

The data sets included in the Martin-Roberts-Stirling-Thorne (MRST 2002) (Martin *et al.*, 2002a, 2003) param-

[3]http://durpdg.dur.ac.uk/HEPDATA/PDF
[4]http://www.phys.psu.edu/~cteq/

TABLE II. For illustration, parameters characterizing the MRST 2001 NLO parton distribution functions at $Q_0^2=1$ GeV$^2$, defined in Eq. (5.2).

| Parton | $A_0$ | $\alpha$ | $\beta$ | $\gamma$ | $\delta$ | $\eta$ |
|---|---|---|---|---|---|---|
| $d_v(x,Q_0^2)$ | 0.040 | 0.27 | 3.88 | 52.73 | 0.5 | 30.65 |
| $u_v(x,Q_0^2)$ | 0.158 | 0.25 | 3.33 | 5.61 | 0.5 | 55.49 |

etrization are the following: H1; ZEUS, both neutral current and charge-current data; BCDMS; SLAC; FNAL E665; CCFR; Drell-Yan data (FNAL E605, E772, and E866); and FNAL CDF and D0 data. The MRST parametrization has a starting scale of $Q_0^2=1$ GeV$^2$ and accepts data down to $Q^2=2$ GeV$^2$. Thus, the SLAC data have an influence at large values of $x$.

A parametrization of the parton distribution functions is given by

$$xf(x,Q_0^2)=A_0x^\alpha(1-x)^\beta(1+\gamma x^\delta+\eta x). \tag{5.2}$$

The parameters at the starting scale are given in Table II for the MRST 2001 parametrization, a NLO fit to the data.

The chief difference between the MRST 2003 set (Martin *et al.*, 2004b) and MRST 2002 is the exclusion of data below $Q^2=10$ GeV$^2$ and below $x=0.005$, whereas, the MRST 2004 analysis (Martin *et al.*, 2004) included new HERA data at moderate values of $x$ and high $Q^2$. The MRST 2004 NNLO set was the first to use the full NNLO splitting functions. The newer MSTW parametrization (Watt *et al.*, 2008; Martin *et al.*, 2009) represents an update of MRST. This update has a number of new theoretical features aimed at the NNLO parametrization, e.g., NNLO corrections to the Drell-Yan data. This parametrization also includes NuTeV and Chorus data, the CDFII data, HERA inclusive jet data, and direct high-$x$ data on the $F_L$ structure function. The most interesting feature of these updates is apparent in the valence region of Fig. 25. The NLO MSTW evaluation gives a much smaller $xd(x)$ distribution at very high $x$ than the previous work. Nevertheless, it is apparent in the differences between the parametrizations at large $x$ that the $d$ quark distribution is poorly constrained above $x=0.6$. This further emphasizes the need for new data in the very high $x$ region.

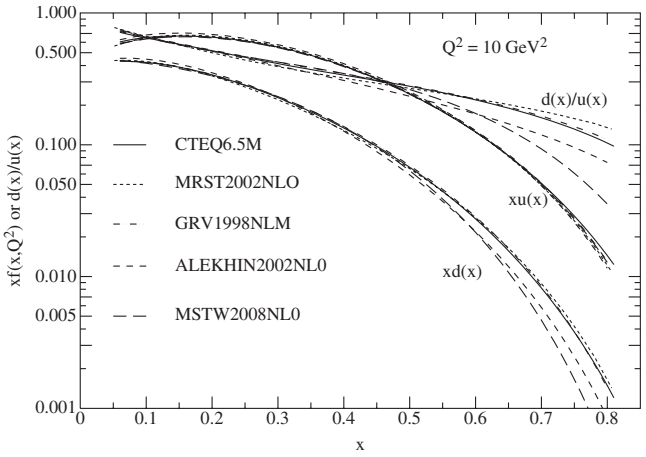


FIG. 25. Five parton distribution evaluations at NLO in the $\overline{\text{MS}}$ factorization scheme at $Q^2=10$ GeV$^2$ in the valence region. There are three families of curves: the $d(x)/u(x)$ ratios, the $xu(x)$ distributions, and the $xd(x)$ distributions.

### B. CTEQ parametrization

The most recent parametrizations from the Coordinated Theoretical-Experimental Project on QCD (CTEQ) is the CTEQ6 series (Pumplin *et al.*, 2001, 2002, 2007; Stump *et al.*, 2003; Lai *et al.*, 2007; Nadolsky *et al.*, 2008). The CTEQ Collaboration omits data for $Q^2\leqslant 4$ GeV$^2$. In particular, CTEQ6 omits SLAC data as well as some high-$Q^2$ H1 data. CTEQ uses 10% systematic errors in quadrature with the statistical errors for the Drell-Yan data in comparison with 5% systematic errors assumed by MRST 2002. CTEQ uses a starting scale of $Q_0^2=1.69$ GeV$^2$.

The functional form of the CTEQ6 parametrization of the distribution functions is given by

$$xf(x,Q_0^2)=A_0x^{A_1}(1-x)^{A_2}e^{A_3x}(1+e^{A_4}x)^{A_5}. \tag{5.3}$$

The parameters at the starting scale are given in Table III for the CTEQ6M parametrization, a NLO fit to the data.

### C. GRV/GJR distribution functions

The Gluck-Reya-Vogt (GRV) parton distribution functions were developed in the 1990s (Glück *et al.*, 1992a, 1993, 1995, 1998). They are dynamical distributions, which are generated radiatively from valencelike inputs at a low resolution scale. The latest of this series makes use of the 1994–1995 HERA data for $Q^2\geqslant 2$ GeV$^2$ as well as the SLAC, BCDMS, NMC, and E665 data with $Q^2\geqslant 4$ GeV$^2$ and the simply extracted ratios $F_2^n/F_2^p$ from the NMC, BCDMS, and E665 experiments. This analysis takes into account the Drell-Yan data and the $u_v/d_v$ ratios extracted from the CERN CDHSW and WA21 neutrino data.

The GRV parton distribution functions are parametrized as

$$xf(x,Q_0^2)=A_0x^\alpha(1-x)^\beta(1+\delta\sqrt{x}+\eta x). \tag{5.4}$$

In Table IV we report the parameters at the starting scale for the GRV98 LO parametrization, a leading-order fit to the data, and the parameters at the starting scale for the GRV98 NLO parametrization, a next-to-

TABLE III. Parameters at $Q_0^2=1.69$ GeV$^2$ for the CTEQ6M parton distribution functions, defined in Eq. (5.3).

| Parton | $A_0$ | $A_1$ | $A_2$ | $A_3$ | $A_4$ | $A_5$ |
|---|---|---|---|---|---|---|
| $d_v(x,Q_0^2)$ | 1.4473 | 0.6160 | 4.9670 | −0.8408 | 0.4031 | 3.0000 |
| $u_v(x,Q_0^2)$ | 1.7199 | 0.5526 | 2.9009 | −2.3502 | 1.6123 | 1.5917 |
| $g(x,Q_0^2)$ | 30.4571 | 0.5100 | 2.3823 | 4.3945 | 2.3550 | −3.0000 |
| $(\bar{u}+\bar{d})(x,Q_0^2)$ | 0.0616 | −0.2990 | 7.7170 | −0.5283 | 4.7539 | 0.6137 |
| $s(x,Q_0^2)=\bar{s}(x,Q_0^2)$ | 0.0123 | −0.2990 | 7.7170 | −0.5283 | 4.7539 | 0.6137 |

leading-order fit to the data in the $\overline{\text{MS}}$ scheme. It is interesting that the value of $\beta$ for $u_v$ and $d_v$ systematically increases in going from LO to NLO. This is expected and consistent with the effect of gluon radiation reducing the hardness of the parton distribution.

These distributions are characterized by a relatively low starting scale for evolution: LO, $Q_0=0.5$ GeV, and NLO, $Q_0=0.63$ GeV. One might question whether therefrom it is valid to employ pQCD evolution equations. In this connection, we observe that it is the combination $\alpha(Q_0)/[2\pi]$ which appears in the evolution equations. At leading order, $\alpha(Q_0=0.5\ \text{GeV})/[2\pi] \approx 0.17$ and hence $\{\alpha(Q_0)/[2\pi]\}^2<0.03$. Therefore both the procedure and a physical interpretation of the distributions at this scale might be meaningful if higher-twist and essentially nonperturbative effects are not too important. At present one cannot answer whether the latter is true. Notwithstanding this, the procedure alone can be useful as a fitting and correlating tool.

A more recent analysis (Glück *et al.*, 2008) extends the GRV98 analysis. The distribution functions are generated from a radiated valencelike positive input with $Q_0 \leqslant 1$ GeV, where valencelike refers to Eq. (5.4). With these constraints, the predictions for $F_L$ remain positive throughout the accessible kinematic region. Constraining the starting distribution to be valencelike leads to smaller quoted uncertainties in the very low-$x$ region than those analyses without this constraint.

### D. Distributions in relief

A comparison of five modern parton distributions on the valence domain at $Q^2=10$ GeV$^2$ is shown in Fig. 25. All five evaluations are in remarkably good agreement for the $xu(x)$ distribution. Despite the large uncertainty in the $d/u$ ratio discussed in Sec. II.G, three of the distributions (MRST 2002 NLO, CTEQ6.5M, and GRV98) are in remarkably good agreement for the $d/u$ ratio. The newest evaluations, MSTW 2008 (Martin *et al.*, 2009), differ here largely because of a more flexible parametrization of the $d$ quark distribution, and the inclusion of new data from FNAL on the lepton charge asymmetry from $W$ decays and the $Z$ rapidity distribution.

The ALEKHIN 2002 parametrization (Alekhin, 2003) is a somewhat different case. This parametrization is based on the SLAC, BCDMS, NMC, and HERA data existing at the time. The cuts on the data included $2.5<Q^2<300$ GeV$^2$ and $x<0.75$. The model function was parametrized for $Q_0^2=9$ GeV$^2$, much higher than most other forms. The cuts in $Q^2$ and $x$ give this parametrization more emphasis on the high-$x$ SLAC data than CTEQ or MRST. This could possibly explain the differences in the high-$x$ $d$-quark distribution. Later

TABLE IV. Upper five rows—Parameters for the GRV98 LO parton distribution functions at $Q_0^2=0.26$ GeV$^2$, defined in Eq. (5.4), where $\Delta\equiv\bar{d}-\bar{u}$ and $xs(x,Q_0^2)=x\bar{s}(x,Q_0^2)$. Lower five rows—Parameters for the GRV98 NLO parton distribution functions at $Q_0^2=0.40$ GeV$^2$.

| Parton | $A_0$ | $\alpha$ | $\beta$ | $\delta$ | $\eta$ |
|---|---|---|---|---|---|
| $d_v(x,Q_0^2)$ | 0.761 | 1.48 | 3.62 | −1.8 | 9.5 |
| $u_v(x,Q_0^2)$ | 1.239 | 0.48 | 2.72 | −1.8 | 9.5 |
| $x\Delta(x,Q_0^2)$ | 0.23 | 0.48 | 11.3 | −12.0 | 50.9 |
| $x(\bar{u}+\bar{d})(x,Q_0^2)$ | 1.52 | 0.15 | 9.1 | −3.6 | 7.8 |
| $xg(x,Q_0^2)$ | 17.47 | 1.6 | 3.8 | — | — |
| $d_v(x,Q_0^2)$ | 0.394 | 1.43 | 4.09 | — | 18.2 |
| $u_v(x,Q_0^2)$ | 0.632 | 0.43 | 3.09 | — | 18.2 |
| $x\Delta(x,Q_0^2)$ | 0.20 | 0.43 | 12.4 | −13.3 | 60.0 |
| $x(\bar{u}+\bar{d})(x,Q_0^2)$ | 1.24 | 0.20 | 8.5 | −2.3 | 5.7 |
| $xg(x,Q_0^2)$ | 20.80 | 1.6 | 4.1 | — | — |

ALEKHIN parametrizations include Drell-Yan data (Alekhin *et al.*, 2006) as well as even lower momentum-transfer data (Alekhin *et al.*, 2008). However, the differences between these updated PDFs and the ALEKHIN 2002 distributions do not exceed one standard deviation.

Notwithstanding differences between the groups' PDFs, it is evident from the figure and the tables that all fits are consistent with

$$d(x)/u(x) \overset{x\sim 1}{\sim} 0. \tag{5.5}$$

However, this empirical statement has large uncertainties, some of which are discussed by Owens *et al.* (2007). It reflects primarily upon the fact that $u$ quarks dominate proton cross sections and hence it is difficult to tightly constrain the proton's $d$-quark distribution.

MRS (Sutton *et al.*, 1992) and GRV (Glück *et al.*, 1992b, 1999) also produced analyses of the parton distribution function in the pion. The pion distribution functions were extracted from Drell-Yan and prompt photon data. As discussed in Sec. III.E, a more recent NLO reanalysis of the FNAL E615 pionic Drell-Yan data (Wijesooriya *et al.*, 2005) indicated that there was more curvature in the pion distribution at very large values of $x$ than given by either of these fits. As shown in Fig. 41, this result strengthens the disagreement between the data and contact-interaction models but does not produce as much curvature as expected from either pQCD (Ezawa, 1974; Farrar and Jackson, 1975) or nonperturbative DSE calculations (Hecht *et al.*, 2001). This discrepancy persists to this day and is one of the outstanding problems in understanding the application of QCD to real-world data. We therefore discuss it at length in Sec. VI.

### E. Neural network parton distribution functions

In recent years another approach to the parametrization of parton distribution functions has emerged, namely, the neural network method (NNPDF) (Ball *et al.*, 2009). In this approach, instead of using predetermined functional forms to parametrize the PDFs, such as Eq. (5.2), which might introduce unanticipated prejudices, flexible neural networks are used as unbiased interpolants. In addition, a Monte Carlo method for error propagation is used to avoid Gaussian assumptions. This method, which aims to avoid bias, could give significant differences on the large-$x$ domain, of interest herein, whereupon mysteries have become apparent. In particular, the determination of pion NNPDFs would be welcome. The first global parton distribution determination based on neural networks (NNPDF 2.0) and a description of the approach are given by Ball *et al.* (2010). This latest work includes both DIS and hadron data, and uses NLO QCD consistently throughout.

## VI. THEORETICAL INTERPRETATION OF THE DISTRIBUTION FUNCTIONS

### A. Evolving insight from models

We noted at the outset that while parton distribution functions are basic elements of factorized perturbative QCD, they are essentially nonperturbative; viz., they can only be calculated using a nonperturbative framework. Their calculation is a problem that has been with us for more than 30 years [e.g., Politzer (1974)]. The interim has seen the proposal and elucidation of numerous models for the phenomena of low-energy QCD, many of which have been employed to estimate the valence-quark distribution functions.

#### 1. MIT bag model

Soon after it had been proposed, the MIT bag model (Chodos, Jaffe, Johnson, and Thorn, 1974; Chodos, Jaffe, Johnson, Thorn, and Weisskopf, 1974) was being used to calculate structure functions (Jaffe, 1975). It is still being used to make estimates, now of generalized parton distribution functions [Pasquini *et al.* (2005) and Scopetta (2005)].

The basic difficulties with this approach were noted at the outset. The bag is treated as a static cavity, namely, a spherical chamber with fixed radius $R_0$. Among other things, this places a lower bound on the domain of $x$ for which distribution functions can be calculated, i.e., $x \gtrsim 1/(2MR_0) \sim 0.1$, where $M$ is the nucleon's mass. Moreover, the bag boundary cannot realistically be static. It should respond to the action of currents on the quarks it contains and that would affect the form of the distribution functions. The target is treated as being at rest but the framework is not Poincaré covariant and hence momentum is not conserved through the intermediate Compton scattering state. This entails that the calculated structure functions do not possess the correct support; e.g., they do not vanish for $x>1$. In addition, in an independent-particle picture arising from a spin-flavor symmetric Hamiltonian the ratio in Eq. (2.45) is particularly simple, viz.,

$$\forall x: \frac{F_2^n(x)}{F_2^p(x)} = \frac{2}{3} \quad \{\mathrm{SU}(6)\ \text{symmetric}\}, \tag{6.1}$$

because the pointwise behavior of the distributions is the same for both $u$ and $d$ quarks. This prediction conflicts with data (Fig. 10). Moreover, while the momentum sum rule is satisfied, which is achieved with all the target's momentum being carried by the quarks, experimentally, the quarks' momentum fraction should only be $\sim 50\%$, i.e., $\langle x \rangle \sim \frac{1}{2}$.

From a modern perspective, the last of these outcomes is not seen as a critical impediment. The distribution functions are known to be scale dependent in QCD and, in principle, once determined at a particular scale, QCD predicts their pointwise form at any and all other scales. It should nonetheless be noted that, owing to the

role played by gluons in binding the compound hadron, there is no scale at which the momentum fraction carried by valence quarks can be equal to 1.

In practice, one views a model computation as providing the distribution functions at some infrared resolving scale $Q_0$. The evolution equations, discussed in Sec. II.D, are then used to obtain their form at some other scale, typically $Q=2$ GeV. In applying a model, $Q_0$ is fixed *a posteriori* by requiring that the evolved distribution functions yield $\langle x\rangle \approx 0.4$, which is an empirical feature of the PDFs described in Sec. V, as evident, e.g., in Fig. 2 of Glück *et al.* (1992a). In contrast to modeling, however, in a truly nonperturbative solution of QCD the scale $Q_0$ would be known *a priori*.

The bag model does yield some insight and positive results, on the other hand. For example, as treated, Bjorken scaling is recovered for $W_1$ and $(\nu/M^2)W_2$ in Eq. (2.13). Moreover, in the Bjorken limit [Eq. (2.9)], $W_L$ vanishes and $\nu W_L$ scales and is calculable. Thus one preserves the Callan-Gross relation. The structure functions obey quantum number sum rules, such as the Adler relation,

$$\int_0^1 dx \frac{1}{x}[F_2^{\nu p}(x) - F_2^{\bar{\nu} p}(x)] = 2, \tag{6.2}$$

where $F_2^{\nu p,\bar{\nu} p}$ are neutrino scattering analogs of the usual $F_2^p$. In addition, $F_1$ and $F_2/x$ are peaked at $x_0=1/N$, where $N$ is the number of quanta in the target: if three valence quarks are all the model possesses, then these functions peak at $x_0=1/3$. The width of the peak is related to the model's confinement radius.

Primary among the problems identified above, in part because it also affects other models, is the absence of translational invariance and hence momentum conservation. In the usual mean-field approach the quarks move independently within a spherical cavity of fixed radius and definite location. The Hamiltonian associated with this problem is not translationally invariant. From this arises the so-called center-of-mass problem: particles moving independently within the volume cannot constitute an eigenstate of the total momentum, in particular, they cannot properly describe a hadron at rest.[5]

In general, the removal of spurious center-of-mass motion from the hadron's wave function is not a well-defined problem and has no unique solution (Lipkin, 1958). The illness is typical of shell-like models. A number of prescriptions exist, which serve to mitigate the undesirable effects that this spurious motion has on physical observables. Among these, the Peierls-Yoccoz projection (Peierls and Yoccoz, 1957) has been most widely discussed. It projects exact eigenstates of the center-of-mass momentum by forming a linear superposition of at-rest bag states at different locations. Artifacts remain, however, e.g., some expectation values exhibit unexpected momentum dependence. A remedy may be found in the Peierls-Thouless projection (Peierls and Thouless, 1962) but that is difficult to implement. Note that the Peierls-Yoccoz projection is a nonrelativistic prescription and hence cannot properly account for the boost experienced by the intermediate state in the forward Compton scattering process. This means that for an initial state at rest, the procedure can only be internally consistent for $|\vec{k}| < M_{qq}$, in the notation of Fig. 26, which corresponds to $x \lesssim 0.6$.

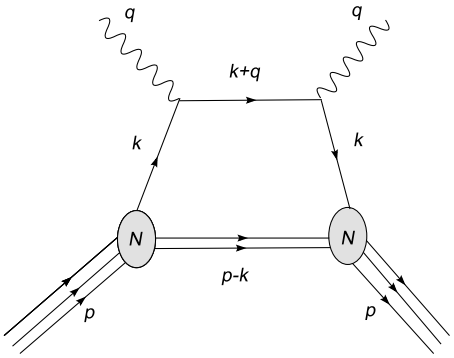


FIG. 26. "Handbag diagram" contribution to the virtual-photon-nucleon forward Compton scattering amplitude: $\gamma^*(q)N(p) \to \gamma^*(q)N(p)$. The intermediate state (or nucleon remnant in the DIS process) here is assumed to be a scalar or axial-vector diquark, with masses $M_s$ and $M_v$, respectively.

In an infrequently used alternative (Szymacha, 1984; Jasiak, 1997), one may augment the independent-particle (bag-model) Hamiltonian for the composite state by a fictitious attractive potential, which depends on the center-of-mass coordinate, viz.,

$$H = \frac{P^2}{2M} + H_{\rm BM}$$
$$\to \tilde{H} = \frac{P^2}{2M} + V(R) + H_{\rm BM} = H_{\rm CM} + H_{\rm BM}, \tag{6.3}$$

where $H_{\rm BM}$ is a bag-model Hamiltonian. With the potential tuned such that the spectra of $H_{\rm CM}$ and $H_{\rm BM}$ are approximately the same, then one has an equivalence between the nonlocal composite and a translationally invariant pointlike state. Unlike the Peierls-Yoccoz prescription, this method ensures that the valence-quark distribution functions are correctly normalized (Jasiak, 1997); namely, Eqs. (2.27) are satisfied independent of model details.

With a prescription for removing the spurious center-of-mass motion one can be confident that computed valence-quark distribution functions will possess the correct support, i.e., are nonzero only for $0 \leqslant x < 1$. Typical of such calculations are Steffens and Thomas (1994, 1995), which employ the Peierls-Yoccoz projection following Signal and Thomas (1988) and achieve a fair degree of phenomenological success.

In this connection it is notable that having overcome the problem of incorrect support, one can ask for more; e.g., models of the nucleon can be classified and perhaps

[5]A perhaps even greater difficulty is that in an interacting relativistic theory, which the model is aimed to be, Lorentz boosts change the particle number of a given state.

retained or discarded according to whether or not they comply with the perturbative QCD constraint on the valence-quark distribution function (Brodsky *et al.*, 1995; Avakian *et al.*, 2007),

$$q_v(x) \overset{x\sim 1}{\sim} (1-x)^{2n-1+2\delta\lambda}, \tag{6.4}$$

where $n$ is the minimal number of fermion spectator lines in the quark-level scattering process, and $\delta\lambda = |\lambda^q - \lambda^H|$ is the difference in helicities between the struck parton and the hadron; e.g., $\delta\lambda$ is 0 for a struck quark with helicity parallel to that of the $J=\frac{1}{2}$ hadron and 1 for a struck quark with helicity antiparallel. These counting rules are first-principles predictions of QCD, in which the power increases logarithmically under evolution to a higher scale, and they satisfy Gribov-Lipatov reciprocity (Gribov and Lipatov, 1971, 1972); namely, that at leading order spacelike and timelike parton cascades are identical so that structure and fragmentation functions are algebraically related.

For the proton, Eq. (6.4) means

$$q_v^p(x) \overset{x\sim 1}{\sim} (1-x)^{\beta}, \quad \beta = 3 \tag{6.5}$$

for both $u$ and $d$ quarks unless nonperturbative effects somehow preclude either the valence $u$ quarks or $d$ quark from sharing in the proton's helicity on a domain that includes the neighborhood of $x=1$. Subsequently, in connection with Eq. (6.98), we describe a quantitative bound on the $x$ domain within which Eq. (6.5) should be observable.

A naive consideration of the isospin and helicity structure of the proton's light-front quark wave function at $x \simeq 1$ leads one to expect that $d$ quarks are five times less likely than $u$ quarks to possess the same helicity as the proton they comprise. This leads to the prediction (Farrar and Jackson, 1975)

$$\frac{d(x)}{u(x)} \overset{x\to 1}{=} \frac{1}{5}. \tag{6.6}$$

However, as we saw in Sec. V, while fitted PDFs produce $\beta_u \approx 3$, they yield $4 \lesssim \beta_d \lesssim 5$, the feature which leads to Eq. (5.5). This may be understood as an indication that the probability for a $d$ quark at $x=1$ to possess the same helicity as the proton is actually much less than the naive expectation. Given the large uncertainties in the fits, however, it does not necessarily require that $\beta_d > \beta_u$. A reliable nonperturbative approach to nucleon structure is required in order to determine the relative strength of the $\beta_d=3$ and 5 components in the proton.

As explained by Brodsky *et al.* (1995) and we subsequently elucidate,[6] Eq. (6.4) is applicable at the infrared resolving scale $Q_0$. The exponent is a lower bound and increases under QCD evolution to a larger momentum scale. This is described in Sec. II.D. Equation (6.5) can therefore serve as a stringent discriminator. It is satisfied

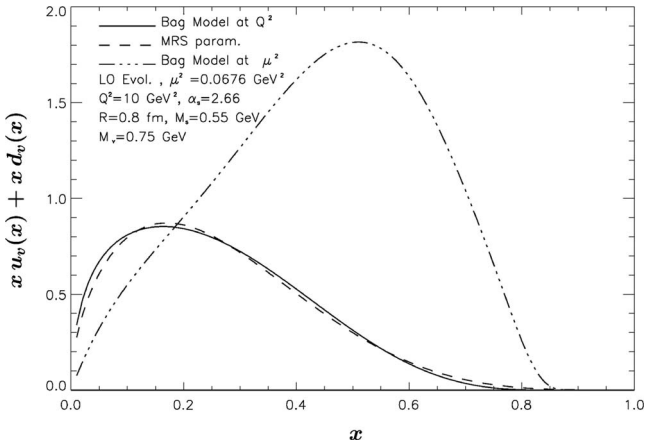


FIG. 27. A bag-model result for the $x$-weighted sum of valence-quark distributions in the proton. The model parameters are the following: bag radius $R=0.8$ fm; scalar and axial-vector diquark masses, $M_s=0.55$ GeV and $M_v=0.75$ GeV; and infrared resolving scale $Q_0=\mu=0.26$ GeV. Adapted from Steffens and Thomas, 1995.

with bag-model valence-quark wave functions that fall as $1/|\vec{p}|^2$ for large momentum $|\vec{p}|$ (Margolis *et al.*, 1993), whereas the often used independent-particle wave functions with Gaussian decay fail this test [see Eq. (6.11) and associated discussion].

The computation described by Steffens and Thomas (1995) is formulated with four parameters: a bag radius $R$; the masses of the two valence-diquark spectator states in an impulse approximation to the forward Compton scattering amplitude—scalar, $M_s$, and axial-vector, $M_v$ (see Fig. 26); and the infrared resolving scale at which the computation is supposed to be valid, denoted by $Q_0$ above and $\mu$ therein.[7] Naturally, the calculated valence-quark distribution functions depend on these parameters, which may therefore be fixed by applying leading- or next-to-leading-order evolution to the calculated distributions and requiring a good least-squares fit to the MRS parametrization (Martin *et al.*, 1993) of experimental data at $Q^2=10$ GeV$^2$.

At leading order (Fig. 4), the values $R=0.8$ fm, $M_s=0.55$ GeV, $M_v=0.75$ GeV, and $Q_0=\mu=0.26$ GeV yield the results shown in Fig. 27. The diquark masses are roughly 20% lower than estimates derived from QCD's Dyson-Schwinger equations [Eq. (B1)] (Burden *et al.*, 1997; Maris, 2002). Of more material concern is the small value of $Q_0$, in which case the evolution equations involve the coupling $\alpha(Q_0)/[2\pi]=0.4$ (cf. the values considered reasonable in Sec. V.C).

Since this value of $\alpha(Q_0)$ might be considered too large for the fitting-by-evolution procedure to be valid, Steffens and Thomas (1995) repeated the analysis using the next-to-leading-order evolution equations [Eqs.

[6] A quantitative definition of $Q_0$ is presented in Sec. VI.B.3 and specifically in connection with Eq. (6.83).

[7] A comparison between bag-model results and those of other nontopological soliton models is presented by Bate and Signal (1992). Marked quantitative differences can be found in spin-dependent structure functions.

(2.30)–(2.35)] and in this way obtained $R=0.8$ fm, $M_s=0.7$ GeV, $M_v=0.9$ GeV, and $Q_0=\mu=0.34$ GeV. While the value of $Q_0$ is still small, these diquark masses agree with contemporary estimates and now $\alpha(Q_0)/[2\pi]=0.1$. In comparison with Fig. 27, the NLO prescription cannot significantly change the evolved distribution because that is the quantity fitted. On the other hand, there is a significant difference in the valence-quark distribution at the new infrared scale $Q_0=0.34$ GeV: $x[u_v(x;Q_0)+d_v(x;Q_0)]$ peaks at $x=0.4$ (reduced by 30%), has a maximum value of 1.4 (reduced by 20%), and material support only for $x<0.8$ (domain contracted by 10%). These differences owe primarily to the accelerated production of sea quarks through valence-quark depletion in NLO evolution as compared with the rate of this effect in LO evolution. The change in diquark masses serves to fine tune the initial condition: more massive intermediate states produce a $Q_0$ distribution that peaks at smaller $x$, a feature required to fit the data parametrization when evolving from a larger value of $Q_0$.

As one might have expected, the computation reviewed here does not ensure correct normalization of the valence-quark distribution functions: roughly 20% of the strength is missing. They argue plausibly that this defect owes to modeling and parametrization of the intermediate state as opposed to its internally consistent calculation. They assert that the missing strength is probably localized in the sea-quark region, viz., $x<0.3$, and one might therefore be justified in supposing that this weakness affects only modestly the pointwise behavior of the valence-quark distribution on the domain of interest.

Upon the domain within which perturbative QCD is unarguably valid the parametrizations of valence-quark distribution functions are infinite at $x=0$ while $xq_v(x;Q^2_{\rm pert})=0$. The divergence is associated with parton splitting (see Fig. 4) and may be understood intuitively by observing that infinitely many $x\sim 0$ partons are required to carry any fixed fraction of the proton's momentum. On the other hand, by assumption, model calculations, such as that just described, generate $q_v(x;Q_0^2)<\infty$ because only a fixed number of valence quarks (three for the proton) interact with the photon probe, and the valence quark's structure is not resolved; i.e., there is no mechanism for them to fragment. While the property $q_v(x;Q_0^2)<\infty$ is not incompatible with the evolution equations, it does disagree with data parametrizations (see, e.g., Sec. V).

#### 2. Constituent quark models

In the minds of many, potential models framed in terms of constituent-quark degrees of freedom are exemplified by Isgur and Karl (1978). The application of such models to the spectra and strong and electromagnetic couplings of baryons is reviewed by Capstick and Roberts (2000). It is noteworthy that as long as the potential between $N$ quarks depends only on the relative coordinates within two-quark subsystems, $\{r_{i,j}=r_i-r_j|i,j=1,\ldots,N\}$, and/or on the conjugate relative momenta, one can exactly eliminate the spurious center-of-mass motion in nonrelativistic constituent-quark models (CQMs) and hence they can be used effectively as a tool to study the spectrum. However, one should bear in mind that the absence of Poincaré covariance is a problem when studying scattering, in general, and deep inelastic scattering, in particular.

These models are defined by a Hamiltonian, which is typically diagonalized in a harmonic-oscillator basis. The Hamiltonian contains a hyperfine interaction, whose structure is modeled according to a practitioner's taste. In many cases it is based on notions of one-gluon exchange [Isgur and Karl (1978)], in others, on pseudoscalar-meson exchange [Glozman *et al.* (1998)]. Here it is only important that the Hamiltonian eigenvectors do not exhibit SU(6) spin-flavor symmetry and hence results other than Eq. (6.1) are possible.

Relevant here is a relationship that appears empirically to hold between the anomalous magnetic moments of the neutron and proton $\kappa_{n,p}$ and the valence-quark distribution functions [see Sec. 4.2.3 of Goeke *et al.* (2001)], viz.,

$$\frac{\kappa_p}{\kappa_n}=-\frac{1}{2}\left[\frac{4\langle x\rangle_{d_v}^{Q_0}+\langle x\rangle_{u_v}^{Q_0}}{\langle x\rangle_{d_v}^{Q_0}+\langle x\rangle_{u_v}^{Q_0}}\right], \tag{6.7}$$

where

$$\langle x\rangle_{q_v}^{Q_0}=\int_0^1 dx x q_v(x;Q_0) \tag{6.8}$$

is the fraction of the proton's momentum carried by a valence quark of type $q$ $(=u,d,\ldots)$ at the scale $Q_0$. Direct computation shows that even though the numerator and denominator on the right-hand side (rhs) in Eq. (6.7) are separately scale dependent, the ratio is not. We reiterate and emphasize that Eq. (6.7) holds in a phenomenological sense: it is satisfied to within 1% by modern parametrizations of parton distribution functions but has not been proven theoretically.

The model described in Sec. VI.A.1 yields $\langle x\rangle_{u_v}=2\langle x\rangle_{d_v}$ and hence, unsurprisingly, $\kappa_p=-\kappa_n$ from Eq. (6.7). It is therefore evident that the magnitude of any deviation from this result can serve as one gauge of the amount by which SU(6) symmetry is broken within the nucleon. Experimentally, $\kappa_p/\kappa_n\approx -0.94$, so the breaking is small by this measure.

It has been argued (Traini *et al.*, 1997) that in CQMs, if one assumes

$$\frac{1}{(2\pi)^3}|\phi_q(\vec{k})|^2=m_q n_q(|\vec{k}|), \tag{6.9}$$

where $\phi_q(\vec{k})$ is the momentum-space wave function for a constituent quark of type $q$ within a nucleon of mass $M$, and $m_q(Q_0)$ and $n_q(|\vec{k}|)$ are the constituent quark's mass and momentum density distribution, respectively, then the virtual-photon-nucleon Compton scattering amplitude, shown in Fig. 26, can yield ($k^+=k_0+k_3$; see Appendix A)

$$xq_v(x;Q_0) = \frac{m_q(Q_0)}{M}\int d^3k n_q(|\vec{k}|)\,\delta\left(x-\frac{k^+}{M}\right). \quad (6.10)$$

This expression can satisfy the momentum sum rule if sea quarks and gluons are absent at $Q_0$ and $m_q(Q_0)=M/3$. However, the distribution does not have correct support: it is nonzero for $x>1$, nor does it satisfy the normalization conditions (2.27).

Both flaws are overcome if one adopts the prescription (Traini *et al.*, 1997)

$$xq_v(x;Q_0) = \frac{1}{(1-x^2)}\int d^3k \frac{k^+}{M} n_q(|\vec{k}|)\,\delta\left(\frac{x}{1-x}-\frac{k^+}{M}\right), \quad (6.11)$$

which exhibits two modifications. The simpler is the replacement $m_f \to k^+$, which provides the struck parton with an amount $k^+$ of the target's momentum, whereas it was at rest in Eq. (6.10). This ensures that Eqs. (2.27) are satisfied.[8] More complicated is the modification of the Dirac $\delta$ function's argument. It was inspired by an observation that only inelastic processes can contribute to the distribution functions. In this case the intermediate fermion line in Fig. 26 should carry momentum $k+q'$, where $q'=(\nu',\vec{q}')$ with $\nu'=\nu-\nu_{\rm el}$ and $\nu_{\rm el}=Q^2/(2M)$. With this prescription the valence-quark distribution function is defined such that the energy transfer does not include the part absorbed in elastic scattering. An additional factor of $1/(1-x)^2$ is necessary to preserve the normalization.

Equation (6.11) is a reasonable definition, which can be applied to a large class of CQMs. That of Isgur and Karl (1978) is included. In this case the wave functions are Gaussian, from which it follows immediately that the model yields valence-quark distribution functions that violate Eq. (6.5), namely, $q_v(x)\sim \exp[-x^2/(1-x)^2]/(1-x)^2$ for $x\simeq 1$.

It is plainly the high-momentum components of constituent-quark relative-momentum wave functions that determine this behavior and Eq. (6.5) can be obtained from Eq. (6.11) if and only if

$$n_q(|\vec{k}|) \overset{|\vec{k}|\to\infty}{\sim} 1/|\vec{k}|^7. \quad (6.12)$$

[The behavior $1/|\vec{k}|^6$ gives $(1-x)^2$, while $1/|\vec{k}|^8$ gives $(1-x)^4$.] Hence, while the constituent-quark wave functions in the CQMs of Bijker *et al.* (1994), Ferraris *et al.* (1995), and Giannini *et al.* (2001) provide greater support at high momentum than those of Isgur and Karl (1978), in all cases it is still insufficient to give agreement with Eq. (6.5) via Eq. (6.11). We know of no CQM that can.

Notwithstanding this, an illustration of the impact of SU(6) symmetry breaking via CQMs might be valuable. Such illustrations are provided by Traini *et al.* (1992) and Pasquini *et al.* (2002). The more recent study compares distribution functions calculated in the models of Isgur and Karl (1978) and Glozman *et al.* (1998). Results are shown in Fig. 28. It is apparent that evolution does not dramatically affect the computed ratio, e.g., compare with the large effect evident in Fig. 27. Hence a comparison between the models' predictions is straightforward. The Hamiltonian defining each model breaks SU(6) symmetry, albeit in slightly different ways, and therefore both produce curves which deviate from Eq. (6.1). Notably, the models exhibit quite different behavior at large $x$. This is primarily because, in contrast to Isgur and Karl (1978), a relativistic kinetic-energy operator is used by Glozman *et al.* (1998) and that increases the wave function's support at high momentum.

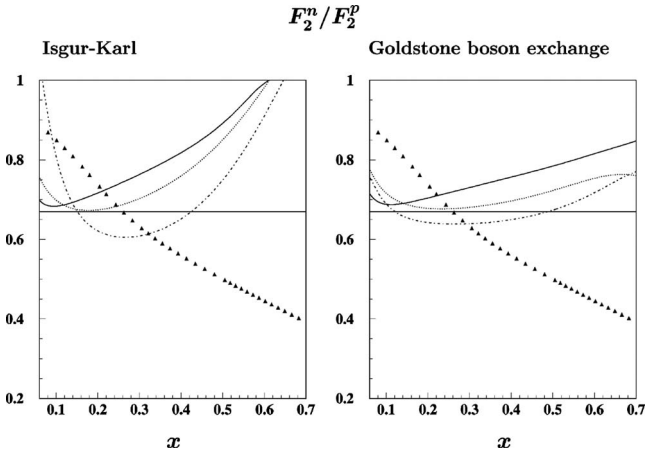


FIG. 28. $F_2^n(x)/F_2^p(x)$. Left panel, computed in the model of Isgur and Karl (1978): dot-dashed curve, at hadronic scale $Q_0 \sim 0.4$ GeV; dotted curve, leading-order evolution to $Q_0^2 = 10$ GeV$^2$; and solid curve, next-to-leading-order evolution. Right panel—computed in the model developed by Glozman *et al.* (1998). In both panels—triangles, CTEQ5 fit to experimental data (Lai *et al.*, 2000); straight line, Eq. (6.1). Using Eq. (2.45) and assuming $s_v(x)=0$ on the valence-quark domain, the large-$x$ behavior in these panels corresponds to $d_v(x)/u_v(x) \gtrsim 1.0$. Adapted from Pasquini *et al.*, 2002.

Along with the two CQM calculations, Fig. 28 shows the behavior of $F_2^n/F_2^p$ that is inferred from the CTEQ5 parametrizations of experimental data (Lai *et al.*, 2000). In this connection it is instructive to recall Fig. 10 and the discussion in Sec. II.G, which emphasizes that $F_2^n/F_2^p$ is well known for $x<0.7$. The parametrization ratio can therefore be viewed as a good representation of data on this domain. The absence of a free neutron target only introduces material uncertainty for $x\gtrsim 0.7$, a domain not reproduced in the figure.

It is therefore significant that neither CQM yields behavior for $F_2^n/F_2^p$ that is consistent with the parametrization ratio, not even for $x\gtrsim 0.4$, i.e., the valence-quark domain, whereupon they are supposed by proponents to provide a veracious description of the nucleon via its salient degrees of freedom. For $0.4<x<0.7$ the ratio in both panels lies well above the data parametrization. This is in contrast to models wherein the struck quark is partnered by scalar- and axial-vector-diquark intermediate states (Close, 1973; Carlitz, 1975; Close and Thomas, 1988; Meyer and Mulders, 1991) to which we shall re-

[8] In the Bjorken limit, $k^+=xM$ in the target rest frame.

turn. Pasquini *et al.* (2002) argued that the large-$x$ behavior of the distribution functions is greatly influenced by proper implementation of the Pauli principle. That is neglected by Close (1973), Carlitz (1975), and Close and Thomas (1988), which treat the diquarks as an elementary degree of freedom whose quark constituents are not active in the scattering process. Naturally, this is a weakness of those models, whose impact should be explored. (N.B. That can be done within a Faddeev equation treatment of the nucleon; see, e.g., Sec. VI.A.7 and Appendix B).

With the information described hitherto one can examine Eq. (6.7) within CQMs. To this end three different SU(6)-breaking Hamiltonians were considered in Giannini *et al.* (2003); namely, those associated with the models of Isgur and Karl (1978), Ferraris *et al.* (1995), and Giannini *et al.* (2001): Eq. (6.7) is satisfied to within 1% in each case. However, despite their differences, this collection of models belongs to a class[9] whose characteristic is $\kappa_p=-\kappa_n$ precisely. It seems therefore that nature employs a different mechanism to break SU(6) symmetry than that expressed in this class of models.

### 3. Pion cloud

Chiral symmetry and the pattern by which it is broken are fundamental to the nature of hadron structure. Neither the MIT bag model nor constituent-quark models express QCD's chiral-symmetry correctly. In working toward a theoretical understanding of distribution functions it is therefore important to explore the influence of correcting this defect.

Pseudoscalar mesons come naturally to mind when considering chiral symmetry in QCD and mesons mean antiquarks. The addition of $q\bar{q}$ pairs or correlations to the intermediate state that is shown in Fig. 26 has long been considered a plausible mechanism by which to solve the normalization problem encountered in computing the valence-quark distribution functions (Schreiber *et al.*, 1991).

This idea is canvassed by Kulagin *et al.* (1996) within the framework of a dispersion representation of the valence-quark distribution function (Kulagin *et al.*, 1994),

$$q_v(x;Q_0)=\int dw\int_{-\infty}^{k^2_{\max}(w,x)} dk^2\rho(w,k^2,x;Q_0). \quad (6.13)$$

Here $\rho$ is the probability density associated with an intermediate spectator state of invariant mass $w=(P-k)^2$ and

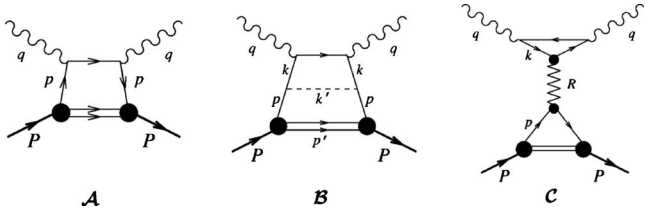


FIG. 29. Depiction of three invariant-mass sectors conjectured by Kulagin *et al.* (1996) to contribute to deep inelastic scattering. Left image $\mathcal{A}$: low $w$—diquark spectators. Central image, $\mathcal{B}$: intermediate $w$—compound spectator system involving a pion (dashed line), constituent quarks and diquarks. Right image, $\mathcal{C}$: large $w$—Regge-trajectory model for $q\bar{q}$ scattering from a constituent quark. Adapted from Kulagin *et al.*, 1996.

$$k^2_{\max}(w,x)=x\left(M^2-\frac{w}{1-x}\right), \quad (6.14)$$

where $M$ is the nucleon mass, is the maximum kinematically allowed value of the struck quark's squared-four momentum, which is equivalent to its virtuality if the quark is massless. In connection with Eq. (6.13), convergence and internal consistency suggest that the probability density can only have material support for $k^2\lesssim -M^2$. The condition

$$k^2_{\max}(w,x)=-M^2\Rightarrow w^2=M^2(1-x^2)/x. \quad (6.15)$$

Hence, in this case it follows that only intermediate states with $w\lesssim M^2$ are important for $x\gtrsim 0.6$. This explains the spectator diquark assumption of Fig. 26. However, as $x$ decreases below $x=0.6$, intermediate states with $s>M^2$ will play an increasingly important role and must be included in order to obtain a pointwise-accurate result for $q_v(x;Q_0)$.

A concrete model is used by Kulagin *et al.* (1996) to illustrate these points. It is notable that by combining the components indicated below, this study aims to produce a valence-quark distribution function that is valid at a resolving scale $Q_0=1$ GeV, i.e., at a scale which may lie within the perturbative domain. We judge that perturbative QCD evolution from such a scale is sounder than from the manifestly infrared scales employed in Secs. VI.A.1 and VI.A.2.

The study divides the space of intermediate states into three sectors, which are shown in Fig. 29 and described here.

$\mathcal{A}$: $w\lesssim M^2$. This is the diagram of Fig. 26, involving diquark spectators, which the studies described in Secs. VI.A.1 and VI.A.2 computed as the sole process contributing to the valence-quark distribution function. It is represented by a probability density

$$\rho_{\mathcal{A}}(w,p^2,x;Q_0)=\sum_{D=0^+,1^+}\delta(w-m_D^2)f^D_{Q/N}(p^2,x;Q_0), \quad (6.16)$$

with $f^D_{Q/N}(p^2,x;Q_0)$ identified as the probability distribution for finding a constituent quark in the nucleon with invariant mass $p^2$, proton light-cone momentum

[9]It appears that this class includes the model of Glozman *et al.* (1998) if a point-form spectator model (PFSM) is employed for the electromagnetic current operator (Melde *et al.*, 2007). Of the currents considered in this connection, only the PFSM can produce results in fair agreement with experiment.

fraction $x$ and partnered by a diquark with $J^P=D$. The Faddeev equation models of nucleon structure provide an appropriate framework for its evaluation (see, e.g., Appendix B).

$\mathcal{B}$: $M^2 \lesssim w \lesssim w_0, w_0 \sim 2M^2$. One model for the addition of $q\bar{q}$ pairs or correlations to the intermediate state is to dress constituent quarks with pseudoscalar mesons.[10] In Kulagin *et al.* (1996) the dressing sum is truncated at just one-pion rung, shown in the central image of Fig. 29. The remainder is shifted to sector $\mathcal{C}$.

$\mathcal{C}$: $w \geqslant w_0$. The large invariant-mass spectator component is modeled via a Regge trajectory, with intercept $\alpha_R \approx 1/2$, to describe $q\bar{q}$ scattering from a constituent quark. This piece provides a contribution to the valence-quark distribution function that behaves as $x^{-\alpha_R}$ for small $x$. As reported in Sec. VI.A.1, this is a desirable feature.

The model is elaborate and has numerous parameters. Their values are fixed through comparison with data and an eye to avoiding large discrepancies with legitimate theoretical constraints. Important among the parameters are the constituent-quark mass, $m_Q=0.45$ GeV; the diquark masses, with the large values[11] $m_{0^+}=1.0$ GeV and $m_{1^+}=1.2$ GeV appearing to be favored by data in this framework; momentum-space widths used in parametrizations of constituent-quark–diquark Faddeev wave functions, $\Lambda_{0^+}=1.0$ GeV and $\Lambda_{1^+}=1.2$ GeV, and exponents for these vertex functions, $n_{0^+}=2.0$ and $n_{1^+}=3.5$, chosen to guarantee Eq. (6.5); a hard-cutoff scale for the constituent-quark–pion vertex, $\Lambda_{Q\pi} \sim 1.0$ GeV; and a power-law form factor to model the $p^2$ and $k^2$ dependences of the Regge exchange quark-quark scattering amplitude, which is defined by a mass scale, $\Lambda_R=0.25$ GeV, and a power, $n_R=4$.

Combining these ingredients, the valence-quark distribution functions are computed at $Q_0=1$ GeV from the sum

$$q_v(x;Q_0) = Z_q(Q_0)\{q_{\mathcal{A}}(x) + q_{\mathcal{B}}(x) - \bar{q}_{\mathcal{B}}(x) + q_{\mathcal{C}}(x) - \bar{q}_{\mathcal{C}}(x)\}, \quad q = u,d, \tag{6.17}$$

with the normalization constants fixed by Eqs. (2.27) subject to the additional constraints $\int dx u_{\mathcal{A}}(x)=2$, $\int dx d_{\mathcal{A}}(x)=1$. The relative normalizations of the contributions in Fig. 29 are determined once the model's parameters are fixed; i.e., they are not additional independent quantities. Hence, in this model, defined at $Q_0=1$ GeV, the total valence-quark normalization is constituted from the diagrams in Fig. 29 as follows:

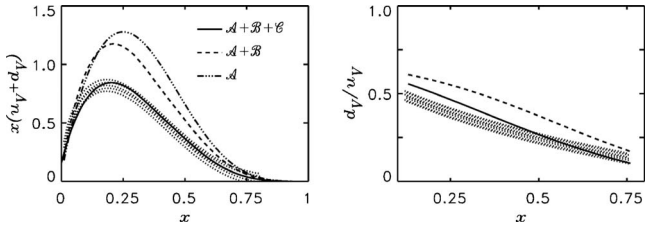


FIG. 30. Results illustrative of the pion-cloud model described in connection with Fig. 29. Left panel: Total valence-quark distribution function. Complete calculation, combining all sectors (solid curve); $\mathcal{A}+\mathcal{B}$ (dashed curve); and $\mathcal{A}$ alone (dash-dotted curve). Right panel: Contribution from sector $\mathcal{A}$ to the ratio of valence-quark distribution functions. $m_{0^+}=1.0$ GeV, $m_{1^+}=1.2$ GeV (solid curve) and $m_{0^+}=0.6$ GeV, $m_{1^+}=0.8$ GeV (dashed curve). Both panels: Computed results are reported at $Q_0^2=10$ GeV$^2$ after LO evolution from $Q_0=1$ GeV, whereat $\alpha/[2\pi] \approx 0.03$. Parametrizations of data (Martin *et al.*, 1994; Lai *et al.*, 1995) are provided for comparison (shaded band). Adapted from Kulagin *et al.*, 1996.

$$\int_0^1 dx\{u_v(x;Q_0) + d_v(x;Q_0)\} = \mathcal{A}(56\%) + \mathcal{B}(16\%) + \mathcal{C}(28\%). \tag{6.18}$$

Moreover,

$$\int_0^1 dx x\{u_v(x;Q_0) + d_v(x;Q_0)\} = \mathcal{A}(41\%) + \mathcal{B}(6\%) + \mathcal{C}(0.06\%) = 0.47, \tag{6.19}$$

which leaves 53% of the proton's momentum to be carried by nonvalence-quark degrees of freedom.

Figure 30 shows features of the model's distribution functions. Although the sector-$\mathcal{A}$ contribution is always dominant on the valence-quark domain, it is evident from the left panel that the renormalization effected by adding the sector-$\mathcal{B}$ and -$\mathcal{C}$ contributions plays an important part within the model: it is a surrogate for evolution, shifting support to lower $x$ at the model's mass scale of $Q_0=1$ GeV. The right panel exhibits that behavior for the valence-quark flavor ratio which is typically identified with diquark models: $d_v(x)/u_v(x)$ decreases monotonically with increasing $x$. The ratio plotted is formed only from the sector-$\mathcal{A}$ contributions. On the valence-quark domain the full result may be estimated by multiplying the value plotted in Fig. 30 by the ratio of normalization constants, namely, $Z_d/Z_u \approx 2/3$.

It is now clear that by implementing a scheme which resolves some of the structure of a constituent quark it is possible to shift the model scale $Q_0$ to a point wherefrom perturbative evolution may plausibly be justified *a priori*. In this way one can reproduce experimental data and provide an interpretation. However, the price appears high: with many ingredients needing to be carefully constrained and combined, the predictive power of an elaborate model is diminished.

[10]This can be sensible even when one unfolds and understands the structure of constituent quarks (Blaschke *et al.*, 1996; Oertel *et al.*, 2001; Cloët and Roberts, 2008). Indeed, it is an integral step in a systematic truncation of QCD's Dyson-Schwinger equations.

[11]These values are roughly 20% larger than extant computations of the mass scales associated with diquark correlations [Eq. (B1)] (Burden *et al.*, 1997; Maris, 2002).

#### 4. Topological soliton models

Attempts to describe baryons as topological solitons are usually motivated by emphasizing the importance of chiral symmetry and the pattern by which it is broken in QCD; the notion that when a carefully defined large-$N_c$ limit is considered, QCD is a theory of weakly interacting mesons (and glueballs) and strongly interacting baryons; and the observation that a simple form of classical nonlinear $\sigma$ model supports strongly interacting static topological soliton solutions, which can be quantized as fermions. Given this starting point, which possesses no explicit quark degrees of freedom, a connection with the parton model and DIS looks problematic.

A straightforward calculation (Jaffe, 1975) of distribution functions for localized field configurations is possible when the current operator is at most quadratic in the fundamental fields and the associated propagators are free-particle-like. The first of these conditions is difficult to satisfy in topological soliton models expressed in terms of elementary meson fields because the nucleon is a nonperturbative object involving all orders of the pion field and hence the current operator cannot be quadratic. This difficulty can be circumvented (Diakonov *et al.*, 1996; Weigel *et al.*, 1997) by realizing the nonlinear $\sigma$ model through a truncated bosonization of a four-fermion theory (Cahill and Roberts, 1985; Ebert and Reinhardt, 1986; Roberts *et al.*, 1988, 1989). Point coupling models of the Nambu–Jona-Lasinio type are often used. A regularization prescription and an associated ultraviolet mass scale $\Lambda_{\rm UV}$ are an essential part of the definition of this model. In general, one cannot guarantee *a priori* that $\Lambda_{\rm UV}$ plays no role in the Bjorken limit, namely, that $Q^2/\Lambda_{\rm UV}^2$ scaling violations are absent.

It has been argued that within this framework the singlet unpolarized quark distribution function in a nucleon at rest may be written as (Diakonov *et al.*, 1996)

$$u(x)+d(x)=\frac{MN_c}{2\pi}\int\frac{d^2p_\perp}{(2\pi)^2}\sum_{n\ \text{occup.}}\Phi_n^\dagger(\vec{p})\times[(I_D+\gamma^0\gamma^3)]\Phi_n(\vec{p})\Big|_{p_3=xM-E_n},\tag{6.20}$$

where $\Phi_n$ is an eigenfunction, with energy $E_n$ of a Dirac Hamiltonian constructed using a so-called hedgehog soliton *Ansatz* for the pion field; the sum runs over the Dirac sea and the single discrete (valence) level bound in the soliton background, with $-m_Q<E_v<m_Q$, containing $N_c$ constituentlike quarks; and $x\in[-1,1]$. In defining Eq. (6.20) one must follow the usual soliton model steps of projection and quantization to arrive at states with the correct spin and isospin, and three-momentum. Moreover, it is necessary to employ a Poincaré invariant Pauli-Villars regularization of the underlying Nambu–Jona-Lasinio model or an equivalent in order to preserve, among other things, completeness of the eigenfunctions and positivity of the rhs in Eq. (6.20). The singlet case is simplest in this approach because effects associated with cranking the topological soliton can be neglected. The distributions in Eq. (6.20) satisfy

$$q(x)=\begin{cases}q(x), & x>0\\ -\bar{q}(-x), & x<0.\end{cases}\tag{6.21}$$

It can be shown algebraically within the model that

$$\int_{-1}^{1}dx[u(x;Q_0)+d(x;Q_0)]=\int_0^1 dx[u_v(x;Q_0)+d_v(x;Q_0)]=N_c,\tag{6.22}$$

which may be compared with Eqs. (2.27). It is notable that the rhs of Eq. (6.22) is saturated by the discrete level alone and hence that the Dirac continuum, distorted by the presence of the large pion field, contributes nothing to the soliton's baryon number. In addition, with the Pauli-Villars regularization,

$$\int_{-1}^{1}dxx[u(x;Q_0)+d(x;Q_0)]=:\int_0^1 dxx\Sigma(x;Q_0)=\int_0^1 dxx[u(x;Q_0)+\bar{u}(x;Q_0)+d(x;Q_0)+\bar{d}(x;Q_0)]=1,\tag{6.23}$$

so that at the resolving scale for which the model is assumed to be defined, viz., $Q_0\simeq\Lambda_{\rm UV}=0.6$ GeV, the proton's complete momentum is carried by the model's constituent quarks and antiquarks.

Distributions typical of a topological soliton model are shown in Fig. 31: left panel, valence-quark distribution, and right panel, the nonzero antiquark distribution. In this model the discrete level contributes to both the DIS valence-quark and antiquark distributions. Furthermore, the Dirac continuum, distorted by the soliton, produces unequal distributions of quarks and antiquarks and hence should not be solely identified with the sea. It will be observed that while the model's antiquark distribution is incorrect in detail, it does have the important property of possessing little support on the valence-quark domain. Moreover, owing to the nonzero antiquark distribution, which only vanishes as $N_c\to\infty$, the valence-quark distribution peaks at $x\lesssim 1/N_c$.

A comparison between the left panels of Figs. 30 and 31 is instructive. Allowing for the difference in normalization, there is a semiquantitative similarity between the soliton model result and that produced by the sum of sectors $\mathcal{A}$ and $\mathcal{B}$ in the model of Kulagin *et al.* (1996), i.e., constituent-quark plus pion (see Fig. 29). This highlights the omission of sea-quark effects in the soliton model at its resolving scale and also the role that sea quarks play in general; e.g., with their inclusion, $xq(x)$ has far greater support at low $x$ and commensurately less support on the valence-quark domain.

It is interesting to compare the approach discussed here with that in Sec. VI.A.1. In contrast to the static cavity treatment of bag models, wherein the three constituent quarks contribute only to quark distributions, here they also generate an antiquark distribution owing to the strong pion mean field, which distorts the

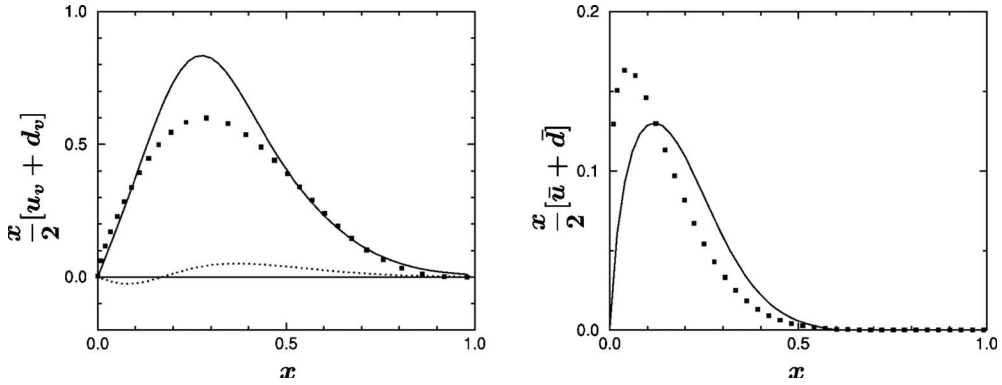


FIG. 31. Results obtained in a topological soliton model whose infrared resolving scale is argued to be $Q_0 \sim 0.6$ GeV. Left panel: $(x/2)\{u_v(x;Q_0)+d_v(x;Q_0)\}$, proportional to the valence-quark distribution: contribution from the single discrete (valence) energy-level bound in the soliton background (solid curve) and from the Dirac continuum (dotted curve). Right panel: $(x/2)\{\bar{u}(x;Q_0)+\bar{d}(x;Q_0)\}$, proportional to the antiquark distribution. Both panels: squares, NLO data parametrization drawn from Glück *et al.* (1995), associated with $Q_0=0.56$ GeV. Adapted from Diakonov *et al.* (1996): $\Lambda_{\rm UV}=0.56$ GeV, the calculated nucleon mass is 1170 MeV, and $N_c=3$ with $1/N_c$ corrections neglected.

negative-energy continuum of the Dirac Hamiltonian. In the context of Sec. VI.A.1, this might be mimicked by incorporating effects of feedback between the constituent quarks and the bag surface.

In the approach outlined here the baryon number and momentum sum rules are automatically preserved. However, again owing to a lack of translational invariance in the formulation, the model's distribution functions do not vanish at $x \geqslant 1$ but behave as $\exp(-\text{const} \times N_c x)$. That problem was considered in Gamberg *et al.* (1998), which argues that distribution functions in the infinite-momentum frame (IMF) may be obtained from those calculated in the nucleon rest frame via the substitution[12]

$$q_{\rm IMF}(x) = \theta(1-x)\frac{1}{1-x} q_{\rm RF}(-\ln[1-x]). \tag{6.24}$$

The same formula was derived in formulating a translationally invariant bag model in 1+1 dimensions (Jaffe, 1981), with the operation $x \to -\ln(1-x)$ identified as expressing Lorentz contraction of the baglike object. Akin to Eq. (6.11), Eq. (6.24) maps a function with support on $[0,\infty)$ to one with support restricted to [0,1] and preserves normalization, i.e.,

$$\int_0^1 dx q_{\rm IMF}(x) = \int_0^\infty dz q_{\rm RF}(z). \tag{6.25}$$

For a typical distribution, it increases the peak height and suppresses the tail. The effects are large, perhaps too large for favorable comparison with experiment, and soliton rotation was not considered in the derivation (Wakamatsu and Kubota, 1998). While the alternative of merely neglecting the support problem is not meritorious, the prescription of Eq. (6.24) is not widely employed.

[12]Recall that in the infinite-momentum frame the target's momentum is equivalent to its light-front momentum and hence Bjorken $x$ coincides with the fraction of the target's light-front momentum carried by a parton. It is only in the IMF that $q_v(x)$ can be interpreted as a single-parton probability density.

#### 5. Pion structure function in the topological soliton model

In topological soliton models chiral symmetry is emphasized and a strong pion mean field is indispensable in order to realize a baryon. This said, it is natural to ask what the model predicts for the pion's valence-quark distribution functions. Suppose, as above, one specifies the theory via a bosonization of a point-coupling Nambu–Jona-Lasinio model and, in addition, completes its definition using a two-subtraction Pauli-Villars regularization scheme for the real part of the action. Under these conditions it has been argued (Gamberg and Weigel, 2000) that the pion's valence-quark distribution function is

$$q_v^\pi(x;Q_0) = \frac{\mathcal{P}(m_\pi^2,x;Q_0)}{\int_0^1 dx \mathcal{P}(m_\pi^2,x;Q_0)} \tag{6.26}$$

with

$$\mathcal{P}(m_\pi^2,x;Q_0) = \frac{d}{dq^2} q^2 \Pi(q^2;Q_0)|_{q^2=m_\pi^2}, \tag{6.27}$$

$$\Pi(q^2;Q_0) = -i\sum_{i=0}^{2} c_i \int \frac{d^4k}{(2\pi)^4} \times \frac{1}{[-k^2 - x(1-x)q^2 + m_Q^2 + \Lambda_{i\rm UV}^2]^2}, \tag{6.28}$$

where $\{c_i,\Lambda_{i\rm UV}\}$ are the Pauli-Villars parameters. It follows that in the chiral limit, viz., $m_\pi^2=0$, an analytic point in this calculation $q_v^\pi(x;Q_0)$, is a constant whose integral over $x \in [0,1]$ is unity. Hence,

$$q_v^{\pi\ \mathrm{soliton}}(x;Q_0)=1, \tag{6.29}$$

which means that at the model's resolving scale it is equally likely for the $u$ quark to carry any fraction of the pion's momentum: all, none, or some fraction in between, with the same probability.

To place Eq. (6.29) in context, the parton-model prediction for the pion's valence-quark distribution function is (Ezawa, 1974; Farrar and Jackson, 1975; Berger and Brodsky, 1979; Brodsky and Lepage, 1979)[13]

$$q_v^{\pi}(x;Q_0)\overset{x\sim 1}{\sim}(1-x)^2. \tag{6.30}$$

Plainly, Eq. (6.4) is also applicable to $J=0$ hadrons since $n=1$ and $2\delta\lambda=1$ in this case (Brodsky, 2005). The extra multiplicative factor of $1-x$ is present because $x=1$ corresponds to elastic scattering and hence $\sigma_T$ must vanish for a spin-0 target. This imposes a helicity selection rule at the parton level, which causes $\sigma_T$ to vanish a single power faster as $x\to 1$ than one would anticipate from dimensional counting (Llewellyn Smith, 1980). Owing to this, Eq. (6.30) is consistent with the Drell-Yan-West analyses (Drell and Yan, 1970b; West, 1970; Lepage and Brodsky, 1980). The soliton model prediction in Eq. (6.29) conflicts conspicuously with the parton-model result.

#### 6. Pion in the Nambu–Jona-Lasinio model

Models of the Nambu–Jona-Lasinio (NJL) type have long been used in connection with the strong interaction. As described in Sec. VI.A.4, the NJL model provides a framework within which quark distribution functions may be defined in topological soliton models. However, it is more common for NJL studies to emphasize dressed-quark degrees of freedom and realize hadrons as poles in $n$-point Green functions. Following this path the model can be viewed from a Dyson-Schwinger equation (DSE) perspective (Roberts and Williams, 1994; Gutiérrez-Guerrero *et al.*, 2010).

The continuing appeal of the NJL model can be explained by two features; namely, it is defined by a simple interaction and exhibits dynamical chiral-symmetry breaking (DCSB). This latter aspect, which the models of Secs. VI.A.1–VI.A.3 do not possess, suggests that it might sensibly be used to explore the structure function of the pion. As noted above, the pion is special in QCD because it is both a dressed-quark-antiquark bound state and the Goldstone mode arising from DCSB (Maris *et al.*, 1998).

By analyzing the Bjorken limit of the parton-model expression for DIS from a pion target, one can derive a model-independent formula for the quark distribution function, which describes the quark-parton number density in the IMF,

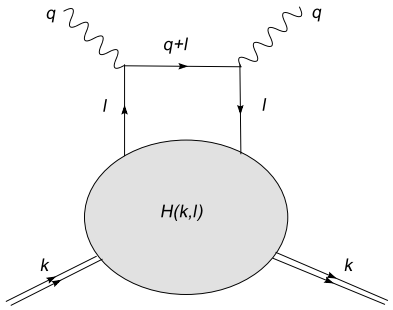


FIG. 32. Depiction of the general handbag diagram contribution to deep inelastic scattering from the pion. As we saw in Fig. 26, with an explicit expression for the single-flavor removal amplitude $\mathcal{H}(k,\ell)$ one defines a model framework within which to complete the calculation.

$$q_v^{\pi}(x;Q_0)=\frac{1}{8\pi}\int d\xi^- e^{(i/2)xk^+\xi^-}\times\langle\pi(k)|\bar{\psi}_q(0)\gamma^+\psi_q(\xi^-)|\pi(k)\rangle, \tag{6.31}$$

where $k^2=m_\pi^2$ or, equivalently, $k^-=(k_\perp^2+m_\pi^2)/k^+$. It follows from Eq. (6.31) that

$$\int_0^1 dx q_v^{\pi}(x;Q_0)=\frac{1}{2k_+}\langle\pi(k)|\bar{\psi}_q(0)\gamma^+\psi_q(0)|\pi(k)\rangle=1, \tag{6.32}$$

independent of $Q_0$, because the last matrix element is simply the contribution of a single quark flavor to the pion's electromagnetic form factor.

Equation (6.31) can be expressed in momentum space as follows:

$$q_v^{\pi}(x;Q_0)=\frac{1}{2}\int\frac{d^4\ell}{(2\pi)^4}\delta(\ell^+-xk^+)\times\mathrm{tr}_{\mathrm{CD}}\gamma^+\mathcal{H}_\pi(k,\ell;Q_0) \tag{6.33}$$

$$=\frac{1}{4}\int\frac{d\ell^- d\ell_\perp}{(2\pi)^4}\mathrm{tr}_{\mathrm{CD}}\gamma^+\mathcal{H}_\pi(k,\ell;Q_0)\Big|_{\ell^+=xk^+}. \tag{6.34}$$

Here the matrix trace applies to color and spinor indices, and $\mathcal{H}_\pi(k,\ell;Q_0)$ is the amplitude defined in Fig. 32: it is partially amputated; i.e., the external pion legs are removed. In this form,

$$\int_0^1 dx q_v^{\pi}(x;Q_0)=\frac{1}{2k^+}\int\frac{d^4\ell}{(2\pi)^4}\mathrm{tr}_{\mathrm{CD}}\gamma^+\mathcal{H}_\pi(k,\ell;Q_0), \tag{6.35}$$

and one recovers Eq. (6.32) because the integral on the rhs is merely an expression of the matrix element describing a single flavor's contribution to the form factor. As we may readily establish, this identity is preserved in the commonly used rainbow-ladder truncation as long as in constructing $\mathcal{H}_\pi(k,\ell;Q_0)$ the quark-photon vertex satisfies the Ward-Takahashi identity and the pion Bethe-

[13]Equation (6.30) generalizes to $q_v^{0^-}(x;Q_0)\sim(1-x)^{2n}$ for a pseudoscalar meson with $n+1$ valence quarks. Again, the exponent $2n$ is a lower bound, saturated at the infrared resolving scale. The value is increased by QCD evolution.

Salpeter amplitude is canonically normalized (Roberts, 1996).

Within the NJL model, Eqs. (6.33) and (6.34) are not yet meaningful. A regularization scheme must be specified and the result for $q_v^\pi(x;Q_0)$ depends critically on the prescription adopted. To illustrate this we write explicitly the formal NJL-model expression for the rhs of Eq. (6.34),

$$q_v(x;Q_0) = \frac{1}{4}\int \frac{d\ell^- d\ell_\perp}{(2\pi)^4} \mathrm{tr}_{\mathrm{CD}} i\gamma_5 g_{\pi\bar{q}q} \times S(\ell)\gamma^+ S(\ell) i\gamma_5 g_{\pi\bar{q}q} S(k-\ell)\Big|_{\ell^+ = xk^+}, \tag{6.36}$$

where $g_{\pi\bar{q}q}$ is the Bethe-Salpeter amplitude for the pion[14] and $\gamma^+$ is the quark-photon vertex. Both are independent of the quark-antiquark relative momentum in a symmetry-preserving regularization of the NJL model owing to the momentum-independent interaction.

One feature of a symmetry-preserving regularization is translational invariance, following from which one can use the Ward identity to rewrite

$$q_v(x;Q_0) = \frac{1}{4}\int \frac{d\ell^- d\ell_\perp}{(2\pi)^4} \mathrm{tr}_{\mathrm{CD}} i\gamma_5 g_{\pi\bar{q}q} \times S(\ell)\gamma^+ S(\ell) i\gamma_5 g_{\pi\bar{q}q} S(k-\ell)\Big|_{\ell^+ = xk^+} \tag{6.37}$$

$$= -\frac{\partial}{\partial k^2}\Pi(k,x)\Big|_{k^2=m_\pi^2}, \tag{6.38}$$

$$\Pi(k,x) = \frac{k^+}{2}\int \frac{d\ell^- d\ell_\perp}{(2\pi)^4} \mathrm{tr}_{\mathrm{CD}} i\gamma_5 g_{\pi\bar{q}q} \times S(\ell) i\gamma_5 g_{\pi\bar{q}q} S(k-\ell)\Big|_{\ell^+ = xk^+}. \tag{6.39}$$

Although written in a slightly different form, Eqs. (6.38) and (6.39) are simply a restatement of Eq. (6.26). This is natural, given that the NJL model provides the framework within which parton distribution functions are defined in topological soliton models.

At this point it is worth emphasizing that light-front concepts have hitherto appeared only as a result of a change in integration variables and it is generally assumed that the change of variables is nugatory. Hence one is not actually working within a light-front formulation of QCD. This makes no difference in perturbative analyses. However, it does involve significant hidden assumptions in connection with important nonperturbative phenomena. For example, in order to evaluate Eq. (6.39) one requires the light-front form of the nonperturbatively dressed-quark propagator. This quantity is, however, unknown. Thus, in proceeding from Eq. (6.39), Bentz *et al.* (1999), for example, assumed that a dressed-quark mass, two orders of magnitude larger than the $u$-quark current mass, is generated nonperturbatively and that $g_{\pi\bar{q}q}$ is related to the dressed-quark mass via a Goldberger-Treiman relation. Neither of these results has yet been proved in the light-front formulation. This problem was highlighted and considered by Bentz *et al.* (1999) [see, e.g., Eq. (3.31) therein], but it was not solved, merely defined away. Thus, an internally consistent treatment of Eq. (6.39) is wanting, so that a covariant treatment following Landshoff *et al.* (1971) is preferable.

Nonetheless, if one overlooks these caveats and proceeds, then it follows from Eq. (6.39) that in the chiral limit with a translationally invariant regularization,

$$q_v^{\pi\ \mathrm{NJL_{TI}}}(x;Q_0) = q_v^{\pi\ \mathrm{soliton}}(x;Q_0) = 1 \tag{6.40}$$

for all values of $Q_0$ and consequently (Dorokhov and Tomio, 2000)

$$\langle x^n\rangle_{Q_0}^{\pi\ \mathrm{NJL_{TI}}} := \int_0^1 dx x^n q_v^{\pi\ \mathrm{NJL}}(x;Q_0) = \frac{1}{n+1}. \tag{6.41}$$

These results are themselves problematic and can directly be traced to the absence of a length scale characterizing the pion's transverse size when a translationally invariant regularization is employed for a chiral-limit NJL model. In this case both the interaction and the regularization procedure are momentum independent and hence neither can act to bound the relative momentum of the pion's constituents. This explains why the model disagrees with the QCD parton-model prediction [Eq. (6.30)]: in QCD there cannot exist a resolving scale at which the relative momentum of the pion's constituents is unbounded.

However, one need not naively employ a translationally invariant regularization scheme. An ultraviolet cutoff $\Lambda_{\mathrm{UV}}$ can serve to mimic asymptotic freedom in QCD in the sense that it defines an NJL-model quark-antiquark interaction which vanishes for momenta larger than $\Lambda_{\mathrm{UV}}$. This procedure, adopted by Shigetani *et al.* (1993) for analysis of the virtual-photon-pion forward Compton scattering amplitude, yields

$$q_v^{\pi\ \mathrm{NJL_{HC}}}(x;Q_0) \propto -g_{\pi\bar{q}q}^2 \int_0^\infty d\kappa\,\theta(\Lambda_{\mathrm{UV}}^2 - \kappa_E)\frac{\kappa - m_Q^2 - x m_\pi^2}{(\kappa - m_Q)^2} \times \theta[m_\pi^2 x(1-x) - xM^2 - (1-x)\kappa], \tag{6.42}$$

where $\kappa_E = -\kappa + x m_\pi^2 - x m_Q^2/(1-x)$ and the constant of proportionality is fixed by requiring $\int_0^1 dx q_v(x;Q_0) = 1$.

The valence-quark distribution function obtained from Eq. (6.42), with $\Lambda_{\mathrm{UV}} = 0.9$ GeV and $m_Q = 0.35$ GeV, is shown in Fig. 33. It differs markedly from Eq. (6.40).

[14] It is generally true that parton distribution functions are determined by a hadron's Bethe-Salpeter amplitude. In the light-front quantization of QCD the PDFs can be computed from the absolute squares of light-front wave functions, integrated over the transverse momentum up to the resolution scale $Q_0$ (Brodsky *et al.*, 1998).

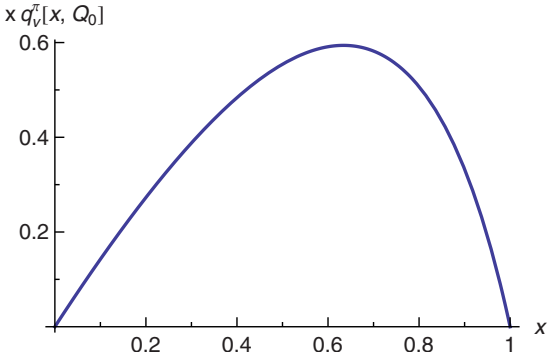


FIG. 33. (Color online) Pion's valence-quark distribution function calculated in a Nambu–Jona-Lasinio model that is regularized by using a hard cutoff (Shigetani *et al.*, 1993). Under one-loop evolution, a resolving scale of $Q_0$=0.5 GeV optimizes agreement with data parametrizations.

As will become clear, this could not have been otherwise because the behavior of $q_v^\pi(x)$ for $x \simeq 1$ depends on the precise form of the cutoff function. If this were not the case, then the valence-quark distribution function would be ineffectual as a discriminator between models for the strong interaction and, furthermore, no behavior could be uniquely identified with a prediction of QCD. With the hard cutoff

$$q_v^{\pi\ \mathrm{NJL_{HC}}}(x;Q_0) \overset{x\simeq 1}{\propto} (1-x). \tag{6.43}$$

From the distribution function shown in Fig. 33 one obtains,

$$\langle x\rangle_{Q_0}^{\pi\ \mathrm{NJL_{HC}}} = 0.39, \quad \langle x^2\rangle_{Q_0}^{\pi\ \mathrm{NJL_{HC}}} = 0.22, \tag{6.44}$$

values which are significantly smaller than those obtained in the absence of a bound-state length scale [Eq. (6.41)]. It is apparent that in a model whose interaction acts at the resolving scale $Q_0$ to bound the relative momentum of the pion's constituents, the valence quarks do not carry all the bound state's momentum. The remainder may be associated with dressed gluons, which affect binding within the pion bound state and are invisible to the electromagnetic probe (Hecht *et al.*, 2001) (see also Sec. V.C).

The kaon's valence-quark distribution functions were also calculated by Shigetani *et al.* (1993). With a current-quark-mass ratio of $m_s/m_d \sim 25$, they obtained $m_S/m_D \approx 1.5$, and given this value for the ratio of constituent-quark-like masses, it is unsurprising that within the kaon the valence *s*-quark distribution is harder than that of the valence *u* quark: the heavier valence *s* quark must typically carry more of the bound state's momentum. It follows from momentum conservation that $u_v^K(x)/u_v^\pi(x) < 1$ on the valence-quark domain. This outcome is consistent with experiment (Badier *et al.*, 1980), as shown in Figs. 21 and 42.

#### 7. Nucleon in the Nambu–Jona-Lasinio model

When emphasizing dressed-quark degrees of freedom, it is natural to describe baryons using a Poincaré covariant Faddeev equation, aspects of which are described in Appendix B. Early attempts to compute the valence-quark distribution functions within this framework are described by Kusaka *et al.* (1997) and Mineo *et al.* (1999). These studies retained only a scalar-diquark correlation and the latter employed a particularly severe truncation of the quark-exchange kernel in Fig. 43, viz., the so-called static approximation, in which all momentum dependence is ignored in the propagator of the exchanged quark. This impacts significantly on the results. The studies also employ a simple current. In the former, the current is built only from diagrams 1 and 2 in Fig. 44. These diagrams are also the basis for the current in Mineo *et al.* (1999) but therein, departing from the purely valence-quark setup, it is augmented by two diagrams argued to provide an estimate of the contribution from a pion cloud.

Unsurprisingly, there are many similarities between the nucleon study of Mineo *et al.* (1999) and that of the pion in Bentz *et al.* (1999). In particular, a translationally invariant regularization prescription is employed so that, in the absence of a pion cloud, the valence quarks carry all the nucleon's momentum at the model's resolving scale, in analogy with Eq. (6.41). Some of this momentum is transferred to the pions following their addition to the current. The amount is related to the pion content of a dressed quark, which is typically ~10% (Cloët and Roberts, 2008).

As found by Kulagin *et al.* (1996) and shown in Fig. 29, Mineo *et al.* (1999) reported that a pion cloud works to soften the valence-quark distribution and increase its support at low *x*. Unlike Kulagin *et al.* (1996), however, Mineo *et al.* (1999) still needed a very low resolving scale, namely, $Q_0 = m_Q = 0.4$ GeV, if agreement with the parametrizations of Martin *et al.* (1994) is to be obtained under NLO evolution. The NJL model, with its momentum-independent interaction, must naturally produce hard distributions but the effect is compounded by the static truncation used by Mineo *et al.* (1999). As a result of this truncation, the nucleon's Faddeev amplitude is independent of the quark-diquark relative momentum, just as the pion's Bethe-Salpeter amplitude is independent of the quark-antiquark relative momentum in the NJL model formulated with a translationally invariant cutoff.

As shown in Fig. 34, the results are also sensitive to details of the regularization scheme. The favored scheme is that adopted by Bentz *et al.* (1999), wherewith a cutoff is placed on $\ell_\perp$ and $q_v(x;Q_0) \neq 0$ on $0 \leqslant x \leqslant 1$. However, in this case $q_v(x;Q_0)$ exhibits a disconcerting sharp and physically unacceptable increase at $x \simeq 0.9$, which must artificially be suppressed before the evolution equations can be used. In practice, the distribution was forced to behave as $(1-x)^{10}$. Owing to the behavior produced by both regularization schemes, this model cannot say anything meaningful about the distributions at $Q_0$ for $x \gtrsim 0.8$. This is a serious limitation because evolution is an area-preserving operation that shifts strength from large to small *x*. Hence, after evolution the behavior in this model of the distributions on the

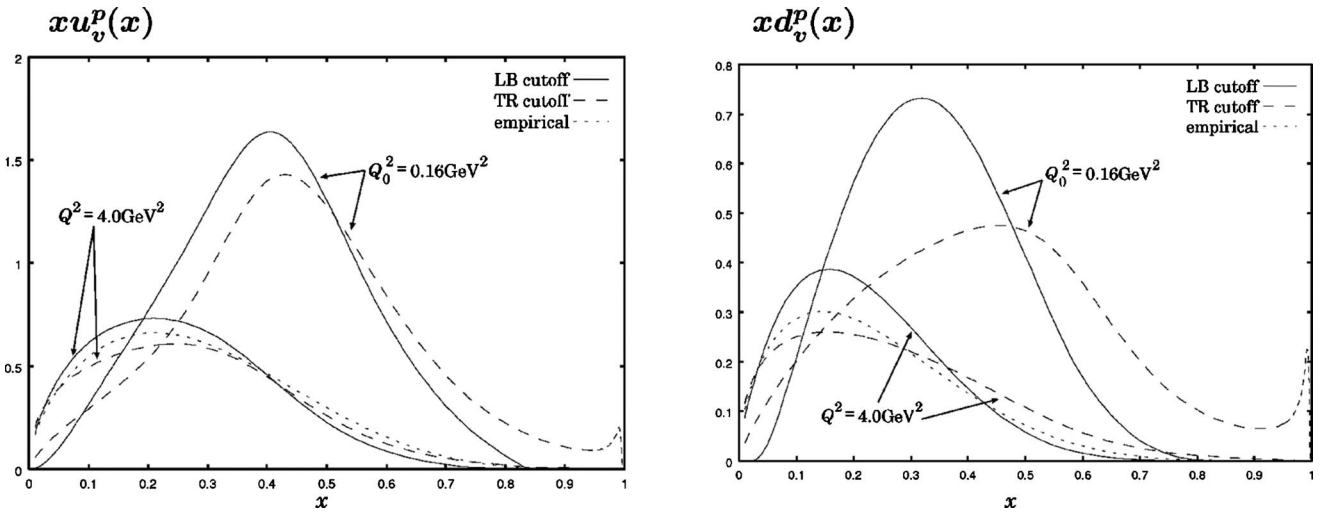


FIG. 34. Valence $u$-quark (left-panel) and $d$-quark (right-panel) distributions computed in a scalar-diquark picture of the nucleon based on an NJL model (Mineo *et al.*, 1999). The results exhibit a marked sensitivity to the manner in which the model is regularized. In this study the TR scheme is judged best. Both schemes lead to unphysical behavior on $x \gtrsim 0.8$. NLO evolution of the model results is performed from $Q_0 = 0.4$ GeV. The parametrization is that of Martin *et al.* (1994). Adapted from Mineo *et al.*, 1999.

valence-quark domain is primarily determined by artifacts induced by the regularization. This is neither a sound basis for prediction nor for comparison with parametrizations of data.

Some general features of the distributions are nonetheless physically reasonable. For example, in this representation of the proton, the $d$ quark appears only as a constituent of a $[u,d]$ scalar diquark with mass $m_Q < m_{0^+} < 2m_Q$. Hence, the probability of finding a valence $d$ quark in the proton is obtained by convoluting two probabilities, viz., that of striking a $0^+$ diquark in the nucleon with that of striking a $d$ quark in the scalar diquark. Naturally, therefore, the valence $d$-quark distribution peaks at smaller $x$ than the valence $u$-quark distribution and is softer for $0.6 \lesssim x \lesssim 0.8$.

A realistic picture of the nucleon must include axial-vector diquark correlations, which generate significant attraction (Hecht *et al.*, 2002), and in Mineo *et al.* (2002) they are added to the model just described. The Faddeev equation is still solved in the static truncation but the regularization procedure denoted by LB in Fig. 34 is adopted. As apparent, it forces the distribution functions to vanish at $x \simeq 0.8$, which, while still unphysical, is less difficult to overlook than the sharp rise produced by the TR scheme. The LB regularization procedure defines a model in which the distributions are extremely soft at $Q_0$. Needless to say, such behavior is inconsistent with Eq. (6.5), which specifies the behavior of distribution functions on a domain that includes the neighborhood of $x=1$.

The model has other internal difficulties. Notably, the axial-vector diquark is unbound and, owing to the absence of confinement, the $\Delta$ resonance cannot be formed without requiring the proton to possess what, within the model, is an unrealistically large axial-vector diquark component. Notwithstanding these problems, one might hope for useful information about the ratio $F_2^n(x)/F_2^p(x)$ on the valence-quark domain. Figure 35 shows this ratio's sensitivity to the strength of the proton's axial-vector diquark component. While the pointwise behavior in $x$ is unlikely to be accurate, we judge that the general trend is a reliable indication of one effect of axial-vector diquark correlations within the nucleon;

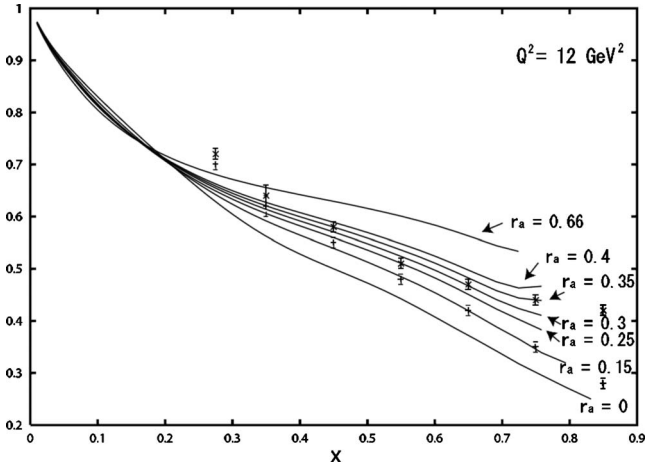


FIG. 35. $F_2^n(x)/F_2^p(x)$ computed by Mineo *et al.* (2002). $r_a$ measures the strength of axial-vector diquark correlations in the proton. It is a free parameter. Used in conjunction with $m_Q = 0.4$ GeV and $m_{0^+} = 0.68$ GeV, the model-preferred value is $r_a = 0.25$, at which the axial-vector correlation contributes just 7% to the proton's normalization. $r_a = 0$ reproduces the scalar-diquark only model (Fig. 34). With $r_a = 2/3$, the axial-vector diquark contributes 39% to the proton's normalization. NLO evolution of the model results is performed from $Q_0 = 0.4$ GeV. An explanation of the experimental points is provided by Melnitchouk and Thomas (1996). Adapted from Mineo *et al.*, 2002.

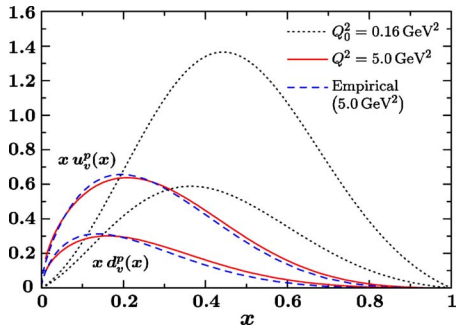


FIG. 36. (Color online) Valence-quark distribution functions computed by Cloët *et al.* (2005), which differs from Mineo *et al.* (1999) primarily in the choice of regularization prescription. The marked sensitivity to regularization scheme in NJL-type models is evident through comparison with Fig. 34. NLO evolution of the model results is performed from $Q_0$=0.4 GeV. "Empirical" denotes the parametrization of Martin *et al.* (2002b). Adapted from Cloët *et al.*, 2005.

viz., a $d$ quark in an axial-vector diquark can possess the same helicity as the proton target.

The analysis of Mineo *et al.* (1999) is updated by Cloët *et al.* (2005), wherein the model is redefined through a proper-time regularization procedure. In addition to the ultraviolet regulator, an infrared cutoff is also used in the reformulation. This expedient serves to mock up confinement (Ebert *et al.*, 1996) and thereby enables an improved description of the Δ resonance.

In effecting a soft cutoff at $Q_0$, the proper-time prescription yields much improved behavior of the distribution functions on the valence-quark domain. This is shown in Fig. 36, which was computed with, (in GeV) $\Lambda_{\mathrm{IR}}$=0.28, $\Lambda_{\mathrm{UV}}$=0.66, $m_Q$=0.4, $m_{0^+}$=0.65, $m_{1^+}$=1.2, and diquark coupling strengths $r_s$=0.5, $r_a$=0.08. The splitting between the scalar and axial-vector diquarks is more than twice the usual size [cf. Eq. (B1)] and the values of $r_s$, $r_a$ suggest that the axial-vector diquark contributes <2% to the proton's normalization.

Both the $u$- and $d$-quark distributions in Fig. 36 behave as (Cloët, 2009)

$$q_v^{\mathrm{NJL_{PT}}}(x;Q_0) \overset{x\simeq 1}{\sim} (1-x)^{\epsilon}, \quad \epsilon \sim 1.5, \tag{6.45}$$

a result which, however, still conflicts with the parton-model constraint [Eq. (6.5)]: $(1-x)^3$. On the other hand, for the flavor ratio one finds

$$d_v^{\mathrm{NJL_{PT}}}(x;Q_0)/u_v^{\mathrm{NJL_{PT}}}(x;Q_0) \overset{x\to 1}{=} 0.2, \tag{6.46}$$

which corresponds to $F_2^n/F_2^p \to 0.43$ as $x \to 1$ [see Eq. (2.45) and cf. Fig. 35]. However, the agreement between Eq. (6.46) and the leading-order vector-gluon prediction of Farrar and Jackson (1975) is incidental. Instead, the value reflects the role and strength of axial-vector diquarks in the proton.

### 8. Pion in the instanton liquid

The instanton liquid model derives from the notion that topological soliton solutions of the classical Euclidean-space Yang-Mills equations might play a role in describing QCD's ground state (Schafer and Shuryak, 1998). This possibility is actively discussed (Lian and Thacker, 2007; Ilgenfritz *et al.*, 2008) and the model meanwhile continues to be used.

In the present context, the instanton liquid model may be viewed as corresponding to a type of NJL model in which the interaction is momentum dependent. With this feature it generates, e.g., a dressed-quark mass and pion Bethe-Salpeter amplitude that are momentum dependent and thereby overcomes a material weakness of the contact-interaction NJL model described above. On the other hand, the momentum dependence differs significantly from that of QCD: it is exponential, not power law, and hence possesses too little support away from zero relative momentum, which is the domain most relevant to the valence-quark distribution.

In this form the instanton liquid model has been employed to calculate the pion's valence-quark distribution function (Dorokhov and Tomio, 2000). As should be anticipated, the momentum dependence of the interaction leads to an $x$-dependent distribution at $Q_0$=0.55 GeV, which vanishes at $x$=0,1, in contrast to that obtained with some regularizations of the contact-interaction NJL model [see, e.g., Eqs. (6.29) and (6.40)].

Following leading-order evolution from $Q_0$ =0.55 GeV to $Q$=2 GeV, the model's result for the distribution function on $0.2 \lesssim x \lesssim 0.9$ is uniformly larger than experiment (see Fig. 41) and the parametrization of Sutton *et al.* (1992) which is based upon it.[15] They attribute this to their omission of gluon, sea, and higher Fock state contributions at $Q_0$, which is plausible given the content of Fig. 30. If the curve is multiplied by 0.65, a factor representing a crude estimate of the renormalization attendant upon inclusion of the omitted effects, then the magnitude is in better agreement with the parametrization. Following this rescaling, one finds that the large-$x$ behavior is softer than that of the parametrization. Indeed, in this model

$$q_v^{\pi\ \mathrm{IL}}(x;Q_0) \overset{x\simeq 1}{\sim} (1-x)^{\epsilon}, \quad \epsilon \sim 1.53-1.56. \tag{6.47}$$

While this behavior also conflicts with the QCD parton-model prediction [Eq. (6.30)], it is a less striking disagreement than any other result described hitherto.

## B. Modern QCD perspective

Today there are a few approaches to the calculation of parton distribution functions that are firmly founded in QCD. There is the numerical simulation of lattice-regularized QCD of course. There are also frameworks which go beyond modeling by incorporating and ex-

[15]Recall the critical reanalysis of the conclusions drawn from the E615 experiment, which is reviewed in Sec. III.E.

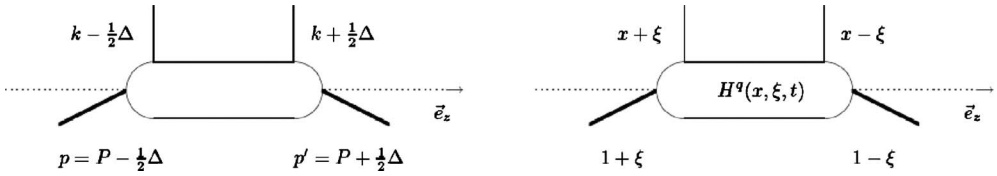


FIG. 37. Handbag diagram contribution to the virtual Compton scattering process: $\gamma^*(q)T(p)\to\gamma(q')T'(p')$. Left panel—kinematic variables in a symmetric reference frame. Right panel—light-front representation of $H^q$ in Eq. (6.48). Adapted from Boffi and Pasquini, 2007.

pressing effects that are rigorously established features of QCD. In the best cases these approaches are directly connected with QCD via a symmetry-preserving truncation so that quantitative calculations can be performed with readily quantifiable errors, which can be estimated *a priori*.

### 1. Generalized parton distributions

These quantities [generalized parton distributions (GPDs)] were considered by Dittes *et al.* (1988) and Müller *et al.* (1998) but have risen to prominence in hadron physics owing to their connection with deeply virtual Compton scattering (Radyushkin, 1996b; Ji, 1997) and hard meson production (Radyushkin, 1996a). Unlike the usual parton distribution functions, GPDs are nondiagonal matrix elements and hence do not have a simple probability interpretation. Instead, GPDs describe interference between amplitudes that represent different partonic configurations within a hadron and provide a means by which to chart correlations between different momentum states of a given parton. They are of interest here because the usual parton distribution functions can be expressed in terms of the GPDs.[16] It follows that either (1) valence-quark distribution functions can be used to constrain the parametrization of GPDs or (2) complete knowledge of GPDs fixes the valence-quark distributions. The former link is used in present-day practice and that will not soon change. Herein we nevertheless elucidate connections between GPDs and PDFs.

In Fig. 37 we show a handbag diagram contribution to a deeply virtual Compton scattering process, in which a high-energy photon with large spacelike virtuality, $Q^2=-q^2$, impacts upon an hadronic target and produces a real photon and an hadronic final state with invariant mass $p^2\ll Q^2$. The amplitude depends on the Bjorken variable $x_B=Q^2/(2p\cdot q)$, defined in Eq. (2.5), and the momentum transfer $t=(p'-p)^2=\Delta^2$. It is assumed that $t\ll Q^2$.

For a spin-$\frac{1}{2}$ hadron $h$ with initial and final helicities, $\lambda$ and $\lambda'$, respectively, one can define eight GPDs. For our purposes it is enough to consider only two of them explicitly, namely, the unpolarized distributions $H_h^q$ and $E_h^q$,

$$\int\frac{dz^-}{8\pi}e^{(i/2)xz^-P^+}\langle h(p',\lambda')|\times\bar{q}\left(-\frac{z}{2}\right)\gamma^+q\left(\frac{z}{2}\right)|h(p,\lambda)\rangle\Big|_{z^+=0,z_\perp=0}=\frac{1}{2P^+}\bar{u}_h(p',\lambda')\left[H_h^q(x,\xi,t)\gamma^+ + E_h^q(x,\xi,t)\frac{1}{2M}\sigma^{+\alpha}\Delta_\alpha\right]u_h(p,\lambda), \tag{6.48}$$

where $x=k^+/P^+$ is the average quark longitudinal-momentum fraction and $\xi=(p^+-p'^+)/(p^++p'^+)$ is the so-called skewness. The GPDs also depend on the resolving scale $Q_0$.

These two GPDs are relevant herein because in the forward limit, i.e., $p'=p$, one has

$$H_h^q(x=x_B,\xi=0,t=0;Q_0)=\begin{cases}q_h(x_B;Q_0), & x_B>0\\ -\bar{q}_h(-x_B;Q_0), & x_B<0,\end{cases} \tag{6.49}$$

from which if follows that

$$\int_{-1}^1 dx x^{2n}H_h^q(x,0,0;Q_0)=\int_0^1 dx x^{2n}q_v^h(x;Q_0)=\langle x^{2n}\rangle_{Q_0}^h. \tag{6.50}$$

Furthermore,

$$\int_{-1}^1 dx H_h^q(x,\xi,t;Q_0)=F_{1h}^q(t),\qquad \int_{-1}^1 dx E_h^q(x,\xi,t;Q_0)=F_{2h}^q(t), \tag{6.51}$$

where, e.g., $F_{1h}^q(t)$ is the contribution to the hadron's Dirac form factor owing to quarks of flavor $q$. The standard normalization is such that

$$F_{1p}^u(t=0)=2, \tag{6.52}$$

$$F_{1p}^d(t=0)=1, \tag{6.53}$$

$$F_{2p}^u(t=0)=\kappa_p^u=2\kappa_p+\kappa_n=1.673, \tag{6.54}$$

[16]For our purposes, we need not consider transversity distributions.

$$F_{2p}^{d}(t=0)=\kappa_p^d=\kappa_p+2\kappa_n=-2.033. \tag{6.55}$$

It is noteworthy that the right-hand sides in Eqs. (6.51) are independent of $\xi$ because integrating over $x$ eliminates all information about the particular light-front direction with respect to which $\xi$ is defined, viz., owing to Lorentz invariance.

Poincaré invariance entails that there is only one generalized quark-parton distribution for the pion (Diehl, 2003),

$$H_\pi^q(x,\xi,t;Q_0)=\int\frac{dz^-}{8\pi}e^{(i/2)xz^-P^+}\langle\pi^+(p')|\bar{q}\left(-\frac{z}{2}\right)\times\gamma^+q\left(\frac{z}{2}\right)|\pi^+(p)\rangle\Big|_{z^+=0,z_\perp=0}. \tag{6.56}$$

Naturally, coupled with the fact that the pion's polarized GPD is identically zero, i.e., $\tilde{H}_\pi\equiv 0$,[17] it follows that $\Delta q_\pi(x)\equiv 0$; i.e., the pion's spin-dependent parton distribution function vanishes. When isospin is a good symmetry, one has

$$H_{\pi^+}^{u+d}:=H_{\pi^+}^u+H_{\pi^+}^d=H_{\pi^-}^{u+d}=H_{\pi^0}^{u+d}, \tag{6.57}$$

$$H_{\pi^+}^{u-d}:=H_{\pi^+}^u-H_{\pi^+}^d=-H_{\pi^-}^{u-d}, \tag{6.58}$$

$$H_{\pi^0}^{u-d}\equiv 0. \tag{6.59}$$

The analogs of Eqs. (6.49) and (6.50) are correct, and, moreover,

$$\int_{-1}^{1}dxH_\pi^q(x,\xi,t;Q_0)=F_\pi^q(t),\quad F_\pi^u(t)-F_\pi^d(t)=2F_\pi(t). \tag{6.60}$$

### 2. Lattice QCD

An operator expression for the pion's quark distribution function is given in Eq. (6.31). We have seen in Sec. VI.B.1 that it is generally true; namely, in a spinless hadron $h$ with total momentum $k$, the distribution function is given by

$$q^h(x;Q_0)=\frac{1}{8\pi}\int_{-\infty}^{\infty}d\xi^-e^{(i/2)xk^+\xi^-}\times\langle h(k)|\bar{\psi}_q(0)\gamma^+\psi_q(\xi^-)|h(k)\rangle. \tag{6.61}$$

This expression is usually understood as representing the distribution in light-cone gauge, i.e., $A_a^+=0$, where $A_a^\mu$ is the gluon field. Equation (6.61) can readily be generalized to bound states with spin.

It is straightforward to modify Eq. (6.61) so that the expectation value is gauge invariant and yet unchanged in light-cone gauge; viz., one introduces a path-ordered exponential (Wilson line)

$$\mathcal{E}(\xi^-):=\mathbf{P}\exp\left\{\frac{i}{2}g\int_{\xi^-}^{0}dz^-\frac{\lambda^a}{2}A_a^+(0,z^-,\vec{0}_\perp)\right\} \tag{6.62}$$

as follows:

$$q^h(x;\mathcal{E};Q_0):=\frac{1}{8\pi}\int_{-\infty}^{\infty}d\xi^-e^{(i/2)xk^+\xi^-}\times\langle h(k)|\bar{q}(0)\gamma^+\mathcal{E}(\xi^-)q(\xi^-)|h(k)\rangle. \tag{6.63}$$

With Eq. (6.63) one has a gauge-invariant expectation value of a bilocal operator evaluated along a lightlike line. It is mathematically precise and provides the pointwise behavior of the distribution function. However, it cannot be evaluated using the numerical approach of lattice-regularized QCD.

Lattice methods can, however, be used to evaluate expectation values of local operators. Consider therefore

$$\langle x^n\rangle_{Q_0}^h:=\int_0^1dxx^n[q^h(x;\mathcal{E};Q_0)-(-1)^n\bar{q}^h(x;\mathcal{E};Q_0)]. \tag{6.64}$$

It is notable that

$$\langle x^0\rangle_{Q_0}^h=\int_0^1dxq_v^h(x;\mathcal{E};Q_0)=N_q^h, \tag{6.65}$$

namely, the number of valence quarks of type $q$ in hadron $h$. Furthermore, in general,

$$\langle x^{2n}\rangle_{Q_0}^h=\int_0^1dxx^{2n}[q^h(x;\mathcal{E};Q_0)-\bar{q}^h(x;\mathcal{E};Q_0)]=\int_0^1dxx^{2n}q_v^h(x;\mathcal{E};Q_0), \tag{6.66}$$

$$\langle x^{2n+1}\rangle_{Q_0}^h=\int_0^1dxx^{2n+1}[q^h(x;\mathcal{E};Q_0)+\bar{q}^h(x;\mathcal{E};Q_0)]. \tag{6.67}$$

It is apparent from these two results that the even moments express properties of a nonsinglet distribution whereas the odd moments probe the singlet distribution. Therefore, they are independent and do not mix under evolution. Importantly, unlike the singlet distribution, a nonsinglet distribution does not receive contributions from disconnected diagrams.

Introducing the Wilson line does not alter the distribution function's domain of support and, moreover, one still has $q^h(x)=-\bar{q}^h(-x)$. Hence,

$$\langle x^n\rangle_{Q_0}^h:=\int_{-1}^1dxx^nq^h(x;\mathcal{E};Q_0)=\int_{-\infty}^{\infty}dxx^nq^h(x;\mathcal{E};Q_0). \tag{6.68}$$

Now, upon insertion of Eq. (6.63), one obtains

[17] With the replacement $\gamma^+\to\gamma^+\gamma_5$ in Eq. (6.48), one arrives at the definition of $\tilde{H}_h$.

$$\langle x^n\rangle_{Q_0}^h = (2k^+)^{-n-1}\langle h(k)|\bar{\psi}_q(0)\gamma^+[iD^+(0)]^n\psi_q(0)|h(k)\rangle, \tag{6.69}$$

where

$$D_\mu(z) = \frac{\partial}{\partial z_\mu} - ig\frac{\lambda^a}{2}A_a^\mu(z) \tag{6.70}$$

is QCD's covariant derivative. [N.B. A connection with Eq. (6.33) is readily established.] The moment on the left of Eq. (6.69) is Poincaré invariant but it only has a probabilistic interpretation in the infinite-momentum frame. Owing to Poincaré invariance, one may equally write

$$2\{k_{\mu_0}k_{\mu_1}\cdots k_{\mu_n}\}\langle x^n\rangle_{Q_0}^h = \langle h(k)|\bar{\psi}_q(0)\{\gamma^{\mu_0}iD^{\mu_1}(0)\cdots iD^{\mu_n}(0)\}\psi_q(0)|h(k)\rangle, \tag{6.71}$$

where the parentheses indicate a symmetrization of indices and the subtraction of traces, e.g., $\{k_{\mu_0}k_{\mu_1}\} = k_{\mu_0}k_{\mu_1} - \delta_{\mu_0\mu_1}k^2$. With Eq. (6.71) one has an expression for the moments of quark distribution functions that can be evaluated using modern lattice-QCD methods (Soper, 1997).

Computations are readily performed for low-order moments; i.e., $n=0,1,2,3$. Of course, owing to Eq. (6.65), there is no information in $\langle x^0\rangle$: it merely provides a check on the numerical procedure. One must also bear in mind that discretized space-time does not possess the full rotational symmetries of the Euclidean continuum. Hence, for $n\geqslant 4$ it is impossible to define lattice operators that are precisely equivalent to those of Eq. (6.71): the lattice analogs cannot transform irreducibly and computations therefore require a numerical determination of the coefficients that describe mixing with operators of lower dimension.

Suppose therefore that one focuses on the $n\leqslant 3$ moments, namely, those most directly accessible within the lattice framework. A typical lattice-QCD result for any one of these moments will contain, in addition to statistical errors, systematic errors from the following sources (Guagnelli *et al.*, 2005): the so-called "quenched approximation"—which is not an approximation but a truncation, and is still common today but will become less so in future; nonperturbative renormalization—the method used to obtain a renormalization-group invariant moment from which continuum results can be inferred; discretization—extrapolation to zero lattice spacing; finite volume—extrapolation to infinite lattice size; and chiral extrapolation—inferring the value of a moment at the real-world current-quark masses from that computed at large unphysical values, which is discussed, e.g., by Detmold *et al.* (2003). The extent to which these errors have been accounted for and the nature of the procedure employed for each type of error must be considered when comparing the value of a moment obtained from a lattice simulation with its empirical or phenomenologically determined value.

TABLE V. Lowest nontrivial moments of the pion's valence $u=d$ quark distribution function. The rows report "Par.92"—moments at $Q_0=2$ GeV determined from the fits of Sutton *et al.* (1992); "Emp.05"—empirical result determined by Wijesooriya *et al.* (2005) at $Q_0=5.2$ GeV. (After evolution, these results are consistent with those in Par.92.) "Lat. 07"—lattice-QCD computation reported by Brommel *et al.* (2007) with nonperturbative evolution to $Q_0=2.0$ GeV (statistical and renormalization error added in quadrature); "Lat. 97$^{\rm Q}$"—quenched computation reported by Best *et al.* (1997), with renormalization scale $Q_0=2.4$ GeV fixed via one-loop chiral-limit lattice perturbation theory (statistical error only); and "Lat. 03"—reanalysis of the results of Best *et al.* (1997) using a different extrapolation to physical current-quark masses (Detmold *et al.*, 2003). The row labeled "DSE 01" is the result obtained using the Dyson-Schwinger equation framework of Hecht *et al.* (2001).

| $\langle x^n\rangle_{Q_0}^\pi$ | $Q_0$ (GeV) | $n=1$ | $n=2$ | $n=3$ |
|---|---|---|---|---|
| Par.92 | 2.0 | 0.24±0.01 | 0.10±0.01 | 0.058±0.004 |
| Emp.05 | 5.2 | 0.217±0.011 | 0.087±0.005 | 0.045±0.003 |
| Lat. 07 | 2.0 | 0.271±0.010 | 0.128±0.008 | 0.074±0.010 |
| Lat. 97$^{\rm Q}$ | 2.4 | 0.273±0.012 | 0.107±0.035 | 0.048±0.020 |
| Lat. 03$^{\rm Q}$ | 2.4 | 0.24±0.02 | 0.09±0.03 | 0.043±0.015 |
| DSE 01 | 2.0 | 0.24 | 0.098 | 0.049 |
| $\langle x^n\rangle_{Q_0}^\rho$ | $Q_0$ (GeV) | $n=1$ | $n=2$ | $n=3$ |
| Lat. 97$^{\rm Q}$ | 2.4 | 0.334±0.021 | 0.174±0.047 | 0.066±0.039 |

Lattice results are available for the first three moments of the pion distribution function; e.g., Best *et al.* (1997) and Brommel *et al.* (2007), with the results reported in Table V. The more recent study (Brommel *et al.*, 2007) employed $O(a)$-improved Clover-Wilson fermions with two flavors of dynamical quarks and pion masses of 430, 600, and 800 MeV. A linear extrapolation in $m_\pi^2$ was used to infer a result at the physical pion mass. They estimated rudimentarily that finite-size effects are of the order of 10% at the smallest pion mass used. Since disconnected diagrams were neglected in calculating all the moments and the simulation pion masses are large, it is reasonable to identify the results with moments of the pion's valence-quark distribution. This interpretation turns lattice artifacts to advantage in order to circumvent practically a problem of principle; viz., it is plain from Eqs. (6.66) and (6.67) that odd moments of the valence-quark distribution are not readily accessible via the vector current operator. The valence-quark distribution is directly accessible though moments of the more complicated $V-A$ current operator.

The earlier study (Best *et al.*, 1997) used Wilson fermions in a quenched simulation, with current-quark masses which correspond to $m_\pi\approx 480$, 650, and 780 MeV. Values for the moments at a physical light-quark current mass were obtained through linear extrapolation in $m_\pi^2$. This could plausibly therein lead to overestimation of the first three moments by 10–20 % (Detmold *et al.*, 2003) (see Table V) and therefore also by Brommel *et al.* (2007).

It is curious that there is little material difference between the results in rows 3–5: all agree within quoted errors even though they were obtained over a ten-year time span in which lattice methods improved greatly. In our view, for this reason and because the pion is so important to strong-interaction physics, the evaluation of the pion's moments is a problem worth renewed attention.

Low moments of the $\rho$ meson's valence-quark distribution functions are also inferred by Best *et al.* (1997). There are three different structure functions for the spin-1 $\rho$: unpolarized, with moments denoted by $a_n$; polarized, with moments denoted by $r_n$; and spin projection, with moments denoted by $d_n$. The spin-projection structure function is absent for a spin-$\frac{1}{2}$ hadron. In the infinite-momentum frame it measures the difference between quark distributions in $J_z=1$ and 0 targets. Here, however, we are concerned with unpolarized distributions and so only $a_{1,2,3}$ are listed in Table V. With the parameters of this lattice simulation, the $\pi$ and $\rho$ moments differ noticeably and the first moments do not agree within statistical errors. It appears to us, therefore, that it is obtuse to claim that the results of Best *et al.* (1997) support an assumption that $F_1^\rho(x) \approx F_1^\pi(x)$, as was done therein.

More attention has focused on the nucleon, with the first computations in Martinelli and Sachrajda (1989) and an overview in Zanotti (2008), but it remains true that disconnected diagrams are neglected in almost all extant studies. It follows that only results for isovector quantities are directly comparable with those determined empirically, i.e.,

$$\langle x^n\rangle_{Q_0}^{u-d} := \langle x^n\rangle_{Q_0}^{p-n}. \tag{6.72}$$

For the reason noted above, calculations are restricted to at most the first three nontrivial moments. We list some results in Table VI.

We present two sets of determinations from Dolgov *et al.* (2002). Both were obtained with Wilson fermions. However, one set was computed in quenched-QCD, while the other was calculated using two degenerate flavors of dynamical sea quarks, with four current-quark mass values that provide for $m_\pi/m_\rho \in [0.69, 0.83]$. Perturbative renormalization was employed to quote results at $Q_0=2$ GeV. The studies possess significant but unquantified finite-size and volume errors, and a linear extrapolation in $m_\pi^2$ was used to infer results at physical current-quark masses.

The fifth row of results in Table VI is compiled from Göckeler *et al.* (2005), a quenched-QCD study that employed an $O(a)$-improved Wilson action and fully nonperturbative renormalization to reach $Q_0=2.0$ GeV. They argued that finite-volume errors were unimportant and were attentive in estimating systematic errors arising from nonperturbative renormalization, operator choice, and continuum and linear chiral extrapolations.

We also list the estimate made by Hägler *et al.* (2008) for the $n=1$ moment, which was the only moment considered therein. This analysis employed a mixed-action approach, namely, domain-wall valence quarks but 2+1 flavors of staggered sea quarks, with light-quark masses corresponding to $m_\pi=350$ MeV. A nonperturbatively improved perturbative renormalization scheme was used to quote a result at $Q_0=2$ GeV. It was argued that finite-volume errors are negligible with respect to statistical errors, while errors associated with nonzero lattice spacing ($a=0.124$ fm) were not discussed. In order to quote a result at the physical pion mass, covariant baryon chiral perturbation theory was employed (Dorati *et al.*, 2008). As anticipated by Detmold *et al.* (2001), an extrapolation nonlinear in $m_\pi^2$ can have an enormous impact: in this instance, a 25% reduction in the value of the moment.

A consideration of Fig. 38 and the results listed in Table VI demonstrate that agreement between the empirical value of $\langle x\rangle^{u-d}$ and that obtained using lattice-QCD is only possible if there is significant nonlinearity in the $m_\pi^2$ dependence of $\langle x\rangle^{u-d}$ on $m_\pi^2 < 0.1$ GeV$^2$. On the other hand, given that a chiral expansion of physical quantities is invalid for $m_\pi^2 \gtrsim 0.2$ GeV$^2$ (Chang *et al.*, 2007) and reliable lattice results are restricted to this domain, it is unsurprising that extant results from lattice QCD do not exhibit nonlinearity.

TABLE VI. Lowest nontrivial moments of the isovector nucleon distribution function, all evolved to $Q_0=2$ GeV, albeit using different methods. While they are all moments of nonsinglet distributions, in principle, only $n=2$ is connected with a difference of valence-quark distributions. The rows report "Emp.90"—empirical result determined from the parametrizations of $x[u_v(x)+d_v(x)]$ and $xd_v(x)$ in Kwiecinski *et al.* (1990), which were fitted to then-extant data via next-to-leading-order evolution from a starting scale of $Q_0=2.0$ GeV [these values are little changed in more modern parametrizations, e.g., using MRST 2002, available through the Durham database (Durham, 2009), $\langle x\rangle_{2\,\mathrm{GeV}}^{u_v-d_v}=0.157\pm0.009$, as indicated in the row labeled "Emp.02"]; "Lat. 02$^{\mathrm{Q}}$" and "Lat. 02"—lattice QCD computations reported by Dolgov *et al.* (2002), the former in quenched QCD, both with perturbative evolution to $Q_0$ and linear chiral extrapolation (statistical error only); "Lat. 05$^{\mathrm{Q}}$"—quenched-QCD study described in Göckeler *et al.* (2005), with renormalization scale $Q_0$ fixed via nonperturbative renormalization and linear chiral extrapolation (error is statistical combined with estimates of systematic errors arising from renormalization, operator choice, and continuum and chiral extrapolations); "Lat. 08"—analysis reported by Hägler *et al.* (2008), with renormalization scale $Q_0$ fixed via nonperturbatively improved one-loop renormalization and extrapolation via covariant baryon chiral perturbation theory (Dorati *et al.*, 2008) (before extrapolation $\langle x\rangle^{u-d}\simeq 0.205\pm0.015$, statistical error only).

| $\langle x^n\rangle_{Q_0}^{u-d}$ | $n=1$ | $n=2$ | $n=3$ |
|---|---|---|---|
| Emp.90 | 0.16 | 0.054 | 0.023 |
| Emp.02 | $0.157\pm0.009$ | | |
| Lat. 02$^{\mathrm{Q}}$ | $0.251\pm0.018$ | $0.098\pm0.068$ | $0.028\pm0.049$ |
| Lat. 02 | $0.269\pm0.023$ | $0.145\pm0.069$ | $0.078\pm0.041$ |
| Lat. 05$^{\mathrm{Q}}$ | $0.245\pm0.009$ | $0.083\pm0.017$ | $0.059\pm0.018$ |
| Lat. 08 | $0.157\pm0.010$ | | |

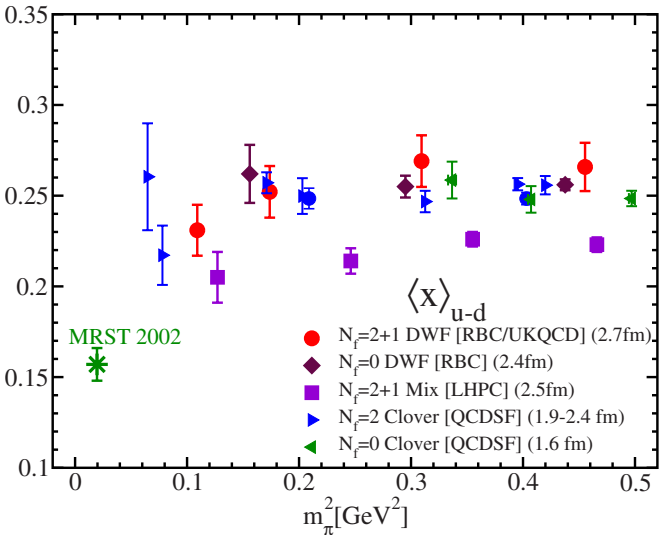


FIG. 38. (Color online) Current-quark-mass dependence of $\langle x \rangle_{Q_0}^{u-d}$, $Q_0$=2 GeV, computed directly through numerical simulations of lattice-regularized QCD: circles (Ohta and Yamazaki, 2008); diamonds (Orginos *et al.*, 2006); boxes (Hägler *et al.*, 2008); right triangles (Brommel *et al.*, 2008); and left triangles (Göckeler *et al.*, 2005). The empirical value is marked by an asterisk. The clover and domain wall fermion results are in excellent agreement, except at the lightest pion mass, a discrepancy which can likely be attributed to finite-size effects. The mixed-action results appear to differ from the others by a normalization factor, which is perhaps understandable given that Hägler *et al.* (2008) does not use the fully nonperturbative renormalization procedure employed in the other studies. Adapted from Zanotti, 2008.

It is evident from the discourse in this section that contemporary lattice QCD provides little aid in understanding the vast amount of DIS data, in general, and the valence-quark distributions, in particular. Practitioners express hope that this will change. However, it should be noted that low moments of parton distribution functions are only very weakly sensitive to the pointwise behavior of $q^h(x;Q_0)$ on $x \gtrsim 0.4$. For example, consider two valence-quark distributions with large-$x$ behavior $(1-x)^{1.15}$ (Sutton *et al.*, 1992) and $(1-x)^{1.80}$ (Hecht *et al.*, 2001). The exponents differ by 60% but the $n=3$ moments, which are the highest accessible in modern lattice-QCD calculations, are indistinguishable within experimental error. One must compute the $n=5$ moments before the difference exceeds 20%. Plainly, pointwise calculations of the distribution functions are vital in order to probe the valence region.

### 3. Dyson-Schwinger equations

As elucidated by Roberts and Williams (1994), the Dyson-Schwinger equations (DSEs) are a system of coupled integral equations that have long been used in nuclear and particle physics. The DSEs provide a nonperturbative approach to QCD in the continuum and are particularly well suited to the study of QCD because of asymptotic freedom, which entails that model dependence can always, in principle, be restricted to infrared momenta, viz., $p \lesssim 1$ GeV. Today, some elements of the approach are well constrained even on that domain owing to positive feedback between DSE and lattice-QCD studies. Applications of DSEs to hadron physics are reviewed by Roberts and Schmidt (2000), Alkofer and von Smekal (2001), Maris and Roberts (2003), Fischer (2006), and Roberts *et al.* (2007).

The physics of hadrons is ruled by two emergent phenomena, namely, confinement and dynamical chiral-symmetry breaking. Confinement is the empirical fact that no quarks have been detected in isolation. Dynamical chiral-symmetry breaking (DCSB), which is responsible among many other things, for the large mass splitting between parity partners in the spectrum of light-quark hadrons, that is present even though the relevant Lagrangian current-quark masses are small, explains the origin of constituent-quark masses and underlies the success of chiral effective-field theory. Neither confinement nor DCSB is apparent in QCD's Lagrangian but yet they play a dominant role in determining the observable characteristics of real-world QCD.

With respect to confinement, it is important to appreciate that the static potential measured in quenched lattice QCD is not related in any simple way to the question of light-quark confinement. It is a basic feature of QCD that light-quark creation and annihilation effects are nonperturbative and thus it is impossible, in principle, to compute a potential between two light quarks (Bali *et al.*, 2005).

On the other hand, confinement can be related to the analytic properties of QCD's Schwinger functions (Roberts *et al.*, 1992; Roberts and Williams, 1994; Roberts, 2008), which are the basic elements of the DSE approach. Hence the question of light-quark confinement can be translated into the challenge of charting the infrared behavior of QCD's universal $\beta$ function.[18] Solving this well-posed problem is an elemental goal of modern hadron physics. It can be addressed in any framework enabling the nonperturbative evaluation of renormalization constants.

Through the DSEs, the pointwise behavior of the $\beta$ function determines the pattern of chiral-symmetry breaking. Moreover, the DSEs connect the $\beta$ function to experimental observables, so that a comparison between computations and observations of, e.g., the valence-quark distribution functions, can be used to learn about the evolution of the $\beta$ function into the nonperturbative domain.

A notable and relevant recent success of the DSE approach to hadron physics is its provision of an understanding of DCSB via QCD's gap equation. The dressed-

[18]This function may depend on the scheme chosen to renormalize the theory but it is unique within a given scheme (Celmaster and Gonsalves, 1979).

quark propagator can be written in a number of equivalent forms, e.g.,[19]

$$S(p) = -i\gamma\cdot p\sigma_V(p^2,\zeta^2) + \sigma_S(p^2,\zeta^2) = \frac{1}{i\gamma\cdot pA(p^2,\zeta^2) + B(p^2,\zeta^2)} = \frac{Z(p^2,\zeta^2)}{i\gamma\cdot p + M(p^2)}. \tag{6.73}$$

It is important that the mass function $M(p^2) = B(p^2,\zeta^2)/A(p^2,\zeta^2)$, shown in Fig. 11, is independent of the renormalization point, $\zeta$. Furthermore, this propagator and, indeed, all colored Schwinger functions are gauge covariant. Therefore, when contracted in the expression for a color-singlet and gauge-invariant observable, all information about the evolution of the quark mass with momentum, shown in Fig. 11, is retained. Hence, this manifestation of DCSB has an impact on cross sections that is truly observable.

The impact is greatly amplified in observables involving the pion, which, as QCD's Goldstone mode, is innately connected with DCSB. Indeed, the DSEs explain the pion as simultaneously both a Goldstone mode and an intricate bound state of a dressed quark and antiquark, described by a Bethe-Salpeter amplitude,

$$\Gamma_\pi(k;P) = \gamma_5[iE_\pi(k;P) + \gamma\cdot PF_\pi(k;P) + \gamma\cdot kk\cdot PG_\pi(k;P) + \sigma_{\mu\nu}k_\mu P_\nu H_\pi(k;P)]. \tag{6.74}$$

Through the axial-vector Ward-Takahashi identity, which is the statement of chiral-symmetry and the pattern by which it is broken, the DSEs yield (Maris *et al.*, 1998) a set of Goldberger-Treiman relations for the pion, which are exact in the chiral limit, viz.,

$$f_\pi E_\pi(k;0) = B(k^2), \tag{6.75}$$

$$F_R(k;0) + 2f_\pi F_\pi(k;0) = A(k^2), \tag{6.76}$$

$$G_R(k;0) + 2f_\pi G_\pi(k;0) = 2A'(k^2), \tag{6.77}$$

$$H_R(k;0) + 2f_\pi H_\pi(k;0) = 0, \tag{6.78}$$

where the functions on the right-hand sides are defined in Eq. (6.73); $f_\pi$ represents here the pion's leptonic decay constant; and $F_R$, $G_R$, and $H_R$ are associated with terms in the axial-vector vertex that are regular in the neighborhood of the pion pole.

The first of these relations [Eq. (6.75)] states that in the chiral limit the dominant pseudoscalar part of the pion's Bethe-Salpeter amplitude is completely determined by the scalar piece of the dressed-quark self-energy. This exact result in QCD expresses an extraordinary fact; viz., owing to DCSB, the solution of the two-body problem in the pseudoscalar channel is known, almost completely, once the quark one-body problem is solved.[20] In combination with the feature that the dressed-quark propagator has a spectral representation when considered as a function of current-quark mass (Langfeld *et al.*, 2003), Eq. (6.75) entails that the chiral-limit dressed-quark scalar self-energy provides an accurate pointwise approximation to $E_\pi(k;P)$ at physical light-quark current masses.

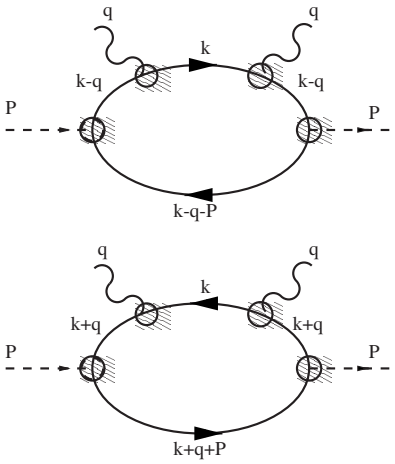


FIG. 39. "Handbag" contributions to the virtual-photon-pion forward Compton scattering amplitude. $\pi$, dashed line; $\gamma$, wavy line; $\mathcal{S}$, internal solid line, dressed-quark propagator [Eq. (6.73)]. The filled circles represent the pion's Bethe-Salpeter amplitude $\Gamma_\pi$, in Eq. (6.74) and the dressed-quark-photon vertex $\Gamma_\mu$, discussed in Appendix B, depending on which external line they begin or end. Adapted from Hecht *et al.*, 2001.

It will now be evident that, through the mesonic analog of Fig. 26, shown in Fig. 39, the leading $x$ dependence of the physical pion's valence-quark distribution function is determined by the chiral-limit dressed-quark scalar self-energy. As with the electromagnetic pion form factor, the leading-order contribution is accurate apart from small corrections to the anomalous dimension (Maris and Roberts, 1998; Maris and Tandy, 2000a). This has far reaching consequences, which can be revealed by considering the gap equation.

Imagine a theory in which the kernel of the gap equation behaves as

$$\alpha(q^2)/q^2 \overset{q^2\gg M_D^2}{\propto} (1/q^2)^{1+\kappa}, \tag{6.79}$$

where $\kappa>0$ and $M_D^2$ is some intrinsic, characteristic scale. Then, using the method of Higashijima (1984) and Roberts and McKellar (1990), one finds

[19] In order to maintain easy contact with existing literature, in this section we employ a Euclidean metric. In concrete terms that means for Dirac matrices $\{\gamma_\mu,\gamma_\nu\}=2\delta_{\mu\nu}$, $\gamma_\mu^\dagger=\gamma_\mu$, $\gamma_5=\gamma_4\gamma_1\gamma_2\gamma_3$, $\mathrm{tr}\gamma_5\gamma_\mu\gamma_\nu\gamma_\rho\gamma_\sigma=-4\varepsilon_{\mu\nu\rho\sigma}$, and $a\cdot b=\Sigma_{i=1}^4 a_i b_i$. A timelike vector $p_\mu$ has $p^2<0$. More information can be found in Sec. 2.1 of Roberts and Schmidt (2000).

[20] The following three relations establish that the pion necessarily has pseudovector components because the dressed-quark wave-function renormalization is not identically one. This fact has an extremely important impact on the pion's electromagnetic form factor at large momentum transfer (Maris and Roberts, 1998; Gutiérrez-Guerrero *et al.*, 2010).

$$B(k^2) \overset{k^2 \gg M_D^2}{\propto} (1/k^2)^{1+\kappa}. \tag{6.80}$$

The case of QCD is similar: the kernel is

$$\frac{\alpha(q^2)}{q^2} \overset{q^2 \gg \Lambda_{\rm QCD}^2}{=} \frac{1}{q^2} \frac{\lambda \pi}{\ln[q^2/\Lambda_{\rm QCD}^2]}, \tag{6.81}$$

where $\lambda = 12/(33-2n_f)$, with $n_f$ as the number of active fermion flavors, and

$$B(k^2) \overset{k^2 \gg \Lambda_{\rm QCD}^2}{\propto} \frac{\lambda}{k^2} \left( \frac{1}{\ln[k^2/\Lambda_{\rm QCD}^2]} \right)^{1-\lambda}. \tag{6.82}$$

The general pattern should now be clear; namely, the momentum dependence of the chiral-limit dressed-quark self-energy replicates, up to an anomalous dimension, that of the quark-quark interaction and this behavior is manifest for $k^2 \gg M_D^2$.

With this perspective, the analysis of Ezawa (1974) can now be understood to predict that, in a theory with an interaction of the type in Eq. (6.79), the pion's valence-quark distribution function must evolve according to

$$q_v^\pi(x;Q_0) \overset{x\sim 1}{\propto} (1-x)^{2(1+\kappa)} \quad \forall\, Q_0 \gg M_D. \tag{6.83}$$

This indicates and interprets the scale at which "counting-rule" behavior should be evident; viz., it is the mass scale at which the asymptotic form of the evolution of the chiral-limit dressed-quark scalar self-energy is manifest.

One can readily translate the preceding argument into a QCD prediction, namely,

$$q_v^\pi(x;Q_0) \overset{x\sim 1}{\propto} (1-x)^{2+\gamma}, \quad Q_0 \simeq 1\ {\rm GeV}, \tag{6.84}$$

where $0 < \gamma \ll 1$ is an anomalous dimension because, as shown in Fig. 11, $1\ {\rm GeV}^2 \approx 20\Lambda_{\rm QCD}^2$ is the mass scale at which the chiral-limit dressed-quark mass function has assumed its asymptotic form [Eq. (6.82)]. Given Eq. (6.83), it is unsurprising that the exponent 2 in Eq. (6.84) is a lower bound. As indicated, the additional logarithmic correction to the momentum dependence of the mass function, a manifestation of asymptotic freedom, leads truly to an exponent greater than 2 at the counting-rule resolving scale. Moreover, this exponent increases under QCD evolution to $Q > Q_0$.

It is now instructive to reconsider Eq. (6.83) in connection with models of the NJL type (Sec. VI.A.6). Such a model, in the chiral limit and regularized in a translationally invariant manner, may be realized through an analytic continuation of Eq. (6.79) to $\kappa = -1$. One then reads the mass function from Eq. (6.80): $\forall k^2$, $B(k^2) = m_Q$, i.e., a constant. The pion's valence-quark distribution function in this model follows from Eq. (6.83): $q_v^{\pi\ {\rm NJL_{TI}}}(x) = 1$. In the absence of any regularization scale, this is the chiral-limit prediction at all resolving scales. Of course, in concrete applications of such models, an ultraviolet regularization scale is finally introduced: typically $\Lambda_{\rm UV} \sim 1$ GeV. The model's practitioners describe this scale as the boundary between the nonperturbative and perturbative domains. As the only scale in the model's description of a chiral-limit pion, it should properly define the model's intrinsic resolving scale. Hence, one arrives at the prediction

$$q_v^{\pi\ {\rm NJL_{TI}}}(x; Q_0 = \Lambda_{\rm UV}) = 1. \tag{6.85}$$

Our modernization of the analysis of Ezawa (1974) serves to eliminate much of the ambiguity in understanding what is meant by the "QCD prediction" for $q_v^\pi(x)$. We have provided a clean definition of the resolving scale at which this prediction should be valid. Moreover, with Eqs. (6.83)–(6.85) and the associated discussion, we have demonstrated that the *pointwise* behavior of the pion's quark distribution function on the valence-quark domain is a sensitive probe of the nature of the quark-quark interaction. To be concrete, if the conclusion of Conway *et al.* (1989) is confirmed, then the theory underlying hadron physics is not QCD. The arguments can be generalized to other hadrons.

Additional information can be explicated through a recapitulation of a calculation of the pion's valence-quark distribution function within the DSE framework. The diagrams in Fig. 39, an explicit realization of Fig. 32, provide the starting point for the computation of Hecht *et al.* (2001). The upper diagram represents the renormalized matrix element,

$$T_{\mu\nu}^+(q,P) = {\rm tr} \int \frac{d^4k}{(2\pi)^4} [\tau_- \Gamma_\pi(k_\Gamma; -P) S(k_t) ie Q \Gamma_\nu(k_t,k) \times \underline{S(k)} ie Q \Gamma_\mu(k,k_t) S(k_t) \tau_+ \Gamma_\pi(k_\Gamma; P) \underline{S(k_s)}], \tag{6.86}$$

where $\tau_\pm = \frac{1}{2}(\tau_1 \pm i\tau_2)$ is a combination of Pauli matrices; $\mathcal{S}(\ell) = {\rm diag}[S_u(\ell), S_d(\ell)]$, with $S_u = S_d = S$, assuming isospin symmetry, and $k_\Gamma = k - q - P/2$, $k_t = k - q$, and $k_s = k - q - P$. The fully dressed-quark-photon vertex $\Gamma_\mu(\ell_1, \ell_2)$ appeared in Eq. (6.34) and here $Q = {\rm diag}(2/3, -1/3)$ is the quark-charge matrix. The matrix element represented by the lower diagram is the crossing partner of Eq. (6.86) and is obvious by analogy. The hadronic tensor relevant to inclusive deep inelastic lepton-pion scattering can be obtained from the forward Compton process via the optical theorem,

$$W_{\mu\nu}(q;P) = W_{\mu\nu}^+(q;P) + W_{\mu\nu}^-(q;P) = \frac{1}{2\pi} {\rm Im}[T_{\mu\nu}^+(q;P) + T_{\mu\nu}^-(q;P)]. \tag{6.87}$$

In the Bjorken limit one finds explicitly (Hecht *et al.*, 2001)

$$W_{\mu\nu}^+(q;P) = F_1^+(x) t_{\mu\nu} + F_2^+(x) q_\mu^t q_\nu^t / 2x, \tag{6.88}$$

$t_{\mu\nu} = \delta_{\mu\nu} - q_\mu q_\nu / q^2$, $q_\mu^t = q_\mu + 2xP_\mu$, and

$$F_2^+(x) = 2xF_1^+(x), \quad F_{1,2}^+(x) \to 0 \text{ as } x \to 1. \tag{6.89}$$

Combining these results with their analogs for $W_{\mu\nu}^-$, one recovers Bjorken scaling of the deep inelastic cross section; namely, the cross section depends only on $x$ and not separately on $P \cdot q$ and $q^2$. One may therefore write

$$F_2^{e\pi}(x) = F_2^+(x) + F_2^-(x) = \tfrac{4}{9}[xu(x) + x\bar{u}(x)] + \tfrac{1}{9}[xd(x) + x\bar{d}(x)] + \cdots, \tag{6.90}$$

where the ellipsis denotes contributions from heavier quarks, which are small. We emphasize that this result is only valid at lowest order in the strict Bjorken limit. It is not preserved under QCD evolution (see Sec. II.D).

In an explicit calculation of the handbag diagrams (Fig. 39), the resolving scale is exposed through the act of taking the imaginary part when employing the optical theorem in Eq. (6.87). At this point a snapshot is taken of the dressed-quark propagators underlined in Eq. (6.86). Their dressing functions are sampled at the particular renormalization point and this defines the resolving scale $Q_0$. One can recover the analysis of Ezawa (1974), augmented by perturbative QCD evolution, by pursuing this route at a resolving scale deep into the perturbative domain.

On the other hand, Hecht *et al.* (2001) employed algebraic *Ansätze* for the elements in Eq. (6.86) whose form is known even on the nonperturbative domain. They are determined by studies of meson properties (Burden *et al.*, 1996; Roberts, 1996; Maris and Roberts, 1998) and exhibit behavior that is broadly consistent with that of QCD's $n$-point functions; viz., the ultraviolet power laws are explicitly expressed but the logarithms are suppressed in order to achieve a level of simplicity. Hence, following the path described above, Hecht *et al.* (2001) delivered a representation of the pion's distribution functions at an infrared resolving scale through the definitions

$$u_v^\pi(x;Q_0) \coloneqq \tfrac{9}{2}F_1^+(x;Q_0), \quad d_v^\pi(x;Q_0) \coloneqq 18F_1^-(x;Q_0). \tag{6.91}$$

How should Eqs. (6.91) be understood? Hecht *et al.* (2001), interpreted the computation within the setting of a rainbow-ladder DSE truncation. Hence, sea-quark contributions are absent because they cannot appear without nonperturbative dressing of the quark-gluon vertex (Cloët and Roberts, 2008; Chang and Roberts, 2009; Chang *et al.*, 2009). Thus, Eqs. (6.91) describe valence-quark distribution functions and one should have

$$\int_0^1 dx u_v^\pi(x;Q_0) = 1 = \int_0^1 dx \bar{d}_v^\pi(x;Q_0), \tag{6.92}$$

viz., the $\pi^+$ contains one and only one $u$-valence quark and one $\bar{d}$-valence quark. Note that one has $\bar{d}_v^{\pi^+}(x;Q_0) = u_v^{\pi^+}(x;Q_0) = d_v^{\pi^-}(x;Q_0)$ in this calculation.

It is a deficiency of this and kindred calculations that the model's resolving scale is not determined *a priori*. This can be overcome by calculating the moments of the pion's distribution via Eq. (6.33), in which case the resolving scale is identical to the renormalization point used in computing the dressed Schwinger functions. The cost of that approach, however, is a loss of direct knowledge about the distribution's pointwise evolution. Hecht *et al.* (2001) choose $Q_0$ so that the computed distribution, when evolved to $Q_0' = 2$ GeV using leading-order formulas, produced first and second moments in agreement with those reported by Sutton *et al.* (1992). This yields[21] $Q_0 = 0.54$ GeV so that Eq. (6.92) is satisfied with a valence-quark mass $M = 0.30$ GeV $\approx M(Q_0)$.

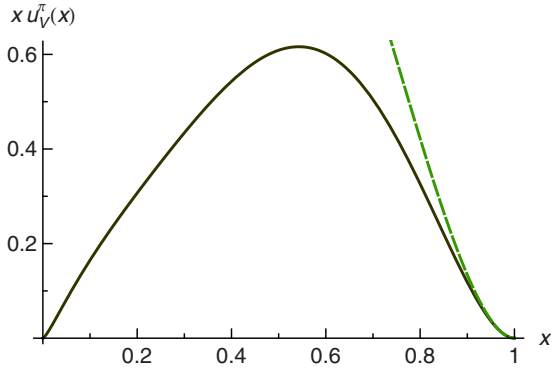


FIG. 40. (Color online) Solid curve, pion's valence-quark momentum distribution computed by Hecht *et al.* (2001). Dashed curve, $A(1-x)^{\eta_2}$, with the parameters drawn from Eq. (6.97).

It is apparent that this procedure views the distributions defined in Eqs. (6.91) as infrared boundary-value input for the valence-quark evolution equations. This is strictly valid only if all nonperturbative corrections are negligible for $Q > Q_0$, a constraint whose faithful implementation would require $Q_0 > 1$ GeV. On the other hand, it might be an efficacious approximation as long as $\alpha(Q_0)^2/(4\pi^2) \ll 1$. In this connection, it is notable that

$$\alpha(Q_0)^2/4\pi^2 = 0.017, \quad Q_0 = 0.54 \text{ GeV}, \tag{6.93}$$

whereas $\alpha(0.5Q_0)^2/(4\pi^2) = 0.60$. Plainly, there is a narrow domain upon which this perspective may be reasonable. This view mirrors that described in Sec. V.C. Furthermore, and significantly, these considerations do not affect the pointwise behavior of the distribution function at $Q_0$.

The valence-quark distribution function computed by Hecht *et al.* (2001) is shown in Fig. 40. From this form one finds the momentum fraction carried by the valence quarks, viz.,

$$\langle x_q \rangle^\pi_{Q_0=0.54 \text{ GeV}} = \int_0^1 dx x[u_v^\pi(x;Q_0) + \bar{d}_v^\pi(x;Q_0)] = 0.72. \tag{6.94}$$

The remainder is carried by the gluons, namely, $\langle x_g \rangle^\pi_{Q_0} = 0.28$, which are invisible to the electromagnetic probe, since the sea distribution is zero at $Q_0$. The pion is a bound state of finite extent formed through the exchange of dressed gluons between a dressed quark and antiquark, and hence gluons are necessarily always present. It is therefore plain that at no resolving scale

[21] The quantitative similarity between this and the mass scale for LO evolution in Sec. V.C is noteworthy.

could all the pion's momentum be carried by the valence quarks. For comparison, the parametrized valencelike pion parton distributions of Glück *et al.* (1999) yield a gluon momentum fraction of[22] $\langle x_g \rangle^{\pi}_{Q_0}=0.29$ at $Q_0=0.51$ GeV. From Hecht *et al.* (2001), the second and third moments are

$$\langle x^2_{u+\bar{d}} \rangle^{\pi}_{Q_0=0.54\ \mathrm{GeV}} = 0.36, \quad \langle x^3_{u+\bar{d}} \rangle^{\pi}_{Q_0=0.54\ \mathrm{GeV}} = 0.21. \tag{6.95}$$

The low moments are primarily determined by the distribution function's behavior at small $x$ (see Sec. VI.B.2). Sensitivity to the nature of QCD's interaction is found at large $x$, which corresponds to large relative momentum between the dressed quark and antiquark. Two questions come immediately to mind, namely, what should one expect for the $x$ dependence of the distribution in Fig. 40 at large $x$ and what truly constitutes the large-$x$ domain?

The first question is readily answered. In this case $Q_0^2 \gtrsim 5\Lambda^2_{\mathrm{QCD}}$, which corresponds to a scale whereat the chiral-limit mass function is dropping rapidly but does not yet exhibit the behavior associated with its truly asymptotic momentum dependence: $Q_0=0.54$ GeV does not lie beyond the inflexion point of the chiral-limit mass function (see Fig. 11). One would therefore anticipate that, for $x\sim 1$, $u_v(x;Q_0=0.54\ \mathrm{GeV}) \approx (1-x)^{\eta}$, with $\eta \lesssim 2$. It was found by Hecht *et al.* (2001) that the distribution in Fig. 40 is pointwise accurately interpolated by the function

$$x u_v^{\pi}(x;Q_0) = A x^{\eta_1}(1-\epsilon\sqrt{x}+\gamma x)(1-x)^{\eta_2} \tag{6.96}$$

with the fit parameters taking the values

| $A$ | $\eta_1$ | $\epsilon$ | $\gamma$ | $\eta_2$ |
|---|---|---|---|---|
| 11.24 | 1.43 | 2.44 | 2.54 | 1.90 |

. (6.97)

These parameters depend on $Q_0$ and the value of $\eta_2$ is fully consistent with expectation.

The second question posed above can now also be answered quantitatively using Eqs. (6.96) and (6.97). The dashed curve in Fig. 40 is the component of Eq. (6.96) which dominates the $x$ dependence of $u_v^{\pi}(x;Q_0)$ at "large $x$." On the domain

$$\mathcal{L}_x = \{x | x > 0.86\}, \tag{6.98}$$

the dominant component agrees at the level of 20% or better with the full curve. The extent of this domain depends weakly on the mass scale $M_D$: it is a little larger in a model with a smaller value of $M_D$ and the disagreement increases to 37% at $x=0.76$

From Hecht *et al.* (2001), using leading-order evolution, the distribution in Fig. 40 is evolved to $Q_0=2$ and 4 GeV. The $u$-quark moments at the former scale are presented in Table V and the curve at the latter scale is presented in Fig. 16.

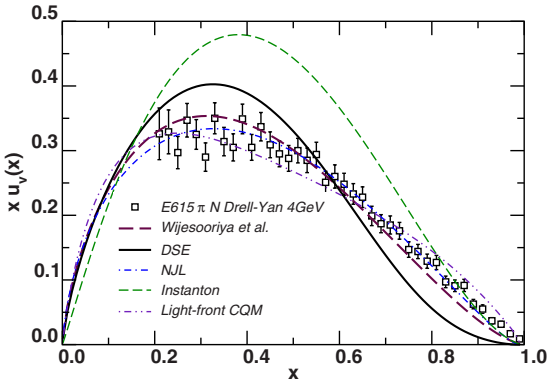


FIG. 41. (Color online) Compilation of results for the valence-$u$-quark distribution in the pion: solid curve, DSE result (Hecht *et al.*, 2001); dotted-dashed curve, NJL model (see Sec. VI.A.6); short-dashed curve, instanton model (Dorokhov and Tomio, 2000); dash-dot-dotted curve, light-front constituent-quark model (Frederico and Miller, 1994); squares, Drell-Yan data presented by Conway *et al.* (1989); and long-dashed curve, reanalysis of that Drell-Yan data described by Wijesooriya *et al.* (2005), which is also shown in Fig. 18. All calculations evolved at leading order to $Q_0=4.0$ GeV using a four-flavor value of $\Lambda_{\mathrm{QCD}}=0.204$ GeV, except that from Wijesooriya *et al.* (2005), which is reported at $Q_0=5.2$ GeV.

In Fig. 41 we display a compilation of results for the valence-$u$-quark distribution in the pion. The elucidation here explains why only the DSE prediction exhibits behavior at large $x$ that is consistent with the QCD parton model [Eq. (6.84)] first derived by Ezawa (1974) and Farrar and Jackson (1975). The discussion of Wijesooriya *et al.* (2005) and Sec. III.E shows that one cannot draw firm conclusions about the large-$x$ behavior of the pion's valence-quark distribution function from the single extant $\pi N$ Drell-Yan experiment (Conway *et al.*, 1989). The status of QCD as the strong-interaction piece of the standard model will seriously be challenged if an improved experiment, such as that canvassed in Wijesooriya *et al.* (2001), is also incompatible with Eq. (6.84).

Computations of the valence-quark distribution functions in other mesons are underway (Nguyen, 2010; Nguyen *et al.*, 2010) using the DSE approach that successfully predicted the pion's electromagnetic form factor (Maris and Tandy, 2000a, 2000b). The impact of the dressed-quark mass function on the ratio $u_v^K(x)/u_v^{\pi}(x)$ is shown in Fig. 42. In comparison with the nonpointlike-pion-regularized NJL result of Shigetani *et al.* (1993), one finds that the momentum-dependent mass function markedly affects the separate behaviors of $u_v^{\pi}(x)$ and $u_v^K(x)$, especially on the valence-quark domain. However, the preliminary indication is that it does not materially affect the ratio, e.g.,

[22] A novel perspective on the magnitude of a hadron's gluon momentum fraction is discussed by Chen *et al.* (2009a, 2009b) and Ji (2009).

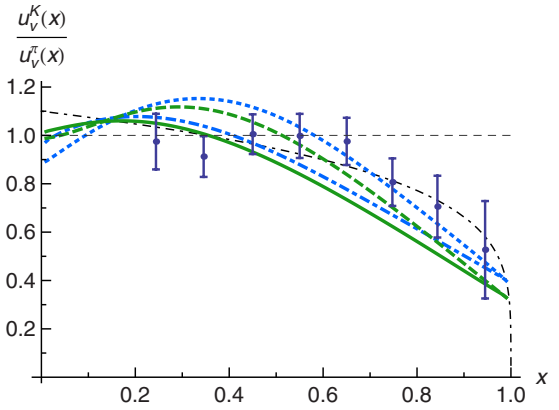


FIG. 42. (Color online) Solid curve, preliminary Dyson-Schwinger equation prediction for the ratio of kaon-to-pion valence-quark distribution functions at $Q_0=5$ GeV, evolved at leading order from the dashed curve, which is the DSE prediction at $Q_0=0.57$ GeV (Nguyen, 2010; Nguyen *et al.*, 2010). Dotted and dash-dotted curves, our reevaluation of $u_v^K(x)/u_v^\pi(x)$ using the model of Shigetani *et al.* (1993); filled circles, the ratio of kaon-to-pion Drell-Yan cross sections obtained from a sample of dimuon events with invariant mass $4.1<M<8.5$ GeV (Badier *et al.*, 1980); thin dashed line, the curve $u_v^K(x)=u_v^\pi(x)$; and thin dashed-dotted curve, fit to the data given in Eq. (3.24).

$$\left.\frac{u_v^K(x)}{u_v^\pi(x)}\right|_{\rm DSE}^{x\to 1} = 0.31 \quad \text{cf.} \quad \left.\frac{u_v^K(x)}{u_v^\pi(x)}\right|_{\rm NJL^{HC}}^{x\to 1} = 0.37. \tag{6.99}$$

We anticipated a nonzero value for the ratio because, in the neighborhood of $x=1$, the $u$-quark distribution should have the same pointwise behavior in all pseudoscalar mesons. These features and predictions add additional emphasis to the need for a much improved measurement of the kaon structure functions. Before claiming understanding of QCD, it is crucial to verify the predicted large-$x$ behavior, especially those properties which are environment dependent and those which are not.

The calculation of baryon valence-quark distribution functions is also possible; e.g., using the Poincaré covariant Faddeev equation described in Appendix B. This approach capitalizes on the importance of scalar and axial-vector diquark correlations within the nucleon. In QCD these correlations are essentially nonpointlike (Maris, 2004; Alexandrou *et al.*, 2006). While no DSE computations of the pointwise behavior of the nucleon structure functions are yet available, based on the diquark-correlation probabilities presented in Table II of the DSE study of nucleon electromagnetic form factors described by Cloët *et al.* (2009) and the fact that the ratio is a fixed-point under evolution, one can estimate

$$d(x)/u(x) \overset{x\to 1}{\approx} 0.12 \Rightarrow F_2^n(x)/F_2^p(x) \overset{x\to 1}{\approx} 0.36 \tag{6.100}$$

[cf. Eqs. (5.5), (6.6), and (6.46) and Figs. 10, 28, and 35]. In addition, the nonzero value highlights the important role of axial-vector diquark correlations: they enable a truly valence $d$ quark to carry the proton's helicity, which is impossible if scalar diquarks are the only correlations present in the proton's Faddeev amplitude.

## VII. PERSPECTIVE AND PROSPECTS

Understanding the physics of hadrons on the valence-quark domain is a definitive task for hadron physics. Indeed, a given hadron is defined by its flavor content and that is a valence-quark property. While significant continuing and new investments in experiment and theory are required in order to acquire this understanding, the potential rewards are great. For example, this information is essential to both an elucidation of the standard model and the provision of reliable parton distribution functions for use in the analysis of large collider experiments—our best tool for uncovering phenomena outside this paradigm.

We have highlighted numerous outstanding and unresolved challenges in the valence region, which experiments must confront. Important among them are the $x>0.8$ region of the nucleon and the pion, and the kaon distribution function. The upgraded Jefferson Laboratory facility is well suited to provide new data for the valence region in the nucleon from both inclusive and semi-inclusive deep inelastic scattering. Moreover, a future electron-ion collider could provide crucial new data for both mesons and nucleons. There is also great potential in using Drell-Yan interactions, at FNAL, CERN, J-PARC, and GSI, to push into the large-$x$ domain for mesons and nucleons.

The challenges for theory are exciting and equally great. The valence-quark domain is the purview of nonperturbative methods in QCD. Hence, true understanding, in contrast to modeling and parametrization as a simple means of identifying and highlighting key features, requires a widespread acceptance of the need to adapt theory: to the lessons learnt already from the methods of nonperturbative quantum-field theory and a fuller exploitation of those methods. Thus, before an elucidation of hadron structure can be achieved, theory must accept the most conspicuous of QCD's challenges. The standard model will not otherwise be solved.

*Note added in proof*. After this manuscript was submitted, a new analysis of extant data on the pion-nucleon Drell-Yan process was performed, which included, for the first time, next-to-leading logarithmic resummation effects (Aicher *et al.*, 2010). As a result, a considerably softer pion $u$-valence distribution is obtained at high $x$, in line with predictions of perturbative QCD and Dyson-Schwinger equations.

## ACKNOWLEDGMENTS

In preparing this paper we benefited greatly from constructive comments and input provided by J. Arrington, S. J. Brodsky, S. Capstick, I. C. Cloët, F. Coester, D. F. Geesaman, S. E. Kuhlmann, A. D. Martin, W. Melnitchouk, J.-C. Peng, P. E. Reimer, P. C. Tandy, R. D.

Young, and J. M. Zanotti. This work was supported by the Department of Energy, Office of Nuclear Physics, Contract No. DE-AC02-06CH11357.

## APPENDIX A: LIGHT-FRONT CONVENTIONS

Unless otherwise specified, we use the following light-front notation:

$$\ell^+ = \ell^0 + \ell^3, \quad \ell^- = \ell^0 - \ell^3, \quad \ell_\perp = (\ell^1, \ell^2), \tag{A.1}$$

where $\ell^\mu$ is any quantity that transforms as a contravariant four-vector. Naturally, $\ell_\pm = \ell^\mp$ and $\ell^2 = \ell^+\ell^- - \ell_\perp \cdot \ell_\perp$. It follows that

$$\int d^4\ell \to \tfrac{1}{2} \int d\ell^- d\ell^+ d^2\ell_\perp. \tag{A.2}$$

The spinor describing a spin-$\frac{1}{2}$ hadron is orthonormalized according to

$$\bar{u}(p',\lambda')u(p,\lambda) = 2p^+(2\pi)^3 \delta_{\lambda\lambda'} \delta(p'-p) \delta^2(p'_\perp - p_\perp), \tag{A.3}$$

where $\lambda$, $\lambda'$ are helicities.

If one considers a particle's momentum, then $k^+ \geqslant 0$ in the light-front frame. Hence, the only way to make a zero-momentum Fock state is for every particle it contains to have $k^+=0$. Although this defines a set of measure zero in the light-front phase space, such states cannot casually be discarded because operators exist which are singular at $k^+=0$. For example, to throw away these states is, perhaps, to preclude dynamical chiral-symmetry breaking, a keystone of nonperturbative QCD and hadron physics.

## APPENDIX B: DRESSED QUARKS, THE FADDEEV EQUATION, AND THE CURRENT

When emphasizing dressed-quark degrees of freedom it is now natural to describe baryons using a Poincaré covariant Faddeev equation. This approach sits squarely within the ambit of the application of Dyson-Schwinger equations (DSEs) in QCD (Roberts and Schmidt, 2000; Maris and Roberts, 2003; Roberts *et al.*, 2007).

One arrives at the Faddeev equation by noticing that in quantum-field theory a nucleon appears as a pole in a six-point quark Green's function. The pole's residue is proportional to the nucleon's Faddeev amplitude, which is obtained from a Poincaré covariant Faddeev equation that sums all possible exchanges and interactions that can take place between three dressed quarks. A tractable Faddeev equation for baryons was formulated by Cahill *et al.* (1989). Shown in Fig. 43, it is founded on the observation that an interaction which describes color-singlet mesons also generates quark-quark (diquark) correlations in the color-$\bar{3}$ (antitriplet) channel (Cahill *et al.*, 1987).

The dominant correlations for ground-state octet and decuplet baryons are scalar ($0^+$) and axial-vector ($1^+$) diquarks because, for example, the associated mass scales are smaller than the baryons' masses (Burden *et al.*, 1997; Maris, 2002), namely (in GeV),

$$\begin{aligned} m_{[ud]_{0^+}} &= 0.7 - 0.8, \\ m_{(uu)_{1^+}} &= m_{(ud)_{1^+}} = m_{(dd)_{1^+}} = 0.9 - 1.0. \end{aligned} \tag{B1}$$

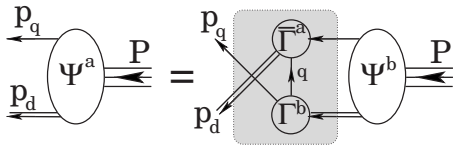


FIG. 43. Poincaré covariant Faddeev equation. $\Psi$ is the Faddeev amplitude for a nucleon of total momentum $P=p_q+p_d$. It expresses the relative-momentum correlation between the dressed quark and diquarks within the nucleon. The shaded region demarcates the kernel of the Faddeev equation, in which the single line denotes the dressed-quark propagator; $\Gamma$ is the diquark Bethe-Salpeter-like amplitude; and the double line is the diquark propagator. [Full explanation provided in Appendix A of Cloët *et al.* (2009), from which this figure is adapted.]

While diquarks do not appear in the strong-interaction spectrum [see, e.g., Bender *et al.* (1996, 2002) and Bhagwat *et al.* (2004)], the attraction between quarks in this channel justifies a picture of baryons in which two quarks are always correlated as a color-$\bar{3}$ diquark pseudoparticle, and binding is effected by the iterated exchange of roles between the bystander and diquark-participant quarks.

The kernel of the Faddeev equation is completed by specifying that the quarks are dressed, with two of the three dressed quarks correlated always as a color-$\bar{3}$ diquark. As shown in Fig. 43, binding is then effected by the iterated exchange of roles between the bystander and diquark-participant quarks. The Faddeev equation yields the nucleon's mass and amplitude.

In order to calculate nucleon distribution functions one must know the manner in which the nucleon described by the Faddeev equation couples to a photon. This is derived in Oettel *et al.* (2000) and shown in Fig. 44. Naturally, the current depends on the electromagnetic properties of the diquark correlations. A detailed explanation of the diagrams in Fig. 44 is presented in Appendix C of Cloët *et al.* (2009). Here we only provide a brief explanation.

Diagram 1 represents the photon coupling directly to the bystander quark. It is a necessary condition for current conservation that the quark-photon vertex satisfies the Ward-Takahashi identity. Since the quark is dressed, the vertex is not bare. It can be obtained by solving an inhomogeneous Bethe-Salpeter equation.

Diagram 2 depicts the photon coupling directly to a diquark correlation. Naturally, the diquark propagators match the line to which they are attached. Moreover, the interaction vertices satisfy Ward-Takahashi identities and obey QCD constraints.

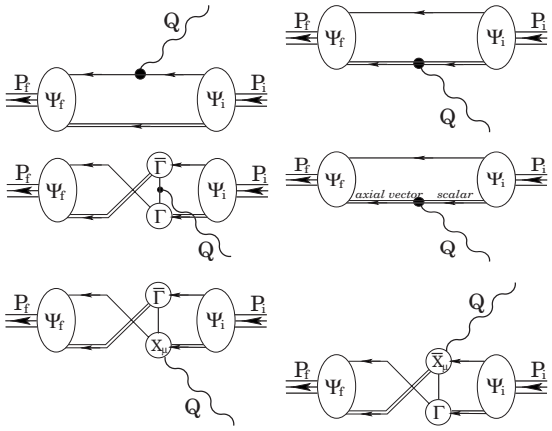


FIG. 44. Vertex which ensures a conserved current for on-shell nucleons described by the Faddeev amplitudes $\Psi_{i,f}$ obtained from the Faddeev equation shown in Fig. 43. The single line represents the dressed-quark propagator; the double line, the diquark propagator; and Γ is the diquark Bethe-Salpeter amplitude. The remaining vertices are described in the text: the top-left image is diagram 1, the top right, diagram 2 etc., with the bottom-right image, diagram 6. In connection with DIS, the photon line is equated with a zero-momentum insertion. [A full explanation of the diagrams depicted here is provided in Appendix C of Cloët *et al.* (2009), from which this figure is adapted.]

Diagram 3 shows a photon coupling to the quark that is exchanged as one diquark breaks up and another is formed. It is a two-loop diagram. It is noteworthy that the process of quark exchange provides the attraction necessary in the Faddeev equation to bind the nucleon. It also guarantees that the Faddeev amplitude has the correct antisymmetry under the exchange of any two dressed quarks. This key feature is absent in models with elementary (noncomposite) diquarks.

Diagram 4 differs from Diagram 2 in expressing the contribution to the nucleons' form factors owing to an electromagnetically induced transition between scalar and axial-vector diquarks. This transition vertex is a rank-2 pseudotensor, kindred, e.g., to the matrix element describing the $\rho\gamma^*\pi^0$ transition (Maris and Tandy, 2002).

Diagrams 5 and 6 are the so-called "seagull" terms, which appear as partners to diagram 3 and arise because binding in the Faddeev equations is effected by the exchange of a dressed quark between *nonpointlike* diquark correlations (Oettel *et al.*, 2000). The new elements in these diagrams are the couplings of a photon to two dressed quarks as they either separate from (diagram 5) or combine to form (diagram 6) a diquark correlation. As such they are components of the five point Schwinger function which describes the coupling of a photon to the quark-quark scattering kernel. These terms vanish if the diquark correlation is represented by a momentum-independent Bethe-Salpeter-like amplitude; i.e., the diquark is pointlike.

## REFERENCES


Abbate, R., and S. Forte, 2005, Phys. Rev. D **72**, 117503.
Accardi, A., and J.-W. Qiu, 2008, J. High Energy Phys. **07**, 090.
Accardi, A., *et al.*, 2010, Phys. Rev. D **81**, 034016.
Ackerstaff, K., *et al.* (HERMES Collaborations), 1998, Phys. Rev. Lett. **81**, 5519.
Adams, M. R., *et al.* (E665 Collaboration), 1993, Phys. Rev. D **48**, 5057.
Adloff, C., *et al.* (H1 Collaboration), 1999, Eur. Phys. J. C **6**, 587.
Afnan, I. R., *et al.*, 2000, Phys. Lett. B **493**, 36.
Afnan, I. R., *et al.*, 2003, Phys. Rev. C **68**, 035201.
Ahmed, M., and T. Gehrmann, 1999, Phys. Lett. B **465**, 297.
Aicher, M., A. Schäfer, and W. Vogelsang, 2010, e-print arXiv:1009.2481.
Alekhin, S., 2003, Phys. Rev. D **68**, 014002.
Alekhin, S., S. Kulagin, and R. Petti, 2008, e-print arXiv:0810.4893.
Alekhin, S., K. Melnikov, and F. Petriello, 2006, Phys. Rev. D **74**, 054033.
Alekhin, S. I., S. A. Kulagin, and S. Liuti, 2004, Phys. Rev. D **69**, 114009.
Alexandrou, C., P. de Forcrand, and B. Lucini, 2006, Phys. Rev. Lett. **97**, 222002.
Alkofer, R., and L. von Smekal, 2001, Phys. Rep. **353**, 281.
Altarelli, G., 1982, Phys. Rep. **81**, 1.
Altarelli, G., R. K. Ellis, and G. Martinelli, 1978, Nucl. Phys. B **143**, 521.
Altarelli, G., R. K. Ellis, and G. Martinelli, 1979, Nucl. Phys. B **157**, 461.
Altarelli, G., and G. Parisi, 1977, Nucl. Phys. B **126**, 298.
Amaudruz, P., *et al.* (New Muon Collaboration), 1991, Phys. Rev. Lett. **66**, 2712.
Amaudruz, P., *et al.* (New Muon Collaboration), 1992, Phys. Lett. B **295**, 159.
Arneodo, M., *et al.* (European Muon Collaboration), 1987, Z. Phys. C **34**, 277.
Arneodo, M., *et al.* (New Muon Collaboration), 1994, Phys. Rev. D **50**, R1.
Arneodo, M., *et al.* (New Muon Collaboration), 1997a, Nucl. Phys. B **487**, 3.
Arneodo, M., *et al.* (New Muon Collaboration), 1997b, Nucl. Phys. B **483**, 3.
Arrington, J., F. Coester, R. J. Holt, and T. S. H. Lee, 2009, J. Phys. G **36**, 025005.
Aubert, J., *et al.*, 1983, Phys. Lett. **123B**, 275.
Aubert, J. J., *et al.* (European Muon Collaboration), 1987, Nucl. Phys. B **293**, 740.
Avakian, H., S. J. Brodsky, A. Deur, and F. Yuan, 2007, Phys. Rev. Lett. **99**, 082001.
Avakian, H., *et al.*, 2006, Jefferson Lab Proposal No. PR12-06-112 (unpublished).
Badier, J., *et al.* (Saclay-CERN-College de France-Ecole Poly-Orsay Collaboration), 1980, Phys. Lett. **93B**, 354.
Badier, J., *et al.* (NA3 Collaboration), 1983, Z. Phys. C **18**, 281.
Baldit, A., *et al.* (NA51 Collaboration), 1994, Phys. Lett. B **332**, 244.
Bali, G. S., H. Neff, T. Duessel, T. Lippert, and K. Schilling (SESAM), 2005, Phys. Rev. D **71**, 114513.
Ball, R. D., *et al.* (NNPDF Collaboration), 2009, Nucl. Phys. B **809**, 1.
Ball, R. D., *et al.*, 2010, Nucl. Phys. B **838**, 136.
Barbieri, R., J. R. Ellis, M. K. Gaillard, and G. G. Ross, 1976, Nucl. Phys. B **117**, 50.
Bardeen, W. A., A. J. Buras, D. W. Duke, and T. Muta, 1978, Phys. Rev. D **18**, 3998.

Barone, V., A. Drago, and P. G. Ratcliffe, 2002, Phys. Rep. **359**, 1.
Bate, M. R., and A. I. Signal, 1992, J. Phys. G **18**, 1875.
Bender, A., W. Detmold, C. D. Roberts, and A. W. Thomas, 2002, Phys. Rev. C **65**, 065203.
Bender, A., C. D. Roberts, and L. Von Smekal, 1996, Phys. Lett. B **380**, 7.
Bentz, W., T. Hama, T. Matsuki, and K. Yazaki, 1999, Nucl. Phys. A **651**, 143.
Benvenuti, A. C., *et al.* (BCDMS Collaboration), 1989, Phys. Lett. B **223**, 485.
Benvenuti, A. C., *et al.* (BCDMS Collaboration), 1990a, Phys. Lett. B **237**, 592.
Benvenuti, A. C., *et al.* (BCDMS Collaboration), 1990b, Phys. Lett. B **237**, 599.
Berger, E. L., and S. J. Brodsky, 1979, Phys. Rev. Lett. **42**, 940.
Berger, E. L., J.-W. Qiu, and R. A. Rodriguez-Pedraza, 2007, Phys. Rev. D **76**, 074006.
Best, C., *et al.*, 1997, Phys. Rev. D **56**, 2743.
Betev, B., *et al.* (NA10), 1985, Z. Phys. C **28**, 9.
Bhagwat, M. S., I. C. Cloët, and C. D. Roberts, 2007, *Proceedings of the Workshop on Exclusive Reactions at High Momentum Transfer* (World Scientific, Singapore).
Bhagwat, M. S., A. Höll, A. Krassnigg, C. D. Roberts, and P. C. Tandy, 2004, Phys. Rev. C **70**, 035205.
Bhagwat, M. S., M. A. Pichowsky, C. D. Roberts, and P. C. Tandy, 2003, Phys. Rev. C **68**, 015203.
Bhagwat, M. S., and P. C. Tandy, 2006, AIP Conf. Proc. **842**, 225.
Bickerstaff, R. P., M. C. Birse, and G. A. Miller, 1984, Phys. Rev. Lett. **53**, 2532.
Bickerstaff, R. P., M. C. Birse, and G. A. Miller, 1986, Phys. Rev. D **33**, 3228.
Bijker, R., F. Iachello, and A. Leviatan, 1994, Ann. Phys. **236**, 69.
Bissey, F. R. P., A. W. Thomas, and I. R. Afnan, 2001, Phys. Rev. C **64**, 024004.
Bjorken, J. D., 1967, *Proceedings of the Third International Conference on Electron and Photon Interactions* (Clearing House of Federal Scientific and Technical Information, Washington, D.C.).
Bjorken, J. D., and E. A. Paschos, 1969, Phys. Rev. **185**, 1975.
Blaschke, D., Y. L. Kalinovsky, G. Roepke, S. M. Schmidt, and M. K. Volkov, 1996, Phys. Rev. C **53**, 2394.
Bloch, J. C. R., C. D. Roberts, and S. M. Schmidt, 2000, Phys. Rev. C **61**, 065207.
Bloch, J. C. R., C. D. Roberts, S. M. Schmidt, A. Bender, and M. R. Frank, 1999, Phys. Rev. C **60**, 062201(R).
Bloom, E., and F. Gilman, 1971, Phys. Rev. D **4**, 2901.
Bloom, E. D., *et al.*, 1969, Phys. Rev. Lett. **23**, 930.
Blumlein, J., H. Bottcher, and A. Guffanti, 2007, Nucl. Phys. B **774**, 182.
Bodek, A., *et al.*, 1973, Phys. Rev. Lett. **30**, 1087.
Bodwin, G. T., S. J. Brodsky, and G. P. Lepage, 1989, Phys. Rev. D **39**, 3287.
Boer, D., 1999, Phys. Rev. D **60**, 014012.
Boer, D., S. J. Brodsky, and D. S. Hwang, 2003, Phys. Rev. D **67**, 054003.
Boer, D., and P. J. Mulders, 1998, Phys. Rev. D **57**, 5780.
Boer, D., and W. Vogelsang, 2006, Phys. Rev. D **74**, 014004.
Boffi, S., and B. Pasquini, 2007, Riv. Nuovo Cimento **30**, 387.
Bowman, P. O., *et al.*, 2005, Phys. Rev. D **71**, 054507.
Brandenburg, A., S. J. Brodsky, V. V. Khoze, and D. Mueller, 1994, Phys. Rev. Lett. **73**, 939.
Brandenburg, A., O. Nachtmann, and E. Mirkes, 1993, Z. Phys. C **60**, 697.
Breidenbach, M., *et al.*, 1969, Phys. Rev. Lett. **23**, 935.
Brodsky, S. J., 2005, AIP Conf. Proc. **792**, 977.
Brodsky, S. J., 2009, Nucl. Phys. A **827**, 327c.
Brodsky, S. J., M. Burkardt, and I. Schmidt, 1995, Nucl. Phys. B **441**, 197.
Brodsky, S. J., and G. F. de Teramond, 2008, Phys. Rev. D **77**, 056007.
Brodsky, S. J., D. S. Hwang, and I. Schmidt, 2002a, Phys. Lett. B **530**, 99.
Brodsky, S. J., D. S. Hwang, and I. Schmidt, 2002b, Nucl. Phys. B **642**, 344.
Brodsky, S. J., and G. P. Lepage, 1979, presented at *Workshop on Current Topics in High Energy Physics*, 1979 (Caltech, Pasadena, CA).
Brodsky, S. J., H.-C. Pauli, and S. S. Pinsky, 1998, Phys. Rep. **301**, 299.
Brommel, D., *et al.* (QCDSF-UKQCD Collaboration), 2007, PoS **LAT2007**, 140.
Brommel, D., *et al.*, 2008, Eur. Phys. J. Spec. Top. **162**, 63.
Burden, C. J., L. Qian, C. D. Roberts, P. C. Tandy, and M. J. Thomson, 1997, Phys. Rev. C **55**, 2649.
Burden, C. J., C. D. Roberts, and M. J. Thomson, 1996, Phys. Lett. B **371**, 163.
Burov, V. V., A. V. Molochkov, G. I. Smirnov, and H. Toki, 2004, Phys. Lett. B **587**, 175.
Cahill, R. T., and C. D. Roberts, 1985, Phys. Rev. D **32**, 2419.
Cahill, R. T., C. D. Roberts, and J. Praschifka, 1987, Phys. Rev. D **36**, 2804.
Cahill, R. T., C. D. Roberts, and J. Praschifka, 1989, Aust. J. Phys. **42**, 129.
Cahn, R. N., 1978, Phys. Lett. **78B**, 269.
Cahn, R. N., 1989, Phys. Rev. D **40**, 3107.
Callan, J., G. Curtis, and D. J. Gross, 1969, Phys. Rev. Lett. **22**, 156.
Capstick, S., and W. Roberts, 2000, Prog. Part. Nucl. Phys. **45**, S241.
Carlitz, R. D., 1975, Phys. Lett. **58B**, 345.
Celmaster, W., and R. J. Gonsalves, 1979, Phys. Rev. D **20**, 1420.
Chang, L., I. C. Cloët, B. El-Bennich, T. Klähn, and C. D. Roberts, 2009, Chin. Phys. **C33**, 1189.
Chang, L., Y.-X. Liu, M. S. Bhagwat, C. D. Roberts, and S. V. Wright, 2007, Phys. Rev. C **75**, 015201.
Chang, L., and C. D. Roberts, 2009, Phys. Rev. Lett. **103**, 081601.
Chekanov, S., *et al.* (ZEUS Collaboration), 2007, Nucl. Phys. B **776**, 1.
Chen, X.-S., W.-M. Sun, X.-F. Lu, F. Wang, and T. Goldman, 2009a, Phys. Rev. Lett. **103**, 062001.
Chen, X.-S., W.-M. Sun, X.-F. Lu, F. Wang, and T. Goldman, 2009b, e-print arXiv:0911.0248.
Chiappetta, P., and M. Le Bellac, 1986, Z. Phys. C **32**, 521.
Chodos, A., R. L. Jaffe, K. Johnson, and C. B. Thorn, 1974, Phys. Rev. D **10**, 2599.
Chodos, A., R. L. Jaffe, K. Johnson, C. B. Thorn, and V. F. Weisskopf, 1974, Phys. Rev. D **9**, 3471.
Cloët, I. C., 2009, private communication.
Cloët, I. C., W. Bentz, and A. W. Thomas, 2005, Phys. Lett. B **621**, 246.
Cloët, I. C., G. Eichmann, B. El-Bennich, T. Klähn, and C. D.

Roberts, 2009, Few-Body Syst. **46**, 1.
Cloët, I. C., and C. D. Roberts, 2008, PoS **LC2008**, 047.
Close, F. E., 1973, Phys. Lett. **43B**, 422.
Close, F. E., and A. W. Thomas, 1988, Phys. Lett. B **212**, 227.
Collins, J., and J.-W. Qiu, 2007, Phys. Rev. D **75**, 114014.
Collins, J. C., 1979, Phys. Rev. Lett. **42**, 291.
Collins, J. C., 1993, Nucl. Phys. B **396**, 161.
Collins, J. C., 2002, Phys. Lett. B **536**, 43.
Collins, J. C., and D. E. Soper, 1977, Phys. Rev. D **16**, 2219.
Conway, J. S., 1987, Ph.D. thesis (University of Chicago).
Conway, J. S., *et al.*, 1989, Phys. Rev. D **39**, 92.
D'Alesio, U., and F. Murgia, 2008, Prog. Part. Nucl. Phys. **61**, 394.
D'Alesio, U., and H. J. Pirner, 2000, Eur. Phys. J. A **7**, 109.
Davidson, R. M., and E. Ruiz Arriola, 1995, Phys. Lett. B **348**, 163.
Derrick, M., *et al.* (ZEUS Collaboration), 1996, Z. Phys. C **70**, 1.
DeRújula, A., H. Georgi, and H. D. Politzer, 1977, Ann. Phys. (N.Y.) **103**, 315.
Detmold, W., W. Melnitchouk, J. W. Negele, D. B. Renner, and A. W. Thomas, 2001, Phys. Rev. Lett. **87**, 172001.
Detmold, W., W. Melnitchouk, and A. W. Thomas, 2003, Phys. Rev. D **68**, 034025.
Diakonov, D., V. Petrov, P. Pobylitsa, M. V. Polyakov, and C. Weiss, 1996, Nucl. Phys. B **480**, 341.
Diehl, M., 2003, Phys. Rep. **388**, 41.
Dittes, F. M., D. Müller, D. Robaschik, B. Geyer, and J. Hořejši, 1988, Phys. Lett. B **209**, 325.
Dokshitzer, Y. L., 1977, Sov. Phys. JETP **46**, 641.
Dolgov, D., *et al.* (LHPC), 2002, Phys. Rev. D **66**, 034506.
Dorati, M., T. A. Gail, and T. R. Hemmert, 2008, Nucl. Phys. A **798**, 96.
Dorokhov, A. E., and L. Tomio, 2000, Phys. Rev. D **62**, 014016.
Drell, S. D., and T. M. Yan, 1970a, Phys. Rev. Lett. **25**, 316.
Drell, S. D., and T. M. Yan, 1970b, Phys. Rev. Lett. **24**, 181.
Drell, S. D., and T.-M. Yan, 1971, Ann. Phys. **66**, 578.
Durham, U. K., 2009, HEP databases, ⟨http://durpdg.dur.ac.uk/⟩.
Ebert, D., T. Feldmann, and H. Reinhardt, 1996, Phys. Lett. B **388**, 154.
Ebert, D., and H. Reinhardt, 1986, Nucl. Phys. B **271**, 188.
Ellis, R. K., W. Furmanski, and R. Petronzio, 1982, Nucl. Phys. B **207**, 1.
Ellis, R. K., W. Furmanski, and R. Petronzio, 1983, Nucl. Phys. B **212**, 29.
Ellis, S. D., and W. J. Stirling, 1991, Phys. Lett. B **256**, 258.
Ezawa, Z. F., 1974, Nuovo Cimento Soc. Ital. Fis., A **23**, 271.
Falciano, S., *et al.* (NA10), 1986, Z. Phys. C **31**, 513.
Farrar, G. R., and D. R. Jackson, 1975, Phys. Rev. Lett. **35**, 1416.
Fenker, H., *et al.*, 2003, Jefferson Lab Experiment No. E03-012 (unpublished).
Ferraris, M., M. M. Giannini, M. Pizzo, E. Santopinto, and L. Tiator, 1995, Phys. Lett. B **364**, 231.
Feynman, R. P., 1969, Phys. Rev. Lett. **23**, 1415.
Feynman, R. P., 1972, *Photon-Hadron Interactions* (Benjamin, Reading, MA), Vol. 1, p. 282.
Field, R. D., and R. P. Feynman, 1977, Phys. Rev. D **15**, 2590.
Fischer, C. S., 2006, J. Phys. G **32**, R253.
Frankfurt, L. L., and M. I. Strikman, 1981, Phys. Rep. **76**, 215.
Frederico, T., and G. A. Miller, 1994, Phys. Rev. D **50**, 210.
Friedman, J. I., 1991, Rev. Mod. Phys. **63**, 615.
Friman, B. L., V. R. Pandharipande, and R. B. Wiringa, 1983, Phys. Rev. Lett. **51**, 763.
Furmanski, W., and R. Petronzio, 1982, Z. Phys. C **11**, 293.
Gamberg, L. P., H. Reinhardt, and H. Weigel, 1998, Int. J. Mod. Phys. A **13**, 5519.
Gamberg, L. P., and H. Weigel, 2000, Czech. J. Phys. **50S1**, 137.
Garvey, G. T., 1987, Nucl. Phys. B **279**, 221.
Garvey, G. T., and J.-C. Peng, 2001, Prog. Part. Nucl. Phys. **47**, 203.
Gaskell, D., *et al.*, 2001, Phys. Rev. Lett. **87**, 202301.
Georgi, H., and H. D. Politzer, 1976, Phys. Rev. D **14**, 1829.
Georgi, H., and H. D. Politzer, 1978, Phys. Rev. Lett. **40**, 3.
Giannini, M. M., E. Santopinto, and A. Vassallo, 2001, Eur. Phys. J. A **12**, 447.
Giannini, M. M., E. Santopinto, A. Vassallo, and M. Vanderhaeghen, 2003, Phys. Lett. B **552**, 149.
Glozman, L. Y., W. Plessas, K. Varga, and R. F. Wagenbrunn, 1998, Phys. Rev. D **58**, 094030.
Glück, M., P. Jimenez-Delgado, and E. Reya, 2008, Eur. Phys. J. C **53**, 355.
Glück, M., E. Reya, and I. Schienbein, 1999, Eur. Phys. J. C **10**, 313.
Glück, M., E. Reya, and A. Vogt, 1992a, Z. Phys. C **53**, 127.
Glück, M., E. Reya, and A. Vogt, 1992b, Z. Phys. C **53**, 651.
Glück, M., E. Reya, and A. Vogt, 1993, Phys. Lett. B **306**, 391.
Glück, M., E. Reya, and A. Vogt, 1995, Z. Phys. C **67**, 433.
Glück, M., E. Reya, and A. Vogt, 1998, Eur. Phys. J. C **5**, 461.
Göckeler, M., R. Horsley, D. Pleiter, P. E. L. Rakow, and G. Schierholz (QCDSF Collaboration), 2005, Phys. Rev. D **71**, 114511.
Goeke, K., M. V. Polyakov, and M. Vanderhaeghen, 2001, Prog. Part. Nucl. Phys. **47**, 401.
Gottfried, K., 1967, Phys. Rev. Lett. **18**, 1174.
Gottfried, K., and J. D. Jackson, 1964, Nuovo Cimento **33**, 309.
Gribov, V. N., and L. N. Lipatov, 1971, Phys. Lett. **37B**, 78.
Gribov, V. N., and L. N. Lipatov, 1972, Sov. J. Nucl. Phys. **15**, 438.
Gross, D. J., and F. Wilczek, 1974, Phys. Rev. D **9**, 980.
Guagnelli, M., *et al.* [Zeuthen-Rome (ZeRo) Collaboration], 2005, Eur. Phys. J. C **40**, 69.
Guanziroli, M., *et al.* (NA10 Collaboration), 1988, Z. Phys. C **37**, 545.
Gutiérrez-Guerrero, L. X., A. Bashir, I. C. Cloët, and C. D. Roberts, 2010, Phys. Rev. C **81**, 065202.
Hägler, P., *et al.* (LHPC), 2008, Phys. Rev. D **77**, 094502.
Hawker, E. A., *et al.* (FNAL E866/NuSea Collaboration), 1998, Phys. Rev. Lett. **80**, 3715.
Hecht, M. B., C. D. Roberts, and S. M. Schmidt, 1999, *Proceedings of the Workshop on Light-Cone QCD and Nonperturbative Hadron Physics* (World Scientific, Singapore).
Hecht, M. B., C. D. Roberts, and S. M. Schmidt, 2001, Phys. Rev. C **63**, 025213.
Hecht, M. B., *et al.*, 2002, Phys. Rev. C **65**, 055204.
Heinrich, J. G., *et al.*, 1991, Phys. Rev. D **44**, 1909.
Herrod, R. T., and S. Wada, 1980, Phys. Lett. **96B**, 195.
Higashijima, K., 1984, Phys. Rev. D **29**, 1228.
Holt, R. J., and P. E. Reimer, 2001, AIP Conf. Proc. **588**, 234.
Holtmann, H., A. Szczurek, and J. Speth, 1996, Nucl. Phys. A **596**, 631.
Ilgenfritz, E. M., *et al.*, 2008, Phys. Rev. D **77**, 074502.
Isgur, N., 1999, Phys. Rev. D **59**, 034013.
Isgur, N., and G. Karl, 1978, Phys. Rev. D **18**, 4187.
Ito, A. S., *et al.*, 1981, Phys. Rev. D **23**, 604.

Jaffe, R. L., 1975, Phys. Rev. D **11**, 1953.
Jaffe, R. L., 1981, Ann. Phys. **132**, 32.
Jasiak, J., 1997, e-print arXiv:hep-ph/9706503.
Ji, X.-D., 1997, Phys. Rev. D **55**, 7114.
Ji, X.-D., 2009, e-print arXiv:0910.5022.
Ji, X.-D., J.-P. Ma, and F. Yuan, 2005, Phys. Lett. B **610**, 247.
Jung, H., 1995, Comput. Phys. Commun. **86**, 147.
Kendall, H. W., 1991, Rev. Mod. Phys. **63**, 597.
Kenyon, I. R., 1982, Rep. Prog. Phys. **45**, 1261.
Kopeliovich, B. Z., J. Nemchik, I. K. Potashnikova, M. B. Johnson, and I. Schmidt, 2005, Phys. Rev. C **72**, 054606.
Kretzer, S., and M. H. Reno, 2004, Phys. Rev. D **69**, 034002.
Kulagin, S. A., W. Melnitchouk, T. Weigl, and W. Weise, 1996, Nucl. Phys. A **597**, 515.
Kulagin, S. A., G. Piller, and W. Weise, 1994, Phys. Rev. C **50**, 1154.
Kumano, S., 1998, Phys. Rep. **303**, 183.
Kusaka, K., G. Piller, A. W. Thomas, and A. G. Williams, 1997, Phys. Rev. D **55**, 5299.
Kwiecinski, J., A. D. Martin, W. J. Stirling, and R. G. Roberts, 1990, Phys. Rev. D **42**, 3645.
Lai, H. L., *et al.*, 1995, Phys. Rev. D **51**, 4763.
Lai, H. L., *et al.* (CTEQ), 2000, Eur. Phys. J. C **12**, 375.
Lai, H. L., *et al.*, 2007, J. High Energy Phys. **04**, 089.
Lam, C. S., and W.-K. Tung, 1980, Phys. Rev. D **21**, 2712.
Landshoff, P. V., J. C. Polkinghorne, and R. D. Short, 1971, Nucl. Phys. B **28**, 225.
Langfeld, K., H. Markum, R. Pullirsch, C. D. Roberts, and S. M. Schmidt, 2003, Phys. Rev. C **67**, 065206.
Lepage, G. P., and S. J. Brodsky, 1980, Phys. Rev. D **22**, 2157.
Lian, Y., and H. B. Thacker, 2007, Phys. Rev. D **75**, 065031.
Lipatov, L. N., 1975, Sov. J. Nucl. Phys. **20**, 94.
Lipkin, H. J., 1958, Phys. Rev. **110**, 1395.
Llewellyn Smith, C. H., 1980, in *High Energy Physics—1980*, edited by L. Durand and L. G. Pondrom, AIP Conf. Proc. No. 68 (AIP, New York), pp. 1346–1377.
Lu, Z., B.-Q. Ma, and I. Schmidt, 2006, Phys. Lett. B **639**, 494.
Lu, Z., B.-Q. Ma, and I. Schmidt, 2007, Phys. Rev. D **75**, 014026.
Malace, S. P., *et al.*, 2009, Phys. Rev. C **80**, 035207.
Margolis, B., J. Ng, M. Phipps, and H. D. Trottier, 1993, Phys. Rev. D **47**, 1942.
Maris, P., 2002, Few-Body Syst. **32**, 41.
Maris, P., 2004, Few-Body Syst. **35**, 117.
Maris, P., and C. D. Roberts, 1998, Phys. Rev. C **58**, 3659.
Maris, P., and C. D. Roberts, 2003, Int. J. Mod. Phys. E **12**, 297.
Maris, P., C. D. Roberts, and P. C. Tandy, 1998, Phys. Lett. B **420**, 267.
Maris, P., and P. C. Tandy, 2000a, Phys. Rev. C **62**, 055204.
Maris, P., and P. C. Tandy, 2000b, Phys. Rev. C **61**, 045202.
Maris, P., and P. C. Tandy, 2002, Phys. Rev. C **65**, 045211.
Martin, A. D., R. G. Roberts, W. J. Stirling, and R. S. Thorne, 2002a, Eur. Phys. J. C **23**, 73.
Martin, A. D., R. G. Roberts, W. J. Stirling, and R. S. Thorne, 2002b, Phys. Lett. B **531**, 216.
Martin, A. D., R. G. Roberts, W. J. Stirling, and R. S. Thorne, 2003, Eur. Phys. J. C **28**, 455.
Martin, A. D., R. G. Roberts, W. J. Stirling, and R. S. Thorne, 2004a, Phys. Lett. B **604**, 61.
Martin, A. D., R. G. Roberts, W. J. Stirling, and R. S. Thorne, 2004b, Eur. Phys. J. C **35**, 325.
Martin, A. D., W. J. Stirling, and R. G. Roberts, 1993, Phys. Lett. B **306**, 145.
Martin, A. D., W. J. Stirling, and R. G. Roberts, 1994, Phys. Rev. D **50**, 6734.
Martin, A. D., W. J. Stirling, and R. S. Thorne, 2006, Phys. Lett. B **635**, 305.
Martin, A. D., W. J. Stirling, R. S. Thorne, and G. Watt, 2007, Phys. Lett. B **652**, 292.
Martin, A. D., W. J. Stirling, R. S. Thorne, and G. Watt, 2009, Eur. Phys. J. C **63**, 189.
Martinelli, G., and C. T. Sachrajda, 1989, Nucl. Phys. B **316**, 355.
McGaughey, P. L., *et al.*, 1992, Phys. Rev. Lett. **69**, 1726.
Melde, T., K. Berger, L. Canton, W. Plessas, and R. F. Wagenbrunn, 2007, Phys. Rev. D **76**, 074020.
Melnitchouk, W., 2003, Eur. Phys. J. A **17**, 223.
Melnitchouk, W., I. R. Afnan, F. Bissey, and A. W. Thomas, 2000, Phys. Rev. Lett. **84**, 5455.
Melnitchouk, W., R. Ent, and C. Keppel, 2005, Phys. Rep. **406**, 127.
Melnitchouk, W., A. W. Schreiber, and A. W. Thomas, 1994, Phys. Lett. B **335**, 11.
Melnitchouk, W., and A. W. Thomas, 1996, Phys. Lett. B **377**, 11.
Meyer, H., and P. J. Mulders, 1991, Nucl. Phys. A **528**, 589.
Mineo, H., W. Bentz, N. Ishii, and K. Yazaki, 2002, Nucl. Phys. A **703**, 785.
Mineo, H., W. Bentz, and K. Yazaki, 1999, Phys. Rev. C **60**, 065201.
Mkrtchyan, H., *et al.*, 2008, Phys. Lett. B **665**, 20.
Moch, S., J. A. M. Vermaseren, and A. Vogt, 2004, Nucl. Phys. B **688**, 101.
Müller, D., D. Robaschik, B. Geyer, F. M. Dittes, and J. Hořejši, 1998, Fortschr. Phys. **42**, 101.
Nachtmann, O., 1972, Nucl. Phys. B **38**, 397.
Nachtmann, O., 1973, Nucl. Phys. B **63**, 237.
Nadolsky, P. M., *et al.*, 2008, Phys. Rev. D **78**, 013004.
Nguyen, T. T., 2010, Ph.D. thesis (Kent State University).
Nguyen, T. T., P. C. Tandy, A. Bashir, and C. D. Roberts, 2010, unpublished.
Oertel, M., M. Buballa, and J. Wambach, 2001, Phys. At. Nucl. **64**, 698.
Oettel, M., M. Pichowsky, and L. von Smekal, 2000, Eur. Phys. J. A **8**, 251.
Ogawa, A., M. Grosse Perdekamp, and R. Seidl, 2007, prepared for Proceedings of the 15th International Workshop on Deep-Inelastic Scattering and Related Subjects (DIS2007) (unpublished).
Ohta, S., and T. Yamazaki (for RBC and UKQCD), 2008, PoS **LAT2008**, 168.
Orginos, K., T. Blum, and S. Ohta, 2006, Phys. Rev. D **73**, 094503.
Owens, J. F., *et al.*, 2007, Phys. Rev. D **75**, 054030.
Pasquini, B., M. Pincetti, and S. Boffi, 2005, Phys. Rev. D **72**, 094029.
Pasquini, B., M. Traini, and S. Boffi, 2002, Phys. Rev. D **65**, 074028.
Peierls, R. E., and D. J. Thouless, 1962, Nucl. Phys. **38**, 154.
Peierls, R. E., and J. Yoccoz, 1957, Proc. Phys. Soc., London, Sect. A **70**, 381.
Peng, J.-C., 2003, Eur. Phys. J. A **18**, 395.
Peng, J. C., *et al.* (E866/NuSea), 1998, Phys. Rev. D **58**, 092004.
Petratos, G. M., *et al.*, 2006, Jefferson Lab Experiment No. E12-06-118 (unpublished).
Pieper, S. C., and R. B. Wiringa, 2001, Annu. Rev. Nucl. Part.

Sci. **51**, 53.
Politzer, H. D., 1974, Phys. Rep. **14**, 129.
Pumplin, J., H. L. Lai, and W. K. Tung, 2007, Phys. Rev. D **75**, 054029.
Pumplin, J., *et al.*, 2001, Phys. Rev. D **65**, 014013.
Pumplin, J., *et al.*, 2002, J. High Energy Phys. **07**, 012.
Radyushkin, A. V., 1996a, Phys. Lett. B **385**, 333.
Radyushkin, A. V., 1996b, Phys. Lett. B **380**, 417.
Reimer, P., *et al.* (Fermilab E906/Drell-Yan Collaboration), 2006, Drell-Yan Measurements of Nucleon and Nuclear Structure with the Fermilab Main Injector, E906: Fermilab Proposal No. 906 (unpublished).
Reimer, P. E., 2007, J. Phys. G **34**, S107.
Reya, E., 1981, Phys. Rep. **69**, 195.
Roberts, C. D., 1996, Nucl. Phys. A **605**, 475.
Roberts, C. D., 2008, Prog. Part. Nucl. Phys. **61**, 50.
Roberts, C. D., M. S. Bhagwat, A. Höll, and S. V. Wright, 2007, Eur. Phys. J. Spec. Top. **140**, 53.
Roberts, C. D., R. T. Cahill, and J. Praschifka, 1988, Ann. Phys. **188**, 20.
Roberts, C. D., and B. H. J. McKellar, 1990, Phys. Rev. D **41**, 672.
Roberts, C. D., J. Praschifka, and R. T. Cahill, 1989, Int. J. Mod. Phys. A **4**, 1681.
Roberts, C. D., and S. M. Schmidt, 2000, Prog. Part. Nucl. Phys. **45**, S1.
Roberts, C. D., and A. G. Williams, 1994, Prog. Part. Nucl. Phys. **33**, 477.
Roberts, C. D., A. G. Williams, and G. Krein, 1992, Int. J. Mod. Phys. A **7**, 5607.
Schafer, T., and E. V. Shuryak, 1998, Rev. Mod. Phys. **70**, 323.
Schienbein, I., *et al.*, 2008, J. Phys. G **35**, 053101.
Schreiber, A. W., A. I. Signal, and A. W. Thomas, 1991, Phys. Rev. D **44**, 2653.
Scopetta, S., 2005, Phys. Rev. D **72**, 117502.
Shifman, M. A., 2000, e-print arXiv:hep-ph/0009131.
Shigetani, T., K. Suzuki, and H. Toki, 1993, Phys. Lett. B **308**, 383.
Signal, A. I., and A. W. Thomas, 1988, Phys. Lett. B **211**, 481.
Sivers, D., 1990, Phys. Rev. D **41**, 83.
Sivers, D., 1991, Phys. Rev. D **43**, 261.
Soper, D. E., 1997, Nucl. Phys. B, Proc. Suppl. **53**, 69.
Speth, J., and A. W. Thomas, 1997, Adv. Nucl. Phys. **24**, 83.
Steffens, F. M., and W. Melnitchouk, 2006, Phys. Rev. C **73**, 055202.
Steffens, F. M., and A. W. Thomas, 1994, Nucl. Phys. A **568**, 798.
Steffens, F. M., and A. W. Thomas, 1995, Prog. Theor. Phys. Suppl. **120**, 145.
Steffens, F. M., and A. W. Thomas, 1997, Phys. Rev. C **55**, 900.
Sterman, G., 1995, *Proceedings of the Theoretical Advanced Study Institute in Elementary Particle Physics (TASI 95): QCD and Beyond* (World Scientific, Singapore).
Sterman, G., *et al.* (CTEQ), 1995, Rev. Mod. Phys. **67**, 157.
Stump, D., *et al.*, 2003, J. High Energy Phys. **10**, 046.
Sutton, P. J., A. D. Martin, R. G. Roberts, and W. J. Stirling, 1992, Phys. Rev. D **45**, 2349.
Szczepaniak, A., C.-R. Ji, and S. R. Cotanch, 1994, Phys. Rev. D **49**, 3466.
Szymacha, A., 1984, Phys. Lett. **146B**, 350.
Taylor, R. E., 1991, Rev. Mod. Phys. **63**, 573.
Thomas, A. W., 1983, Phys. Lett. **126B**, 97.
Thomas, A. W., and W. Melnitchouk, 1998, Nucl. Phys. A **631**, 296c.
Thorne, R. S., A. D. Martin, W. J. Stirling, and G. Watt, 2009, Proceedings of 17th International Workshop on Deep-Inelastic Scattering and Related Subjects (DIS 2009) (unpublished).
Towell, R. S., *et al.* (FNAL E866/NuSea), 2001, Phys. Rev. D **64**, 052002.
Traini, M., L. Conci, and U. Moschella, 1992, Nucl. Phys. A **544**, 731.
Traini, M., V. Vento, A. Mair, and A. Zambarda, 1997, Nucl. Phys. A **614**, 472.
Tvaskis, V., *et al.*, 2007, Phys. Rev. Lett. **98**, 142301.
van Neerven, W. L., and E. B. Zijlstra, 1992, Nucl. Phys. B **382**, 11.
Virchaux, M., and A. Milsztajn, 1992, Phys. Lett. B **274**, 221.
Vogt, A., S. Moch, and J. A. M. Vermaseren, 2004, Nucl. Phys. B **691**, 129.
Wakamatsu, M., and T. Kubota, 1998, Phys. Rev. D **57**, 5755.
Watt, G., A. D. Martin, W. J. Stirling, and R. S. Thorne, 2008, Proceedings of 16th International Workshop on Deep Inelastic Scattering and Related Subjects (DIS 2008) (unpublished).
Webb, J. C., 2003, Ph.D. thesis (New Mexico State University).
Webb, J. C., *et al.* (NuSea), 2003, e-print arXiv:hep-ex/0302019.
Weigel, H., L. P. Gamberg, and H. Reinhardt, 1997, Phys. Lett. B **399**, 287.
Weigel, H., E. Ruiz Arriola, and L. P. Gamberg, 1999, Nucl. Phys. B **560**, 383.
West, G. B., 1970, Phys. Rev. Lett. **24**, 1206.
Whitlow, L. W., E. M. Riordan, S. Dasu, S. Rock, and A. Bodek, 1992, Phys. Lett. B **282**, 475.
Whitlow, L. W., S. Rock, A. Bodek, S. Dasu, and E. M. Riordan, 1990, Phys. Lett. B **250**, 193.
Wijesooriya, K., P. E. Reimer, and R. J. Holt, 2005, Phys. Rev. C **72**, 065203.
Wijesooriya, K., *et al.*, 2001, Jefferson Lab Proposal P01-110 (unpublished).
Wiringa, R. B., 2006, Phys. Rev. C **73**, 034317.
Yang, U.-K., and A. Bodek, 1999, Phys. Rev. Lett. **82**, 2467.
Yang, U.-K., and A. Bodek, 2000, Phys. Rev. Lett. **84**, 5456.
Zanotti, J. M., 2008, PoS **LAT2008**, 007.
Zhu, L. Y., *et al.* (FNAL-E866/NuSea), 2007, Phys. Rev. Lett. **99**, 082301.